BSc. Mohannad Marouf 01610555

Master Thesis 2018 supervised by:
Univ.-Prof. Dipl.-Phys. Dr.rer.nat. Holger Ott
M.Sc. Neda Hassannayebi

Particle Tracing In Saturated Micromodel

Combined with the application of defining colloidal preferential flow pathways in porous media

dpe DEPARTMENT PETROLEUM ENGINEERING

MONTAN UNIVERSITÄT

I would like to dedicate my thesis to my beloved parents, to my second mother Fr. Dorit Bassanel, and to my best friend Mag. Hermin Karout, without whom none of my success would be possible.

Declaration

I hereby declare that except where specific reference is made to the work of others, the contents of this dissertation are original and have not been published elsewhere. This dissertation is the outcome of my own work using only cited literature.

Erklärung

Hiermit erkläre ich, dass der Inhalt dieser Dissertation, sofern nicht ausdrücklich auf die Arbeit Dritter Bezug genommen wird, ursprünglich ist und nicht an anderer Stelle veröffentlicht wurde. Diese Dissertation ist das Ergebnis meiner eigenen Arbeit mit nur zitierter Literatur.

_____

Mohannad Marouf, 24 September 2018

Acknowledgements

I wish to express my sincere gratitude to Univ.-Prof. Dipl.-Phys. Dr.rer.nat. Holger Ott, not only for his support during the course of this work, but also for all the knowledge he provided throughout my two-year master's study in Montanuniversität-Leoben

I sincerely thank M. Sc. Neda Hassannayebi for her guidance and encouragement in carrying out this porject work.

I also thank BSc. Ahmad Kharrat for the help and support during the experimental work

Abstract

The motion of particles plays an essential role in flow visualization and quantification. In the recent years, particle and colloid tracing in saturated and unsaturated porous media have been widely studied in various applications. Nano- and micro-seeding particles are introduced into a flow to record their motion and subsequently estimate the kinematics of fluids flow. This, by means of many techniques, would allow exploring the fluids flow behavior in plenty of applications in various fields of studies (e.g., Underground-water management and treatment, manage and engineer underground environmental contaminants, Enhanced Oil Recovery).

In this work, we apply an experimental technique with the assistance of an image processing and analysis software (ImageJ-2/ Fiji®), and a matrix-based programming language (MATLAB®) to computationally analyze and visualize the fluid flow in porous media. We used microfluidic systems with representative porous structures to define the trajectories (flow lines) of neutrally buoyant micro-polystyrene particles (10-µm diameter), flowing in two-dimensional, water-saturated, microporous networks.

By visually tracking individual particles across the micromodel, measuring their average residence time, and comparing it with the estimated saturating-fluid's residence time, we were able to observe the particle dispersion and breakthrough behavior, as well as their microscopic preferential flow paths.

Moreover, tracing particles in a realistic micromodel enabled us to measure the particles instantaneous and average interstitial velocities in porous structures at different flow rates. The resulting data was used to quantify the microscopic flow field and to prove the existence of preferential pathways.

In this thesis, the developed particle tracing technique to quantify the velocity field at the pore scale, is thoroughly discussed and documented. This includes the conventional and fluorescence microscopic images acquisition, processing, and analyzing procedures; the designed combination between the Particle Tracker 2D/3D plugin of Image-J2/Fiji® tool, and the MATLAB® language; as well as the developed MATLAB® code for the calculation and visualization of the velocity field's vectors and magnitudes.

Finally, as the outlook of this work, we applied this method to compare the preferential flow paths in a water-saturated medium with a pre-established biomass system. This is expected to give a better understanding of the effects of biomasses accumulation on the flow properties.

Keywords: particle tracing, preferential flow paths, saturated porous media, micromodel, ImageJ2/Fiji®, MATLAB®.

Zusammenfassung

Die Bewegung von Partikeln spielt eine wesentliche Rolle bei der Strömungsvisualisierung, sowie auch bei der Strömungsquantifizierung. In den letzten Jahren wurde das Verhalten von Teilchen und Kolloiden in gesättigten und ungesättigten porösen Medien verfolgt und umfassend untersucht.

Die Nano- und Mikropartikel werden in ein Fließverhalten versetzt, um anschließend ihre Bewegung aufzuzeichnen und in Folge die Kinematik der Strömung abzuschätzen. Mit dieser Vorgangsweise wäre es möglich, das Strömungsverhalten in vielen verschiedenen Anwendungsgebieten (z.B.: Grundwassermanagment, Enhanced Oil Recovery) besser zu verstehen.

In der vorliegenden Arbeit wird mit Hilfe einer Bildverarbeitungs- und Analysesoftware ImageJ-2/ Fiji® und einer matrixbasierten MATLAB® Programmiersprache das Strömungsverhalten in porösen Medien rechnerisch analysiert und visualisiert. Wir verwendeten Mikrofluidsysteme mit repräsentativen Mikromodellen, um die Trajektorien (Strömungslinien) von neutral schwimmenden polystyrene Mikropartikeln (10 µm Durchmesser), die in zweidimensionalen, wassergesättigten, mikroporösen Netzwerken fließen, zu definieren.

Durch das Beobachten einzelner Partikel, darauffolgender Messung der durchschnittlichen Verweildauer in den verschiedenen Mikromodellen und anschließendem Vergleich mit der geschätzten Verweildauer der Flüssigkeiten, konnten wir daraus das Vorhandensein von kolloidalem bevorzugtem Strömungsverhalten der Partikel feststellen.

Die Beobachtung der Partikel in einem realen Mikromodell ermöglicht die Messung der momentanen und mittleren interstitiellen Geschwindigkeit der Partikel in porösen Strukturen bei unterschiedlicher Fließgeschwindigkeit. Das ist wichtig, um die bevorzugten Strömungswege zu definieren, sowie auch für weitere vielversprechende Anwendungen.

Diese “Particle tracing technique”, die speziell für diese Studie entwickelt wurde, um das Geschwindigkeitsfeld auf einem Porenmaßstab zu quantifizieren, wird in meiner

Arbeit ausführlich diskutiert und dokumentiert. Dies beinhaltet: the microscopic images acquisition, processing, and analyzing procedures; the designed combination between the Particle Tracker 2D/3D plugin available in Image-J2/Fiji® tool, and the MATLAB® language; as well as the developed MATLAB® code for the calculation and visualization of the velocity field vectors and magnitudes.

Schlussendlich, als Resultat dieser Arbeit, verwendeten wir diese Methode, um die bevorzugten Strömungswege in einem wassergestättigten Medium mit einem vorgefertigten Biomassesystem zu vergleichen. Dies soll zu einem besseren Verständnis führen hinsichtlich der Auswirkungen der Biomasseakkumulation auf die Fließeigenschaften.

Keywords: particle tracing, preferential flow paths, saturated porous media, micromodel, ImageJ2/Fiji®, MATLAB®.

Table of Contents

List of Figures

List of Tables

Abbreviations

EOR	Enhanced Oil Recovery
MEOR	Microbial Enhanced Oil Recovery
R_e	Reynolds Number
P_e	Peclet Number
PIV	Particle Image Velocimetry
μPIV	Micro Particle Image Velocimetry
fps	Camera's frame per second
bpp	bits per pixel

Chapter 1

Introduction

Transport of various suspended particulate matter (e.g., bacteria, viruses, colloids, sands, mineral grains) is widely recognized to occur in subsurface environments with high spatial interconnectivity. Particles originated from several subsurface processes, like precipitation in supersaturated solutions, degradation of biological materials, and rock matrix weathering processes, are all carried with underground fluids within hydrocarbons reservoirs and aquifers (Buffle, et al., 1998). They are in the forms of solutions (ultrafine particles with sizes usually smaller than one nanometer), colloids and suspensions with a wide range of sizes between 1 nanometer and 10 micrometers (Chrysikopoulos & Sim, 1996).

Often, colloid transport and penetration into these porous structures are of great interest for many applications. Fine clay particles for example have a significant effect on flow paths in porous media. In like manner, and to protect aquifers, suspensions of particles are injected into formations as tracers to determine potential pathways for migration of pollutants and hazardous substances such as radionuclides, heavy metals, and organic substances (Zheng & Bennett, 1995). Besides that, nanoparticle (NPs) applications used in underground water protection, have been becoming promising candidates for oil and gas applications, especially in Enhanced Oil Recovery methods (EOR) (Hu, et al., 2017). They are used as property modifiers, i.e., to alter rock wettability and interfacial tension (Karimi, et al., 2012), and as “conformance controllers” like emulsions stabilizers, and gelation materials to block the easy flow paths (Pei, et al., 2015).

In this context, to predict and understand colloid transport, particle-tracing methods in columns and microfluidics’ experiments have increasingly gained a substantial role in exploring many processes in the subsurface. It provides useful information in complex processes like microorganisms transport in porous media, the biofilm and biomass formation, and their

relevant applications in microbial enhanced oil recovery (MEOR), water treatment methods, bioremediation, as well as biodegradation.

Until now, the fluid flow behavior in many of these applications is not fully understood. The influence of **particle size, concentration** and **ionic strength** on particles migration in porous media are still largely incomplete. Moreover, much of the research regarding the transport of colloids and bio-colloids is done for safe water drinking and bioremediation. Only recently, a renewed interest emerged in the petroleum industry in many of the applications of fine particles migrations in oil and gas reservoirs (Hu, et al., 2017). This encouraged the development of several computational modelling methods for particle tracing validated by reliable experimental data in microfluidics systems. Microscopic observation and visualization, when coupled with automated and semi-automated image processing and analyzing means, would provide precious information about several processes occur in the porous media. This includes colloids (and bio-colloids) transport, since they suggest a pore-scale two-dimensional view of colloids flow in artificial micromodels represent the subsurface porous media, and supported by a fast and accurate method for data processing and analysis.

We focused in this thesis on studying the colloidal flow behavior in a saturated porous media. By tracking microparticles trajectories in microfluidics systems, measuring and computing their instantaneous and average interstitial velocities, we had a better understanding of the colloidal flow behavior, as well as many related phenomena such as the colloids preferential flow pathways and their breakthrough behaviors, among many others. This, at the same time, led to more questions about the factors affecting their flow in porous media. Particles size and size exclusion effect, particles concentration, differential pressure, are still to investigate in-depth and address.

Six main chapters in this thesis outline its content. After an introduction to colloidal flow in porous media and particle tracing, a literature review in chapter two focuses on the current state of knowledge in this domain. The experimental methods that were designed for this work will be introduced in chapter three. Afterwards, the experimental steps and techniques will be thoroughly discussed in chapter four. The results interpretation and discussion in chapter five, and a summary of main issues and challenges, as well as the future work will follow in chapter six.

Chapter 2

Literature Review

2.1 Particle/colloid Transport in porous media

The migration of colloids in the geological media is highly dependent on physical, chemical and electrochemical properties of both the colloids and the porous rock. Particles sizes and concentration, the surface charge of both particles and the matrix, as well as porosity, permeability, tortuosity, among many other properties are of great importance to the colloid transport process. The physiochemical interaction between the host rock and the solutes or colloids would keep their velocity less than the transporting fluids due to their sorption on the solid phase (deMarsily, 1986). However, if sorption is negligible, their transport velocity, due to other factors, is expected to be close to or slightly less than the interstitial fluid velocity and hence, migration velocity of any substance (colloidal particles) should be less than a tracer[1] velocity.

Nevertheless, few researchers and authors, based on their field and laboratory studies, have concluded that the velocity of colloidal particles migration in their experiments was higher than solutes velocity (Knapp, 2000) (Artinger, 1998) (Zhuang, et al., 2003). It can even exceed the velocity of the pore fluid by a few times (Malkovsky & Pek, 2009). According to

[1] Tracers are fine solutes commonly used in estimating the interstitial velocity of ground water

another experimental laboratory study, the measured colloid velocities are 4 - 5.5 times greater than the estimated pore-water velocities (Sirivithayapakorn & Keller, 2003).

In fact, all these studies have one thing in common. They drew their conclusions based on the early breakthrough observations of these particles/colloids in their concerned cases. Hence, the velocity they measured was the average velocity or Darcy's velocity derived from Darcy's law in porous media.

A real case example from a safety-assessment field-study on an underground repository of Radioactive Wastes (RW) showed that the actual velocity of radioactive contaminants migration could be much higher than its predicted value obtained from computer simulation. They attributed that to what so-called **colloid-facilitated transport** where radionuclides adsorb on colloidal particles, which have higher sorption properties relative to the rock-matrix sorption properties, and thus they can be transported faster (Smith, 2003) (McCarthy, 1998).

However, since the only process for particles migration in the subsurface, is their transport by the underground fluids, colloid migration at a velocity higher than the transporting fluids seems to be doubtful. Investigations of this phenomenon led to two main mechanisms responsible for the elevated-velocity colloids migration:

- A mechanism is responsible for the **redistribution of the colloids** in the flow channels' cross-sections. It relocates the colloids at the central streamlines where local velocities are higher than the average velocity over the whole cross-section. This mechanism is explained by electrostatic repulsion between the particles and the channel walls, and also as a result of **Magnus effect**, which affects rotating objects inside a fluid flow, and causes a transverse motion of the particles to the center (Loitsyanskii, 1973),

- Another mechanism called the colloid **size exclusion,** which emphasizes the existence of preferential flow pathways of colloidal particles in porous media.

Although the redistribution mechanism seems to be plausible, it was discussed by a theoretical analysis (Malkovsky & Pek, 2009). It argued that electrostatic forces might be repulsive and attractive in the geological media, and they only affect the particles in immediate proximity to the channel walls where the velocity is very low. Whereas drift forces arising from **Magnus effect** are more effective, they are **only** considered when there is a rotation movement of the particles **and** a difference between the longitudinal components of the particle velocity and the local velocity of the fluid. This happens if gravity effect is not trivial (non-horizontal flow).
According to the same study, if gravity effect is neglected, then the excess of colloidal velocity over the liquid phase is attributed to "**mechanical retention** of a colloidal particle

in narrow flow channels which led to reduced number of colloidal flow paths" (Malkovsky & Pek, 2009).

Some authors, from their experiments on colloidal transport in the fractured system, hypothesized that colloids always arrive earlier than tracers do. Because of their relatively large size, they travel through the faster streamlines, which enhances the colloids migration (Chrysicopoulos & Abdel-Salam, 1997). Other argued that they diffuse slower in the dead zones of fractures where low-velocity areas exist (Reimus, et al., 1994).Others from their column experiments suggested that colloids only flow in pores with diameters much bigger than theirs and that the "**exclusion of colloids** from **matrix diffusion** is the crucial difference between colloids and tracers transport" (Niehren & Kinzelbach, 1998).

However, most authors attributed this behaviour to a phenomenon called **size exclusion effect**. An experimental evidence of this **size exclusion** effect was introduced by (Sirivithayapakorn & Keller, 2003). By using realistic micromodels of porous media, and four aqueous suspensions of latex particles with four different sizes (0.05, 1, 2, and 3 μm), they could directly observe this phenomenon at the pore-scale. They proved the existence of what so-called "colloidal preferential flow pathways" by statistically counting and analyzing the number of particles passing through different areas (pore throats) of small aperture sizes (2.4 – 14 μm) in a distilled-water saturated porous structure. In relation with the particles size and pressure gradient, they found out that for a particle to enter a pore body across a pore throat, a minimum threshold ratio of the pore throat to the colloid diameter (T/C) should be around (1.5). This, in turn, will lead to a larger-scale pore exclusion effect, where larger particles are directed through only certain regions of the porous medium, and thus distinct pathways. They also found out that the larger the particles and the higher the pressure gradient, the more evident the preferential flow paths they become. In other words, the throat to colloid size ratio defines the colloids inability to move into a pore space as a reason of the size exclusion effect (Sirivithayapakorn & Keller, 2003).

However, later experimental research was implemented in 2005 (Auset & Keller, 2005) on water-saturated micromodels to investigate the microscale processes governing the particle transport in porous media. It found out that capturing mechanisms like straining, interception and attachment, also play a significant role in this phenomenon depending on the solution ionic strength, flow rate and the surface roughness of the matrix.

Analytically, the actual retardation coefficient R_p in the mathematical model, which describes the colloid transport in homogeneous saturated media with advection-dispersion processes, is lower for heterogeneous media than the expected, since it was calculated from batch experiments. This explains the fast break through of colloids in highly heterogeneous saturated media (Sirivithayapakorn & Keller, 2003).

Additionally, many more studies investigated the colloids transport in unsaturated porous media (DeNovio, et al., 2004) (Cey, et al., 2009). However, they all have in common that larger particles experience faster average velocities due to their preferential pathways. They flow through a reduced number of streamlines resulting in more straight trajectories and therefore lower residence times.

Understanding the colloid behavior in natural systems requires identifying the processes that affect its transport in the subsurface. According to (Ryan & Elimelech, 1996), these are physical perturbations, chemical perturbations, Colloid-Colloid interactions, Colloid-Matrix interactions, pore topology, and Colloid characteristics.

The transport of colloids in porous media is a **convective transport**. Two main transport processes of the fluid molecules are considered in this kind of transport;

- **Advection,** which is the bulk transport of mass. The motion of the fluid itself determines it, hence on a large scale, it is determined by Darcy's velocity (the average linear velocity) in the porous media, but on the pore scale, by interstitial velocity.
- **Diffusion,** which is determined by the random **Brownian motion** of individual particles in the fluid (Incropera & Dewitt, 2005).

If advection is the only colloidal transport process, colloids will have the same average velocity (Darcy's velocity) as the transporting fluids on the large scale. This implies that the pressure gradient, permeability, and fluid viscosity will be the influencing factors in this kind of transport.

However,it is not the case. Dispersion, which arises from different reasons such as the parabolic velocity profile at the pore scale, and the velocity variation from pore to pore because of complex geology (different porosity, permeability, and tortuosity distribution), as well as the Brownian diffusion, then colloids will have different average and pore velocity than fluids Figure 1.

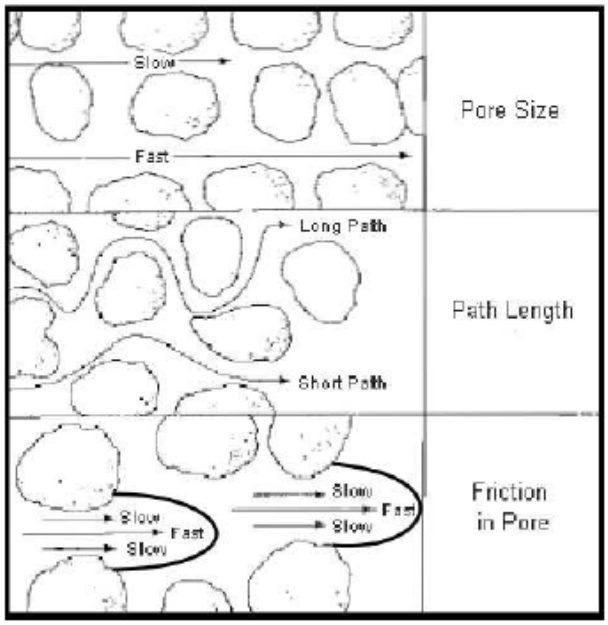

Figure 1-Transport behavior of colloids in porous media (Fetter, 2001)

In fact, Brownian motion which is a random thermal movement of particles is the source of particles diffusion during transport in porous media "If heat is due to kinetic fluctuations of atoms, the particle of interest, that is, a Brownian particle, should undergo an enormous number of random bombardments by the surrounding fluid particles and its diffusive motion should be observable. (Bian, et al., 2016). Therefore, Brownian particles will have different average and pore-scale velocities than the fluid phase. However, diffusion is calculated by the Stokes-Einstein equation:

$$D = \frac{K_B \,.\, T}{6\,\pi \,.\, \mu \,.\, dp/2}$$

Where:

K_B	Boltzmann's constant
T	Temperature
μ	Fluid viscosity
dp	Particle diameter

For particles ≥ 1 μm diameter, diffusion is very small and in most studies is negligible. However, at low fluid velocities, when Peclet number, which is the advection rate over the diffusion rate, $P_e \ll 1$, diffusion is dominated on the particles transport in the porous media.

Other dispersion causes in colloidal transport in porous media is the local flow regime. In very low Reynolds number ($Re \ll 1$) flows, a creeping flow regime will take place and dragging forces will oppose the movement of colloids in fluids (Kirby, 2010). "Reynolds number in the order of 10^{-2} will cause a creeping flow regime" (Lindken, et al., 2009).

Recent and extensive laboratory study to assess whether the dispersivity is dependent on colloid size and interstitial velocity (Chrysikopoulos & Katzourakis, 2015), performed 48 colloid transport columns experiments with 9 different colloids diameters, and various flow velocities. Consequently, they found out that "dispersivity is positively correlated with particles size and increase with interstitial velocity".

Overall, these factors, among many others regarding the colloid-colloid and colloid-matrix interactions, result in colloid's average and pore-scale velocities different from the transporting fluids.

2.2 Particle Tracing:

Direct observation of the porous structures via transparent micromodels (flow cells) provides a valuable tool for studying the processes governing the colloidal transport at the pore scale.
Using transmitted and fluorescent microscopy, an insight into the microscale medium would allow tracking individual particles, record their motion, and using many techniques, explore and quantify the **transport processes** at the pore-scale.
Additionally, single particle tracking has been widely used for visualizing and quantifying the full velocity field at the pore-scale. "Optical whole-field measurement techniques called as micro-scale Particle Image Velocimetry μPIV are useful methods for the detailed characterization and optimization of microfluidics applications in life science, biomedical research, microchemical engineering, and other related fields of research" (Lindken, et al., 2009).
Flow visualization is the best experimental method for detailed investigations of fluid mechanics at the pore scale. "**The idea of flow visualization is to alter the working fluid in a way that the fluid motion stays unchanged while the fluid transport is made detectable**" (Lindken, et al., 2009). By seeding the working fluid with Nano and microparticles, **Quantitative flow visualization** is possible by recording the change in particles distributions over time. Then by processing the acquired images, the flow motion is determined.

Ideally, the seeding particles should faithfully follow the flow, this is theoretically possible by having very small particles with the same density as the working fluid. However, Brownian motion which caused by the thermal motion of water molecules will influence the small particles and "Measurement errors can occur" (Santiago, et al., 1998).
At the same time, according to the detailed study for particle image velocimetry (Lindken, et al., 2009), the large size and weight of the particles will decrease their response time to any changes in the velocity. **Therefore, in microfluidics applications with water as a working**

fluid, the tracer particles are typically made of polystyrene and have diameters of 200 nm to 2 µm to avoid any error in velocity measurements caused by response time.
This means we need particles large enough (>2 µm) to resist Brownian effect, and small enough to respond spontaneously to the change of fluid velocity (response time <0.2 µs for 2µm size particles (Lindken, et al., 2009)).

Many tools for particle tracking and PIV software are available in the market. ImageJ2/Fiji®, for example, is an open source image processing and analysis program; it provides many techniques for image processing, visualization, segmentation, tracking and much more. For fluorescence microscopy for example, several of image-processing algorithms developed at the MOSAIC group and named as MosaicSuite for ImageJ and Fiji. 2D single-particle tracking tool was the first plugin in this MosaicSuite package. Its algorithm was developed to track single particles as bright spots in 2D movies over time (Sbalzarini & Koumoutsakos, 2005), and later was upgraded to include 3D videos and named as Particle Tracker 2D and 3D tool.

Herewith, particle tracking tools available in ImageJ-2/ Fiji® software;

2.2.1 Particle Detector and Tracker 2D / 3D

An ImageJ2/Fiji® Plugin for the automated detection and tracking of particle trajectories from digital videos. It is available under the menu command Plugins → Mosaic → Particle Tracker 2D/3D.

2.2.2 TrackMate

Another ImageJ2/Fiji® plugin for particles tracking. It allows a single particle tracking of spot-like structures. It is available under the menu command Plugins → Tracking → TrackMate.

2.2.3 Spot detection

To detect bright spots and their possible centers. In fact it is the particle detection part of Particle Tracker 2D/3D without the linking part. Available in Plugins → Mosaic → Utility → Spot detector

2.2.4 MTrack 2

Plugins → Tracking → MTrack 2

2.2.5 Manual Tracking

It allows keeping tracking a particle while moving. This tool available under the menu command Plugins → Tracking → Manual Tracking / Manual Tracking with TrackMate / MTrack 2.

Moreover, worth mentioning that ImageJ2/ Fiji® has a PIV tool available under the command Analyse → Optic flow → PIV Analyser

More other available tracking tools for using particle tracking is mentioned in (Meijering, et al., 2012).

Chapter 3

Experimental Method

In this chapter, we present the design of the experimental method, which was developed for performing particle-tracing experiments in saturated micromodels.

The main aim of this study was to observe the colloidal transport behavior at the pore scale and prove the existence of preferential flow pathways by tracing inert colloidal particles in a water-saturated 2D micromodel. Consequently, we aimed to quantify the colloidal flow field by measuring the instantaneous velocity of the particles at different flow rates and different fields of view. To do so, we used aqueous suspensions of fluorescent polystyrene particles with relatively large size (10 µm) and diluted in distilled water. This is expected to enhance the size exclusion effect and observe more distinct colloidal flow pathways.

3.1 Experimental Apparatus and setups

Two experimental setups were mainly used. The principle of the experiments remains constant, but the optical cameras were different.

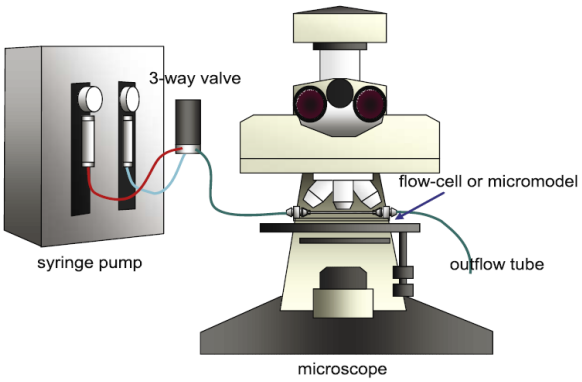

Figure 2 – Particle-Tracing typical setup

As illustrated in Figure 2, the main parts included in this setup are:

3.1.1 Fluorescent Microscope- (Leica-DMI-6000-B inverted microscope)

This microscope can be used for **transmitted light contrasting** as well as for **fluorescence microscopy**.

The difference that in **transmitted light microscopy**, the light is directed to the specimen through a condenser and then passes through it. Absorption of light and other effects produce an image of the sample either at the eyepiece or at a camera.

Whereas, in **fluorescence microscopy**, the excitation light is directed to the specimen through the objective instead of the condenser in order to allow a **filter cube** to generate a specific wavelength of the excitation light (depicted in blue) able to excite the fluorophore in the sample. This will then emits fluorescent light in a specific wavelength range that can be observed via the eyepiece or the camera.

Therefore, the filter cube function as director of the light to the sample and as a filter for the desired excitation and emission wavelength, Figure 3.

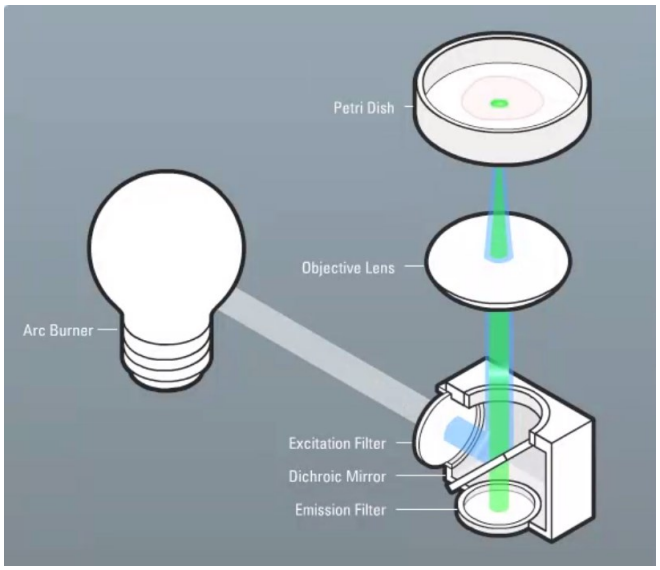

Figure 3 - Detailed beam path for fluorescence microscopy in Leica DMI 6000 B inverted microscope

"In order to build up a successful µPIV experiment, the use of an inverted microscope system is advisable since it is rigid, stable and provide more space for the setup" (Lindken, et al., 2009).

3.1.2 Fluorescent and Bright-field Cameras

Two different cameras were used;

- **Leica DFC320 digital camera**

An sCMOS-type camera works perfectly in bright field microscopy option with up to 16 fps (frame per second). However, this number changes with the desired exposure time and intensity

for the acquired images. For example, the maximum fps in bright field for our experiments was about 4 fps.
The disadvantage of this camera that with low fps, blurring particles will start to appear at high injection rates. This will not allow the detection of the particles after image processing. Therefore, in order to conduct experiments at higher flow rates, it is recommended to have higher fps cameras for particle tracing experiments. Another disadvantage is that it cannot detect moving fluorescent particles in the fluorescence microscopy option.

- **Zyla_sCMOS camera, from ANDOR co**.

With up to 100 fps (53 fps USB 3.0) capability. It works perfectly in the Brightfield and Fluorescent microscopy alike. However, for our experiment, we could achieve up to 25 fps to match with our desired light intensity and exposure time.

3.1.3 Microfluidics chips (micromodels):

2D micromodels with physical-rock network structure from Micronit®. Surrogate rocks etched on the glass to visualize the fluid flow in porous media for experimental purposes. It uses channel structures tolerates high-pressure conditions and represent an actual physical piece of rock with 2 cm length and 1 cm width (45 mm x 15 mm Total size). The full specifications of this micromodels are mentioned in Appendix A.

3.1.4 Chip-holders:

The compatible holder (Figure 4) for the chosen physical-rock micromodel is **Fluidic Connect Pro** from Micronit®. It is robust, easy to use and suitable for standard chips of 45 mm x 15 mm size).

Figure 4 – Fluidic Connect Pro Chip holder from micronit®

3.1.5 Connections and Accessories:

Teflon Connection Kit PRO tubes and ferrules from micronit®: low friction, re-usable, high chemical resistance to a wide range of chemicals, high-temperature resistance (up to 260°c). These specifications are essential for the experiments, specifically when using some aggressive chemicals for cleaning the interior of the micromodels.

Syringe Pumps form Micronit® company; able to operate for different syringes types and sizes with a wide range of flow rates.

Figure 5 - Microfluidic Starter Kit from Micronit®

3.2 Materials

3.2.1 Fluorescent Particles

As we mentioned earlier in this chapter, we diluted fluorescent polystyrene particles with relatively large size (10 µm) in distilled water, in order to enhance the size exclusion effect and observe more distinct colloidal flow pathways.

The particles we used had an almost similar density as water in order to achieve neutrally buoyant particles and avoid gravity effect on the flow as well as any particles precipitations. The table below shows the related particle specifications according to the manufacturer's (micromodel Partikeltechnologie GmbH) technical data sheet:

Table 1 – Fluorescent Particles specifications

Product code:	29-00-104
Surface	Plain
Size	10 µm
Composition	Green fluorescent polystyrene particles
Shape	Sphere
Density	1.03 g/ccm
Optical properties	Green fluorescent
Production from	Suspension in Water
Stable in	aqueous buffer, methanol, ethanol, DMSO

3.2.2 Double distilled Water

To assure that we have no contaminants in the system, and achieve close-to-ideal conditions for particle tracing experiments and flow visualization.

3.3 Ultrasonic Vibrator

In order to correctly clean the micromodel before saturating it with water, as a pre-step for particles tracing experiments, we used an ultrasonic vibrator, which allows water injection within an ultrasonic field at relatively high temperatures. This guarantees the best removal of any contaminants inside the utilized micromodel

.

Chapter 4

Experimental Steps

Two main sets of experiments were conducted in order to develop a robust particle tracing method in the respective microporous media:

1. Experiments to estimate the Particles average residence time, Darcy's Velocity, and colloidal average velocity (analytical preferential pathways calculations).
2. Particle tracing experiments for tracking trajectories, and visualizing potential preferential flow paths.

The table next categorizes the two groups of experiments by their experimental setups:

Table 2 - The conducted Particle-Tracing experiments categorized by their setups

Experiment No.	**Camera type**	**Illumination type & camera's fps**	**Flow rate (ml/hour)**	**magnification**	**Description**
1	**Leica DFC320**	Bright Field 4 fps	0.05	2.5x	Measuring Particles' residence time
2 Includes 5 different locations	=	=	0.005	10x	Bright field trajectories and velocity field calculation
3	=	=	0.005	5x	=
4	=	=	0.02	5x	=
5 (extreme)	=	=	0.05	2.5x	=
6	**Zyla_sCMOS**	Fluorescence 25 fps	0.005	5x	Fluorescent Particles trajectories and velocities

4.1 Particles Average Residence-time T_r and Darcy's Velocity (experiment No. 1)

4.1.1 Visual observations:

In order to justify the existence of preferential paths, we visually observed the particles flow behaviour in a water-saturated micromodel represents a real porous medium with 57% porosity and 2.5 mD permeability. Many obvious colloidal preferential paths were observed at different flow rates and different locations of the micromodel. The figure next illustrates the 10µm-particles preferential paths after 5 minutes of injection with 0.005ml/Hour:

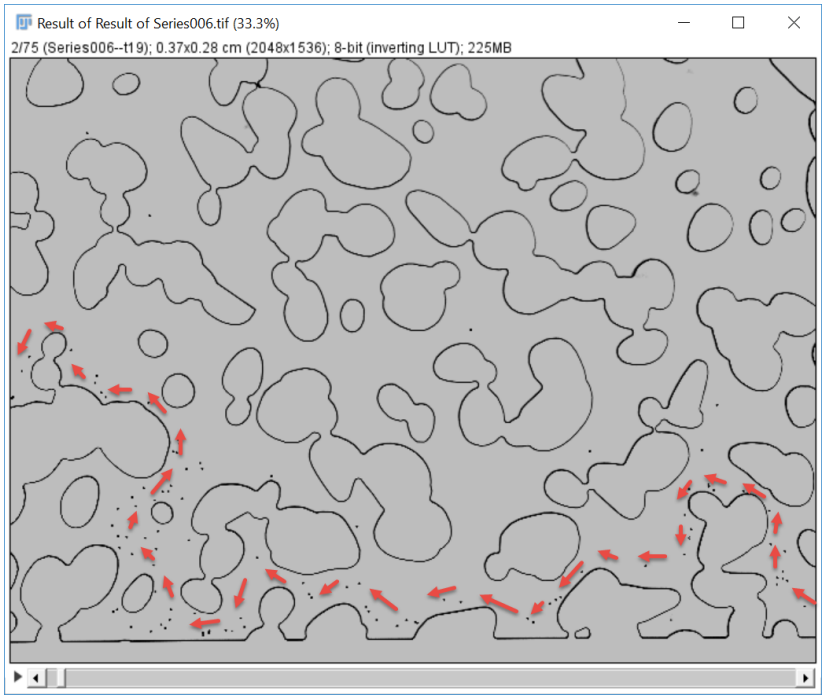

Figure 6: Particles preferential flow paths at 0.005 ml/hour

4.1.2 Reynolds Number:

To analyze and understand this behaviour, we measured the average particle residence-time at a specific flow rate (0.05 ml/hour) and compared it with the estimated water velocity (Darcy's Velocity) across the micromodel.

Technically, this rate was low enough to enable visual tracking of individual particles along the whole micromodel from the inlet to the outlet. At the same time, it was high enough to observe many particles in a short time and to avoid a delicate system sensitive to any tiny pressure changes due to any external effects. This is very important in such situation, especially that the

chip-holder was moved above the microscope objective to keep tracking the individual particles from the moment they enter the micromodel porous structure until they leave it to the outlet channel. This might cause some small, but adequate, disturbances to the steady state situation required in such delicate experimental circumstances.

Moreover, the 0.05 ml/hour flow rate must maintain laminar flow. Due to that, we calculated the Reynolds number to assure this assumption as shown in **eq.1** (Engineering_ToolBox, n.d.):

$$\boldsymbol{Re} = \frac{\boldsymbol{Inertial\ Forces}}{\boldsymbol{Viscous\ Forces}} = \frac{\boldsymbol{\rho.DH.V}}{\mu} = \frac{\boldsymbol{\rho.DH.Q}}{\boldsymbol{A}.\mu} \qquad (1)$$

Where:

ρ is the density of the fluid (for pure water = 1000 kg/m^3),

V is the bulk velocity (average velocity) of the duct's cross section (in our case, in complex geometry, it is the average interstitial velocity in m/sec),

D_H is the hydraulic diameter of the duct;

- For a circular tube, D_H is exactly equal to the inside diameter of the duct D_i.
- for an annular duct, D_H is the difference between the inside diameter of the outer tube and the outside diameter of the inner tube:

$$\mathbf{D_H = D_{o,\,i} - D_{i,\,o}} \qquad (2)$$

- For rectangular or annular ducts where the height and width are comparable:

$$\mathbf{D_H} = \frac{\boldsymbol{4\,A}}{\boldsymbol{P}} \qquad (3)$$

Where:

A is the cross-sectional area.

P is the wetted perimeter (the total perimeter of all channel walls that are in contact with the flow) (Holman, 2002),

- However, for a wide duct, where fluid moving between two plane-parallel surfaces and **the width is much greater than the space between the plates**, then D_H is equal to twice the distance between the plates (20 µm for our micromodel). This is consistent with **eq. 2** and **eq. 3** (Holman, 2002),

Q is the volumetric flow rate (m^3/s),

A is the duct's cross-sectional area (m^2). In our case, it is the rectangular cross section area of the micromodel;

A = micromodel depth (20µm)* micromodel width (10mm) * porosity (0.57)

$$\mathbf{A = 20x10^{-6} * 10x10^{-3} * 0.57 = 114x10^{-9}\ m^2}$$

µ is the dynamic viscosity of the fluid (for pure water = 0.001 Pa.sec)

Since the average interstitial velocity is unknown yet, we used the volumetric flow rate in the calculation ($Q = \frac{0.05 \times 10^{-6}}{3600} = 1.39 * 10^{-11}$ m^3/sec)

$$\boldsymbol{Re = \frac{\rho.DH.Q}{A.\mu} = \frac{1000*40*10^{-6}*1.39*10^{-11}}{114*10^{-9}*0.001} = 0.00487 << 1}$$

An extremely small Reynolds number (< 0.1) assures not only the purely laminar flow (<10 for this case (Rhodes, 2007)), but also creeping motion fully governed by Stokes' law. This flow regime, named as creeping flow or Stokes' flow, applies when drag forces (friction forces) exerted on spherical objects with smooth surfaces and very small Reynolds number in a viscous fluid (Kirby, 2010), (Keith J. Laidler, 1982). This applies on all our experiments since 0.05 ml/hour was the largest flow rate used.

4.1.3 Darcy's Velocity V_d & Colloidal Average Velocity V_c

The residence times for ten randomly picked particles were measured and listed in the table next:

Table 3: different particles' residence-time in the micromodel at 0.05 ml/hour injection rate

Particle No.	Residence time (seconds)
1	135
2	154
3	143
4	144
5	168
6	167
7	163
8	197
9	161
10	162
average	**159.4** seconds

The resulting average residence time was compared afterwards with the estimated average residence time derived from Darcy's velocity in the respective micromodel, assuming that particles are faithfully following the fluid (water) stream lines without any preferential paths or any other effects like Brownian motion effect, drag forces, dispersion effects, etc.;

$$\boldsymbol{V = \frac{Q}{A} = \frac{-K\,.\,\Delta P}{\mu\,.\,L}} \qquad \textbf{(4)}$$

Where:

V is Darcy's fluid flow velocity through the medium in cm/second,

Q is the volumetric fluid flow rate through the medium in cm^3,

A is the cross section area of the medium in cm^2 (corresponds to the cross-section area of the micromodel in z direction),

K is the permeability of the medium in Darcy,

ΔP is the applied pressure difference in atm (corresponds to the pressure difference between the inlet and the outlet of the micromodel),

μ is the dynamic viscosity of the fluid in cP (mPa.s),

L is the length of the medium in cm (corresponds to the micromodel length),

$$\boldsymbol{T_r = \frac{L}{V}} \qquad \textit{(5)}$$

Where:

T_r is the residence time in seconds.

However, to avoid the pressure-differential Δp measurements, we used a simple formula in the calculations as shown in equation (6)

$$\boldsymbol{T_r = \frac{Pore\ Volume}{Q}} \qquad \textit{(6)}$$

The manufacturer already defines the pore volume as 2.3 μl Rock-pore volume (microtechnologies, 2018).

Accordingly, the expected particle residence time for an injection rate of 0.05 mL/hr:

$$\boldsymbol{T_r = \frac{Pore\ Volume\ (ml)}{Q\ (\frac{ml}{hour})}} = \frac{2.3*10^{-3}}{0.05} = 0.046 \text{ hour} = 165.6 \text{ seconds}$$

Compared to the measured particle residence time (as an average) from Table 3, we can infer that particles / colloids have less residence time in the porous network.

The corresponding flow velocities;

- Darcy's Velocity: $\boldsymbol{Vd = \frac{L}{T_r}}$ $= \frac{2*10^4}{165.6} = 120.773$ μm/sec.
- Colloidal average Velocity: $\boldsymbol{Vc = \frac{L}{T_r}}$ $= \frac{2*10^4}{159.4} = 125.471$ μm/sec.

  Where:

  L is the micromodel's porous-part length in μm = $2*10^4$ μm

This indicates that spherical particles (10-µm diameter) are transported with faster average velocity than the transporting fluids (water in the porous medium. This supports the previous assumptions and observations mentioned in Chapter 2.

4.1.4 Results and Discussion:

In this experiment, although our data set was not large enough to generalize its results on hundreds of particles flowing simultaneously across the micromodel, it is, however, a sample of particles observed in a steady state situation from several locations. Moreover, despite the inaccuracy involved in these investigations (Particles were tracked by human eyes, which implies high possibilities of losing or confusing the tracks of the particles of interest), they have shown relatively close results in most of the measurements.

Therefore, as the initial stage, an approximate estimation of the average particles residence-time was accurate enough to provide a first indication about the early colloidal breakthroughs attributed to their preferential paths in porous media.

In order to investigate this phenomenon and many other particle-tracing applications, a more detailed set of experiments were conducted to fulfill the needed observations' accuracy and the intended applications of the experiments.

4.2 Particles tracing experiments for tracking trajectories, and visualizing potential preferential flow paths (experiment No. 2 – 5)

4.2.1 Background and Objectives:

The existence of different-velocity areas within the porous media is intrinsic and depends on the porous channels apertures, curvatures, and their interconnections. Therefore, the highly heterogeneous distributions of these properties will cause the velocities in these channels to differ substantially (Malkovsky & Pek, 2009). According to the conservation of energy

principle in a steady state flow, the sum of all forms of energy (kinetic energy[2], potential energy[3], and internal energy) in a fluid along a streamline remains constant all points on that streamline (Batchelor, 2000).

However, according to Bernoulli's principle, which is a direct application of the conservation-of-energy principle in isentropic flows[4], "an increase in the speed of a fluid occurs simultaneously with a decrease in pressure (internal energy), or a decrease in the fluid's potential energy" (Clancy, 1975) Figure (7).

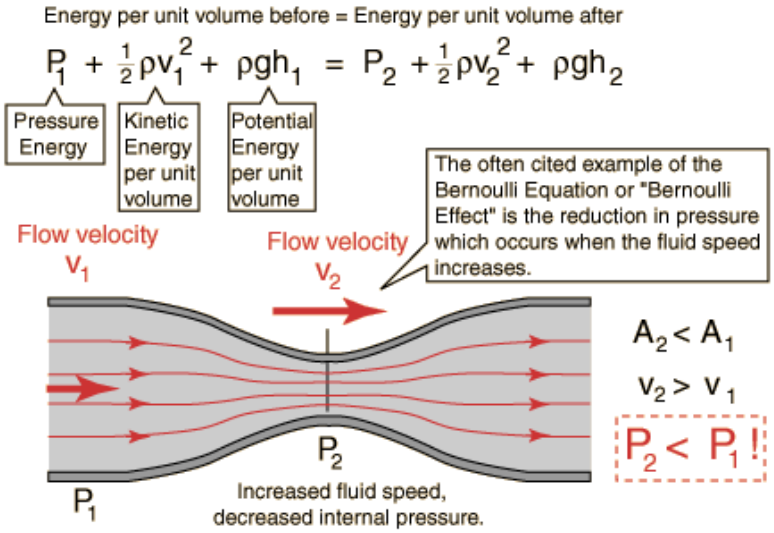

Figure 7: Bernoulli's concept (SCIENCEFORUMS, n.d.)

This implies that in the constant laboratory temperature, a 2D horizontal porous micromodel - with smooth grain boundaries - is considered an isentropic system, if a steady state, laminar, incompressible flow is achieved.

[2] **Kinetic energy** of an object is the energy that it possesses due to its motion. It is the work needed to accelerate a body of a given mass from rest to its stated velocity (Mahesh, 2009).
[3] **Potential energy** of an object is the energy that it processes due to its position relative to other objects, stresses within itself, its electric charge, etc. (Mahesh, 2009)
[4] **Isentropic flow** is both adiabatic (neglects heat transfer), and reversible (neglects friction effect and dissipation effect happen in turbulent flow).

Hence, higher velocities in narrower areas (pore throats) are attributed to energy transformation from internal energy (pressure) to kinetic energy, and vice versa for lower velocities in wider areas (pore spaces).

Whereas, higher velocities in central streamlines across the same pore throat cross-section, is attributed to energy transformation from kinetic energy to potential energy (shear stresses between the laminar flow layers), Figure (8).

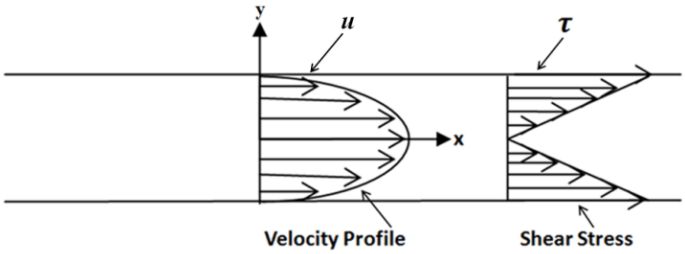

Figure 8: a fully developed velocity profile and shear stress in laminar flow (ResearchGate, n.d.)

In other words, the geometrical heterogeneity of the porous medium explains the different velocities areas along the same laminar flow streamlines. Complex geometries imply a complex spatial distribution of streamlines and complex velocity field at the pore scale. This makes it difficult - by only visualizing the seeding particles in the micromodel - to predict even the single-phase fluid flow behaviour. Darcy's velocities measured or estimated on large scales could not thoroughly explore the fluid flow behaviour. The colloidal preferential paths for example, though it has a significant impact on the overall fluid flow in the porous media, it was not explained by average Darcy's velocity. The latter only indicated such a phenomenon.

Therefore, micro-scale flow investigations - via tracking the particles trajectories - is needed. Moreover, defining the velocity field at the micro-scale was necessary to validate the analytical calculations from the first set of experiments. This is possible by defining the high-velocity particles flow-lines in many areas of interest across the micromodel and use them for the calculation of residence time.

4.2.2 Experiments Description

In this set of experiments, by using the bright field microscopic option (Black and White mode), we observed the particles motion across many areas of interest in the concerned micromodel. We tracked their flow lines (trajectories) by acquiring a sufficient number of image sequences (temporally related images, called stacks, represent a series of images share a single window).

Setting the maximum possible fps (4-6 fps) for the available camera enabled us, by means of the Particle Tracker 2D/3D tool to record the maximum possible number of particle centroids coordinates for each detected particle. Eventually, during a sufficient experimental time in the steady-state conditions, and after implementing proper image processing and analysis procedures, accurate and detailed particles trajectories were attained.

4.2.3 Image Acquisitions Principles and Considerations

The critical issue in this experimental step is the quality of the acquired images. In order to ease the automation of image analysis and avoid any unnecessary steps or challenges posed by the inequality in created images' data, close attention must be paid during image acquisitions. This will considerably improve the quality of the results and decrease the artifacts that might accumulate in successive image processing and analysis procedures.

- **Sufficient spatial resolutions** (the density of pixels or samples in the image) since it can always be down-sampled but never up-sampled. Otherwise, many statistical computations will have a prohibitively high error. Some forms of analysis will not be even possible at all (imagej.net, 2016).

- **Non-Lossy compression image-formats (such as TIFF and PNG)** are recommended when storing the raw acquired images. They preserve the original images' data with the exact pixels values and densities (resolutions). Therefore, they are preferable for precise image analysis as in the case of exact microparticles centroids' coordinates.

- **Lossy compression image-formats (such as JPEGs),** despite their small sizes, they must be avoided. It reduces the size of the original image but at the expense of image quality. They discard valuable image information that causes artifacts considerably affect any image post-processing attempts (imagej.net, 2016) (Rueden & Schindelin, 2017). This would result in images not the same as the original, which makes it inappropriate for our purpose.

- During image acquisition, **even distribution of illumination along the whole field of view**, prevents any reflection artifacts as well as any needed later-corrections for illumination. However, some image processing software can correct for inhomogeneous illumination artifacts. **Background-Subtractor** Plugin in ImageJ2/ Fiji®, for example, implements a robust, histogram-based, rolling-ball algorithm described in (Cardinale, 2008). It is part of MosaicSuite image-processing algorithms in ImageJ2/ Fiji®, developed at MOSAIC Group for fluorescence microscopy, available under Utilities / Mosaic plugin, Figure(9).

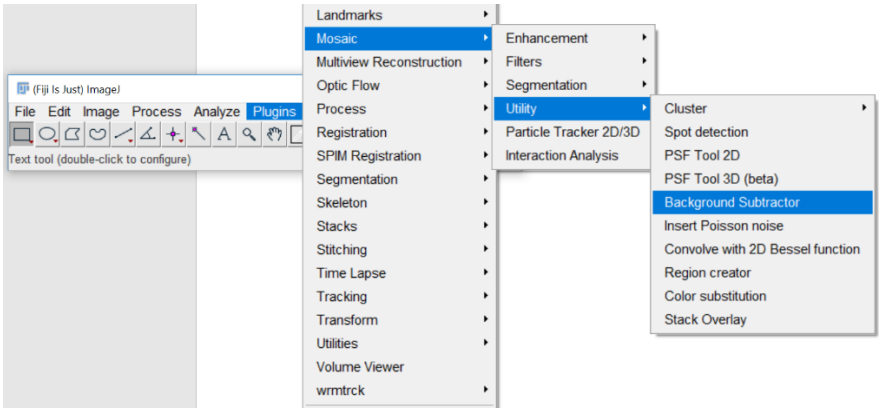

Figure 9 - background Subtractor function in ImageJ2 / Fiji®

Otherwise, Naturalization function under Enhancement option in Mosaic plugin in ImageJ2/Fiji®. It removes the scatter light, noise, and enhance contrast all in one function. The algorithm implemented in this plug-in is described in (Gong & Sbalzarini, November, 2014).

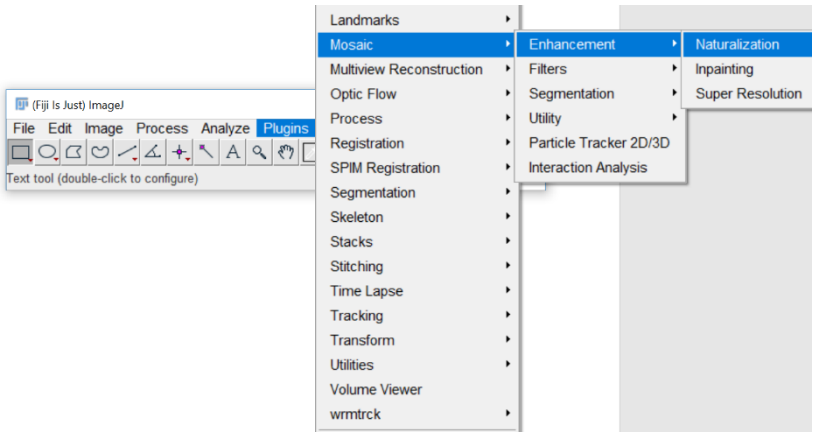

Figure 10 - Naturalization function in ImageJ2 / Fiji®

4.2.4 Image Processing (Principles and Considerations)

In scientific image processing and analysis, a digital image is a regular two-dimensional grid of very fine square elements called pixels, with 1 by1 pixel dimensions. Hence, the number of pixels in X (rows) and Y (columns) directions define the width and the height of the image respectively (Tiago Ferreira, 2012).

In grayscale images (single intensity scale, also called as “Black and White” images), each pixel is presented as a point sample and defined at the vertex points of the grid by a color (grey in this case) intensity value. The intensity values, or as usually called “Pixel values”, are unsigned integers in the range from zero to 255, and represent 256 shades of grey (ranges between black and white). Technically, this unique intensity (brightness) values define the bit depth of the image. A 2-bit image, for example, has $2^2 = 4$ shades (tones) of grey: 00 (black), 01 (grey), 10

(grey), and 11 (white). Whereas, the 4-bit image has $2^4 = 16$ shades ranging from 0000 (black) to 1111 (white) [5], etc.

Regarding bits per pixel (bpp), ImageJ2/Fiji® deals with 8-bit, 16-bit, 32-bit, RGB color[6] types of images, Figure (11). However, only 8-bit is directly displayed on computer monitors, since they can typically show only 256 (= 2^8) shades of grey. Therefore, Black and White 16-bit images and 32-bit images, for instance, which use unsigned integers in the range 0 to 65535 (= 2^{16}), and 0 to 4, 294, 967, 296 (= 2^{32}) respective, they are mapped to 8-bit by windowing the range of grey values (Tiago Ferreira, 2012).

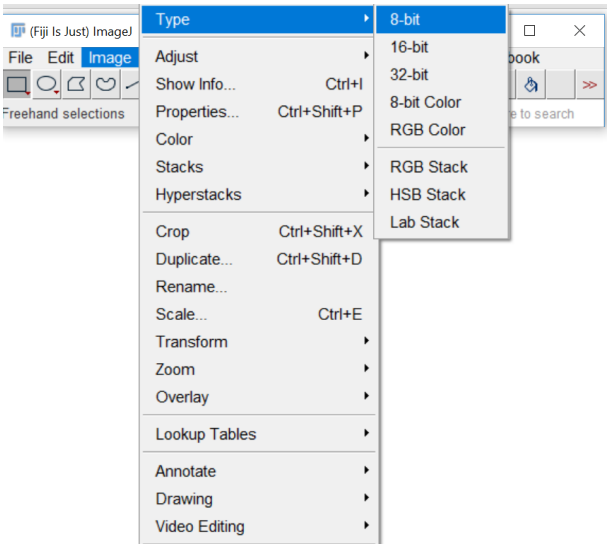

Figure 11 - Image types in ImageJ2/ Fiji®

In this context, many considerations should be taken into account when processing the acquired raw images:

[5] The 16-shades of 4-bit images are: 1) 0000, 2) 0001, 3) 0010, 4) 0100, 5) 1000, 6) 0011, 7) 0101, 8) 1001, 9) 0110, 10) 1010, 11) 1100, 12) 0111, 13) 1011, 14) 1101, 15) 1110, 16) 1111, where 1 is black, 2-15 are grey shades, and 16 is white.

[6] RGB images are coloured images, each pixel contains three sample values (one for each primary colour), also in the range 0 to 255, to represent 256 different shades of the three colours. These are 24-bit ($2^{3 \times 8} = 2^{24}$) images converted to grayscale using the formula Grey = 0.299 red + 0.587 green + 0.114 blue, or the formula Gray = (red + green + blue)/3 if "Unweighted RGB to Grayscale Conversion" is checked in Edit/Options/Conversions in ImageJ2/Fiji®.

- When importing an image sequence in ImageJ-2/Fiji®, we have an option to convert it to 8-bit grayscale. This is highly recommended for particles detection and tracking, if the original sequence is 16-bit, 32-bit, 8-bit color or RGB color images due to high memory consumption of color movies (Levy, 2006).
- **Image Binarization (Segmentation):** in order to define certain image features and objects, we separate them from the background based on their pixels' intensities values. We divide the images into two parts background and features of interest (foreground) with two distinct pixel's values of 0 and 255. To do so, one or two (upper and lower) cut-off values known as thresholds, are set. That is, values below the lower threshold are made black with zero intensity values, while values above the upper threshold are white with 255 intensity values. This would separate the targeted features/objects from the background by their pixel values, figures (12, 13, 14) where the interesting features in Figure 13 are the grain boundaries whereas in figure14 are the aforementioned micro particles.

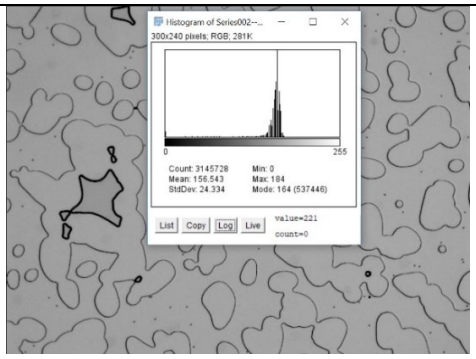

Figure 12 -Original micromodel image with Bright-field illumination option from experiment No.5 and the corresponding intensity Histogram

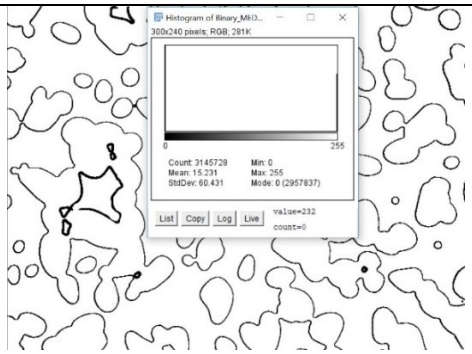

Figure 13 - Binarized micromodel image with Bright-field illumination option from experiment No.5 and the corresponding intensity Histogram

Figure 14 - Binarized Physical-Rock micromodel image with Bright-field illumination option from experiment No.10 and the corresponding intensity Histogram (the objects of interest are the traced micro particles)

- In Manual thresholding (via the menu command Image → Adjust → Threshold), determining a **fixed manual threshold value** and applying it to all the images should be avoided. Although it treats all the images equally to be compared, it will not extract similar features from different images. "This is because there is a certain variability in the images of one single experiment and generally even higher variability between the images of replicated experiments" (magej.net, 2017).

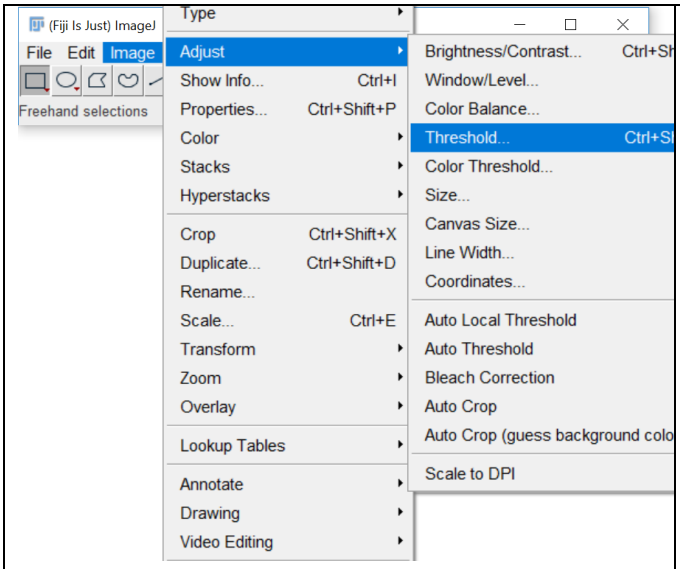

Figure 15 - Thresholding option in ImageJ2 / Fiji®

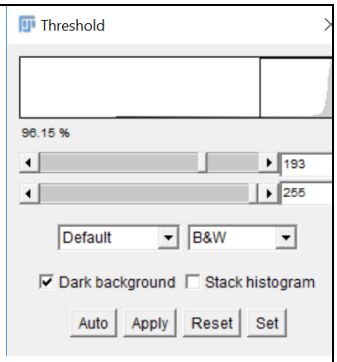

Figure 16 - Thresholding Manual and Automatic options in ImageJ2/ Fiji®

However, manual thresholding should be avoided whenever possible, since it is time-consuming to find an appropriate cut-off value, and most of the time it holds a high user bias and low reproducibility[7]. On the other hand, each automatic thresholding algorithms is appropriate for specific kind of images (image-intrinsic properties). Therefore, applying wise methods for Brightness & Contrast (or any image filters) adjustments, is essential to enhance the features of interest and support the binarization process, but "it may not be feasible to apply the same process to all images" (imagej.net, 2017). In this regard, it is up to the images analyzer to choose the best suitable pre-processing options and methods. A comprehensive description of image binarization principles, the limitations of manual thresholding, and the available automated thresholding methods and their advantages, can be found in (imagej.net, 2017). Additionally, how to manually set a threshold in both Greyscale (Black & White) and Color images is well explained in (imagej.net, 2017), as well as a method

[7] Reproducibility in image binarization methods means that on the same image they will always lead to the same binarization result.

called “Threshold Check”, which is a trial for untrained users to check the quality of the thresholding method, available in (Jan Brocher, 2015).

- Brightness and Contrast option in ImageJ2/Fiji® has the same principle of minimum and maximum intensity cut-off values. Adjusting Brightness and Contrast of an image makes its features and objects more accessible to visualize. Increasing Contrast, for example, make objects in an image more distinguishable.

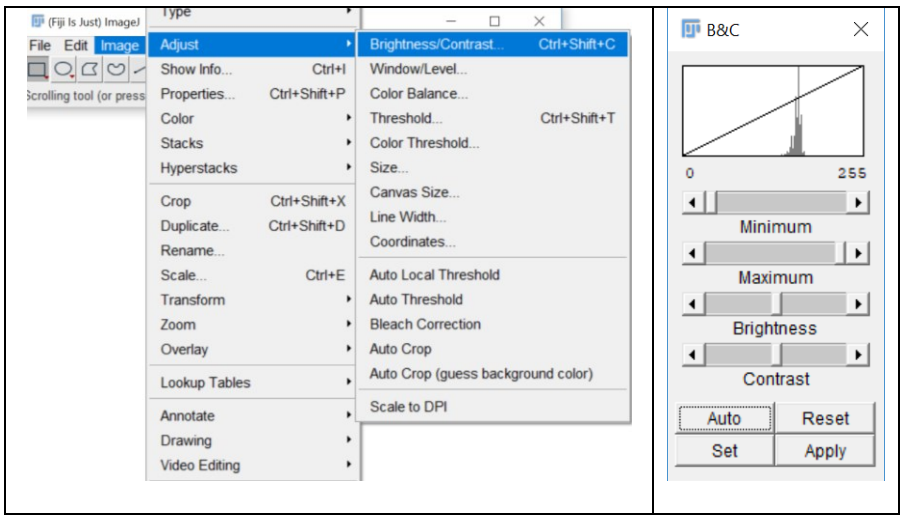

Figure 17 - Brightness and Contrast options in ImageJ2/ Fiji® for an 8-bit image

- Moreover, after being binarized through any thresholding method, many post-processing operations are required based on the purpose of the image processing. Additional binary operations, such as Dilate, Erode, Fill Holes (all under Process → Binary in ImageJ2 /Fiji®), etc., and image combination operation, such as Image Calculator, among many others are subject to the user and the final purpose of the image pre- and post-processing operations. This, alongside many other important considerations in image analysis specifically what concerns Particle Tracker 2D/3D plugin, would be more evident in our experimental cases, where different image acquisition conditions required different processing steps to achieve the best overall results.

4.2.5 Trajectories analysis workflow for Particle-tracing experiments with 10X magnification (experiments No. 2)

In this set of experiments, in order to develop a Particles-Trajectories analysis workflow, we used first a minimal field of view (by using 10X magnification), with an extremely small flow rate (0.005 ml/hour). As a result, relatively large particles were observed moving in a slow motion across many different locations of interest in the micromodel. This was, taking into account the image acquisition principles mentioned before, expected to ease the later implementation of the image processing as well as the particle detection processes via the ImageJ2/ Fiji® plugin; Particle Tracker 2D/3D. Samples of the six acquired TIFF-type image series are shown next:

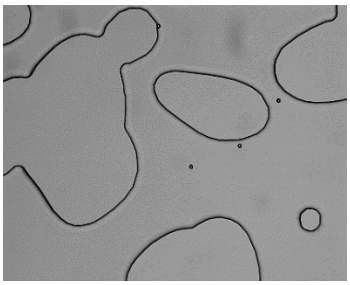

Figure 18 – location-1 in experiment No. 2

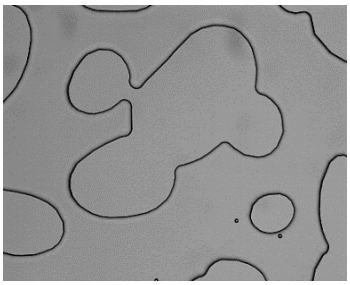

Figure 19 - location-2 in experiment No. 2

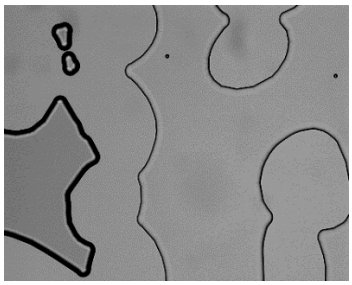

Figure 20 - location-3 in experiment No. 2

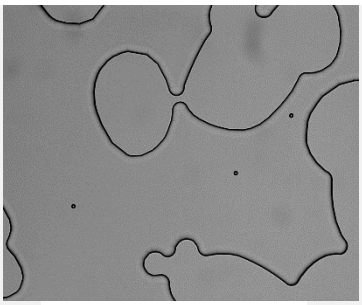

Figure 21 - location-4 in experiment No. 2

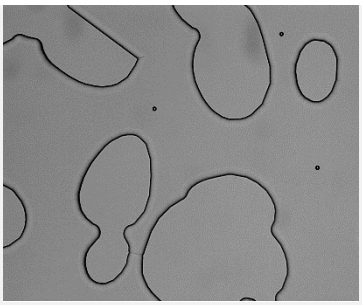

Figure 22 - location-5 in experiment No. 2

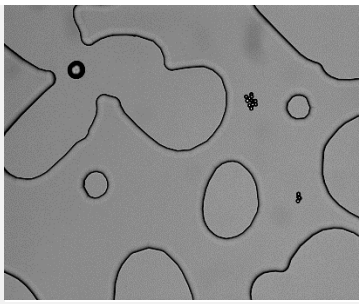

Figure 23 - location-6 in experiment No. 2

The corresponding microscopic image-acquisition settings, which were adjusted on Black and White mode of Bright field illumination with 10x magnification, are shown next:

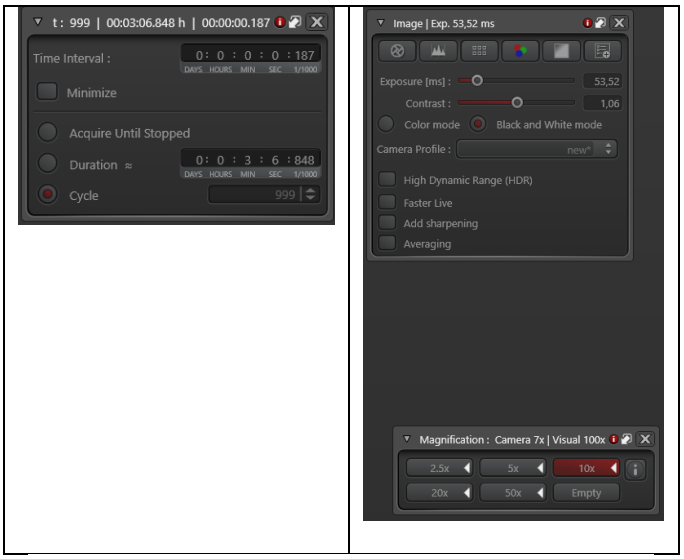

Figure 24 - Image acquisition settings in experiment No. 2

This shows an exposure time of 53.52 milliseconds and a Time interval of 187 milliseconds. In order to implement the particle tracing in ImageJ-2/Fiji ®, we used Particle Tracker 2D/3D Pluginfrom Imagej2/Fiji ®.

Particle Tracker 2D/3D plugin, which implements the feature point detection and tracking algorithm as described in (Sbalzarini & Koumoutsakos, 2005), has been selected in a recent comparative study of many particle-tracking tools as one of the top choices (Chenouard, et al., 2014). It allows visualizing and analyzing the detected particles, as well as previewing their trajectories individually and collectively alike. It saves the exact x, y, and z coordinates with up to three pixel's decimals accuracy, for each particle's centroid within each time frame. Moreover, it discriminates false-particle detections and can handle particles appearance and disappearance from the image region in consecutive time frames.

The key point in particle tracker plugin's proper functionality is the quality of the resulting images after pre- and post-processing, especially the images segmentation process. Due to this, we developed a custom-tailored image processing workflow, which has well suited the acquired digital images in this group of experiments and matched the image processing principles and considerations mentioned earlier in this chapter. The image processing steps and their corresponding results are outlined as the following:

1. Before the plugin can be started, an image sequence, virtual stack, or a movie in ImageJ2/Fiji® must be opened from the file menu (File → Import → Image sequence, TIFF Virtual Stack, or AVI/MPEG for opening a movie file), Figure (25).

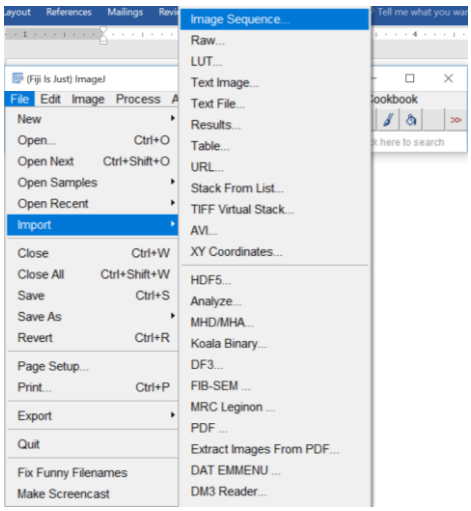

Figure 25 – Importing Image sequences/ AVI videos on Imagej2/Fiji®

2. Convert to 8-bit greyscale format in order to reduce the memory consumption. Then choose the Increment value to define the step between two consecutive images (stack slices if we had imported TIFF Virtual Stack file-type) in the concerned image sequence. This will define the total number of slices (time frames) included in the processing operation. (e.g., an image sequence of 516 images will be reduced to 172 slices if we set the Increment value as 3, figures (26 & 27).

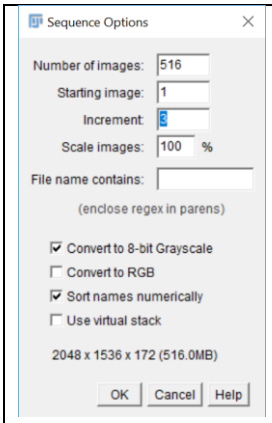

Figure 26 - Convert to 8-bit Grayscale and Increment Options in Imagej2/Fiji®

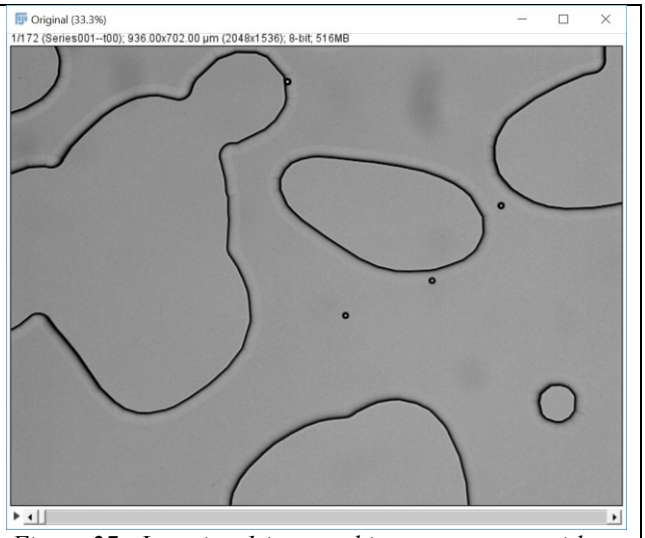

Figure 27 - Location-1 imported image sequence with an Increment of 3, Experiment No. 2

At the upper left corner of figure 27, the number 172 is illustrated. It refers to the total number of slices will be included in the further image processing procedures. Whereas, 516 original images were acquired in experiment No.2, location- 1 as an image-sequence with a 53.52 milliseconds exposure time, and a 187 milliseconds time interval.

3. Subtract the background to eliminate any uneven illumination during image acquisition, and make sure that the field of view is equally lit. From the menu command:
   Process → Subtract Background.

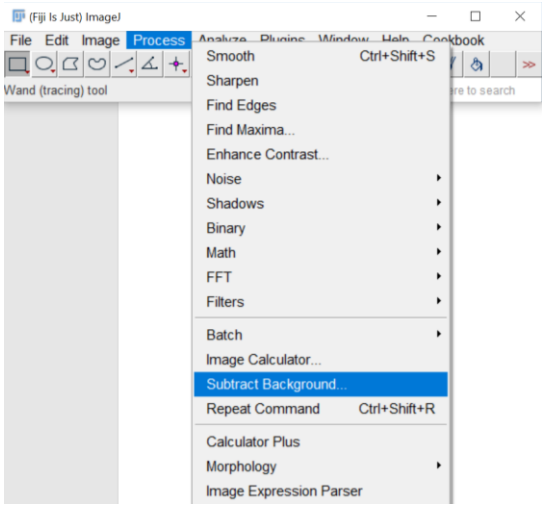

Figure 28 - Subtract Background function in ImageJ2/Fiji®

The corresponding options and results are shown next.

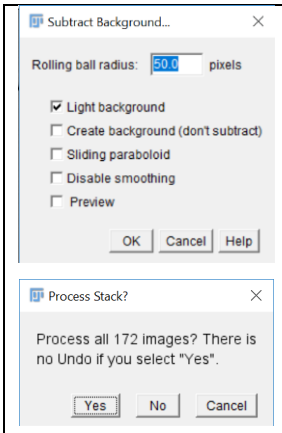

Figure 29 - Background Subtraction options in ImageJ2/Fiji®

Figure 30 – Background Subtracted of a location-1 image sequence with an Increment of 3, experiment No. 2

4. Extract the moving objects (particles) out of the constant background. This is done by first extracting the background, and secondly subtracting it from the concerned image sequence. This is done with the command sequence:
   Image → Stacks → Z-Project → Median. In statistics, "Median" is the middle number in a sorted data set. Therefore, it minimizes the influence of outliers, which are the moving particles in our case, since they have relatively small intensity values

(almost 90 in this set of experiments) compared to the background, which has almost 240-250 intensity values after applying the background subtraction function:

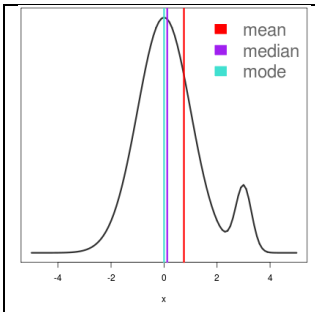

Figure 31 - Mean, Median and Mode concepts in statistics (source www.r-bloggers.com)

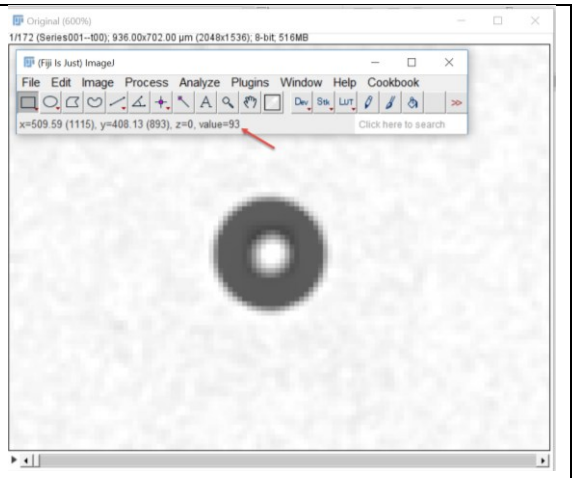

Figure 32 – Particles' low intensity value of 93 in experiment No. 2

Therefore, for 172 slices in this image sequence, a particle represented with distinct intensity-value pixels, will form an outlier when it passes across the field of view during the time of experiment. The faster the particle moves, or the larger the number of image slices to be processed; the less the influence of particles intensity on the overall Median result would be. This will result in a single slice with only static objects exist in the scene. This includes strained particles in pore throats, or attached to grain surfaces, Figures (24 & 25).

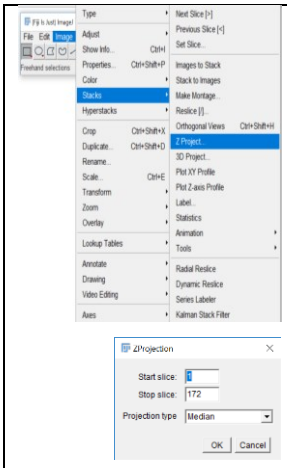

Figure 24 – Z Project options in ImageJ2/Fiji®

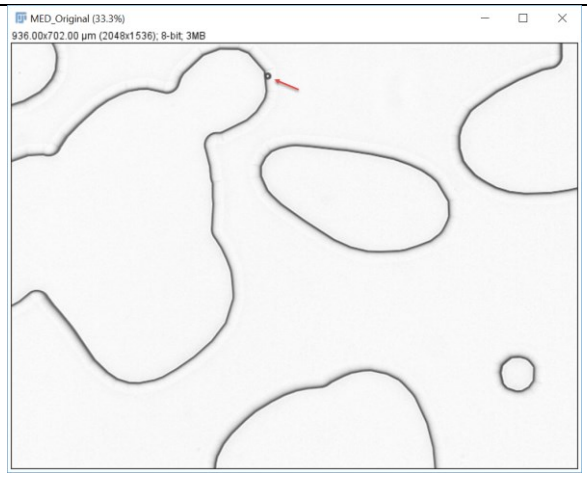

Figure 25 – The Median Z-Projected of a location-1 image sequence with an Increment of 3, Experiment No. 2

By subtracting the resulting Median Z-projected image from the source image sequence, a new image sequence, with only flowing particle in an empty black space, will outcome. This is done from the menu command:

Process → Image Calculator, then by setting **Difference** in the dialog window as shown in figures (33 & 34).

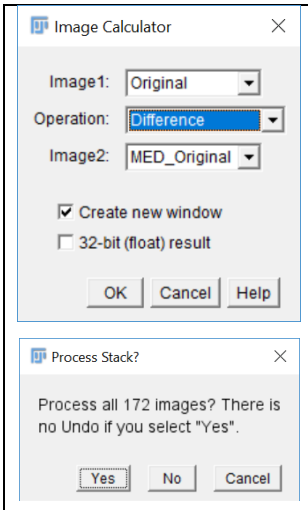

Figure 33- Image Calculator options in ImageJ2/Fiji®

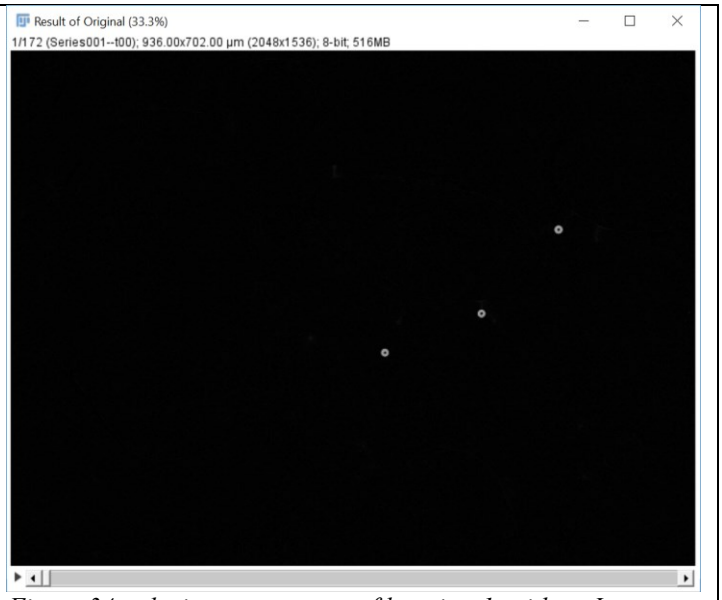

Figure 34 – the image sequence of location-1, with an Increment of 3, after subtracting the Median Z-projected image, experiment No. 2

Important to mention here that both; the image sequence (named as Original in this case), and the Median Z-projected image (named as MED_Original) must be opened with ImageJ2/Fiji® before we implement the previous command. Otherwise, they do not appear in the options of the drop-down lists; Image1, and Image2 in the Image Calculator dialog window. Moreover, the image sequence (Original) must be set as the Image1, whereas the Median Z-projected image (MED_Original) must be set as Image2.

5. However, the intensity histogram (or the intensities list) of the last results shows that most of the pixels' values are of small values, but not fully binarized, **Error! Reference source not found.**.

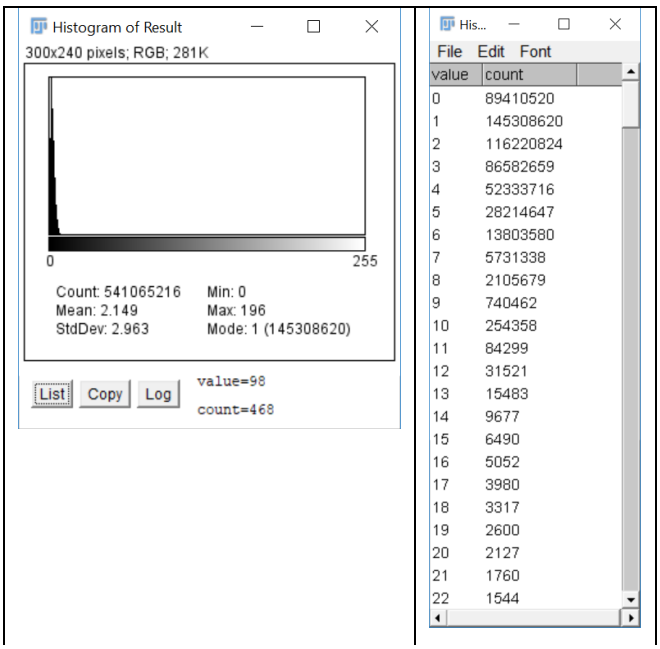

Figure 35 - Intensity Histogram and Intensity list for the image sequence of location-1, with an Increment of 3, after subtracting the Medain Z-projected image, experiment No. 2

To do so, and in order to be able to use Particle Tracker 2D/3D plugin, we should completely separate the flowing particles from the background by applying an appropriate image segmentation (binarization) method. This can be done by several ways, such as adjusting the brightness and contrast; and after that, by making binary.
From the menu command: **Image → Adjust → Brightness/contrast,** and increasing the contrast until we reach the values illustrated in the corresponding results in the figure (36):

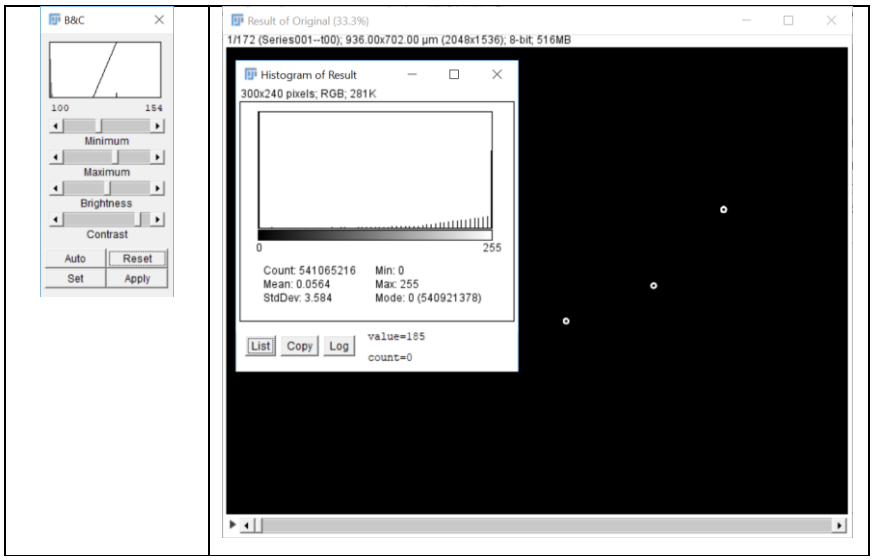

Figure 36 - Brightness and Contrast settings for experiment No. 2 and the corresponding results

Adjusting the contrast allows to increase the minimum intensity threshold and decrease the maximum intensity threshold simultaneously. This gives better results in a shorter time than the manual thresholding, where the minimum and the maximum thresholds

values are set individually, which implies more number of tries and hence, more user bias. Finally, making binary via the following command sequence:
Process → Binary → Make Binary, then **Process → Binary → Fill holes.**
The corresponding settings and results are outlined next:

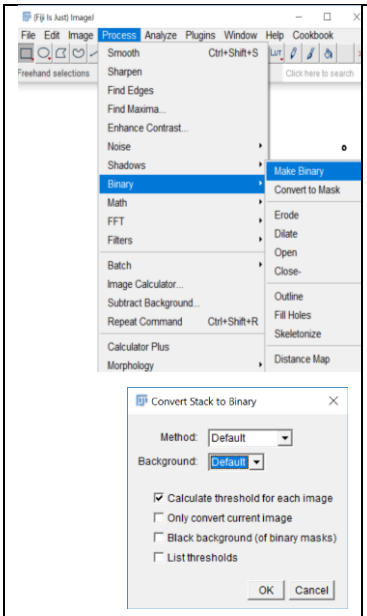

Figure 37 - Make Binary function and settings in ImageJ2/Fiji®

Figure 38 - Make Binary results and the corresponding intensity histogram for the image sequence of location-1, with an Increment of 3, after subtracting the Medain Z-projected image and adjusting contrast, experiment No. 2

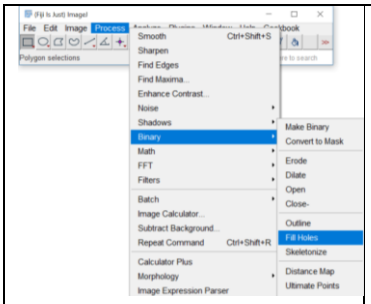

Figure 39 - Fill Holes function in ImageJ2/ Fiji®

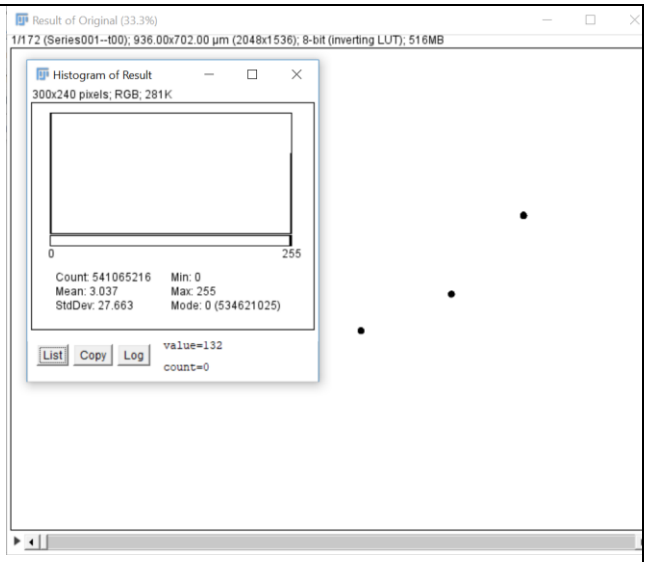

Figure 40 – Fill Holes results and the corresponding intensity histogram for the image sequence of location-1, with an Increment of 3, after subtracting the Medain Z-projected image, adjusting contrast, and making binary, experiment No. 2

6. Up to this level, pre- and post-processing stages were successfully achieved. Further Particles detections and trajectories analysis will require a few additional steps.

   First, we launch the Particle Tracker 2D/3D from the **Plugins menu → Mosaic → Particle Tracker 2D/3D.** A dialog window will pop up and ask if these are 3D data. In our case we are dealing with 2D micromodels. Therefore, we set "No", figure (41).

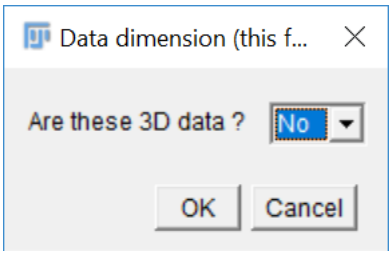

Figure 41 - Particle Tracker 2D/3D toggling window

7. Next, we set the proper settings for this plugin:

   - **Radius**: Approximate radius of the particles in the images in units of pixels. In order to know this value we first measure approximately the particles diameters by zooming in to a particle and using the straight line tool in the tools bar in ImageJ2/Fiji®, and then **Analyze → Measure** (or by pressing **M key** as a keyboard shortcut).

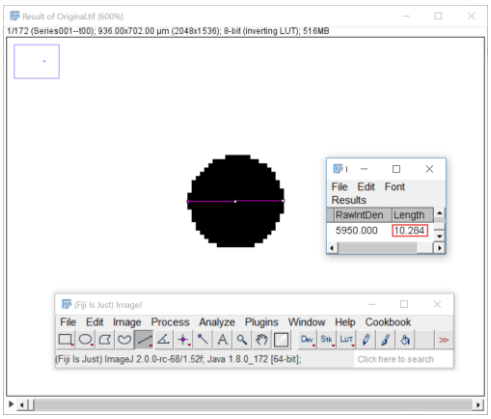

Figure 42 – Measuring particle's diameter by using the "straight line tool" in ImageJ2/Fiji®

This shows a 10.284 particle's diameter.

The units of measurements are set from the Image → Properties command, which calls a dialog window showing the Pixel to the chosen unit-of-measurement conversion factor, Figure (43).

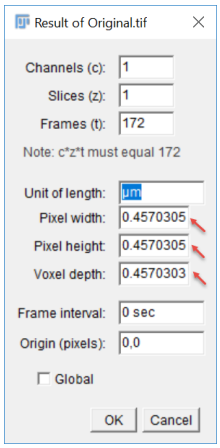

Figure 43 - Image properties dialog window in ImageJ2/Fiji

This means that the previous particle diameter measurement was in **µm.** Therefore, in order to find out the approximate particle radius in the pixel, we use the conversion formula:

$$\boldsymbol{Particle's\ Radius\ in\ Pixel} = \frac{\boldsymbol{Particle's\ Diameter\ in\ the\ unit\ of\ measurement}}{\boldsymbol{2 * Pixel\ width\ (or\ Pixel\ height)}}$$

That is;

$$\boldsymbol{Particle's\ Radius\ in\ Pixel} = \frac{\boldsymbol{10.284}}{\boldsymbol{2 * 0.4570305}} = \boldsymbol{11.25089\ pixel}$$

Thus, the Radius in our case must be set to 12 µm. "The value should be slightly larger than the visible particle radius, but smaller than the smallest inter-particle separation" (MOSAIC Group, 2006).

- **Cut-off:** The score cut-off for the non-particle discrimination. The higher the number in the cut-off field the more suspicious the algorithm is of false particles (MOSAIC Group, 2006)**.**
  In our case, we set it on a small value **0.0001** since our particles are all of a regular spherical shape and precisely same size.
- **Percentile (r):** It determines which bright pixels are accepted as points. The higher this number is, the brighter spots will be considered by the algorithm as detected particles. "All local maxima in the upper (r) percentile of the image intensity distribution are considered candidate points" **(MOSAIC Group, 2006)**. For that, we will keep the default value Per/abs = 0.5; given that the absolute checkbox (abs) is unchecked. In order to evaluate these parameters, the plugin offers an option to preview the detected particles before it implements the second part of the Particle Tracker 2D/3D algorithm, namely the particle linking and particle trajectories analysis algorithm. If the set parameters are correct and accurate, red circles will surround exactly the circumference of the detected particles. Otherwise, we should readjust the particles radius, Cut-off value and Percentile value Figure (45).

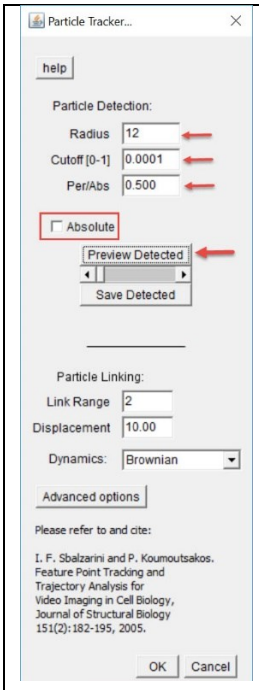

Figure 44 - Particle Tracker 2D/3D parameters for experiment No. 2

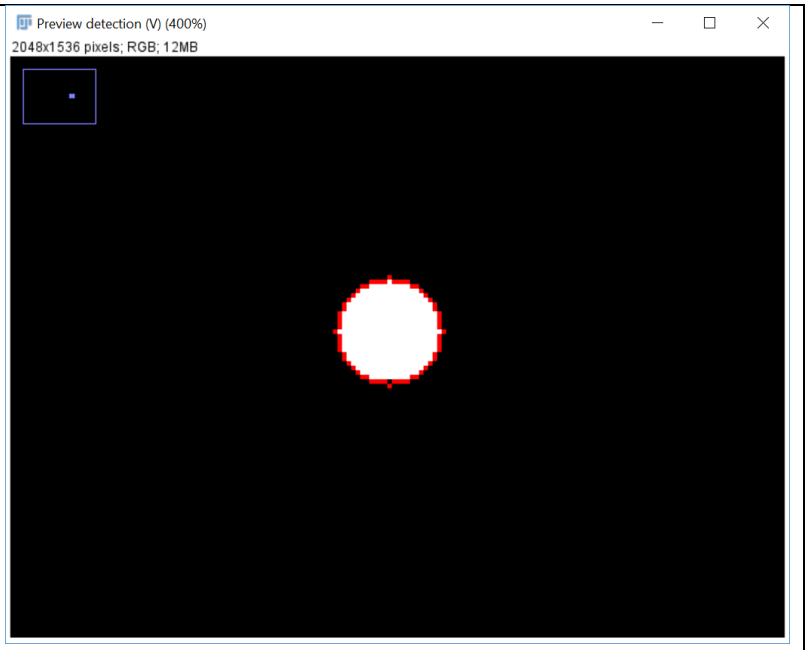

Figure 45 - Previewing the detected particles by Particle Tracker 2D/3D

Now, as long as the Preview detected accurately **all and only** the moving objects (particles) we are tracing, the second part of Particle Tracker 2D/3D is expected to give accurate results.

Particle linking dialog has the following parameters to adjust:

- **Link range**: it defines "the number of subsequent frames that are taken into account to determine the optimal correspondence matching" (MOSAIC Group, 2006). It is best to keep it on the default value = 2.
- **Displacement:** it defines the maximum distance in Pixels a particle can cross between two succeeding frames **(MOSAIC Group, 2006)**. This is very important especially when a large number of particles are traced to a small area (high particles concentration). The algorithm in such a case might mix up which particle is which in two consecutive frames. Due to that, we should have a global look of the field of view within all the time frames to get an excellent approximation of the maximum distance in pixels; the fastest particle can cross between any two subsequent frames. In our case, we used the straight-line tool to measure the potential maximum distance and converted it to the pixel. The corresponding **Displacement** value was approximately **40 pixels**, but we set it to **50 pixels** since only few particles were moving in the field of view and the possibility of mismatching them is almost zero. Hence, a larger value of maximum displacement would increase the quality of the results in case we underestimated this value by any chance.
- **Dynamics:** 3 different options do exist here: Straight lines; Constant Velocity; and Brownian. In fact, this is to define the shape of the connecting line between each two subsequent particle coordinates. It is up to the user how he considers the flow during the time interval between two consecutive detected particles' coordinates. This is more important to fill the gabs when a particle disappears in some frames. In our case since we are using a very slow flow rate of 0.005 ml/hour, We will go for Brownian which is more likely to influence the particles flow behavior in slow motions.
- After setting all parameters, we can start tracking by clicking the OK button in the dialog window; Progress information will be displayed in the main ImageJ2/Fiji® status Bar, Figure (46 & 47).

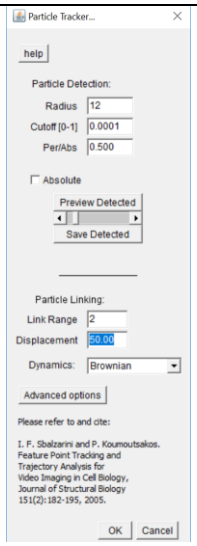

Figure 46 - Particle Tracker 2D/3D parameters for location -1, experiment No. 2

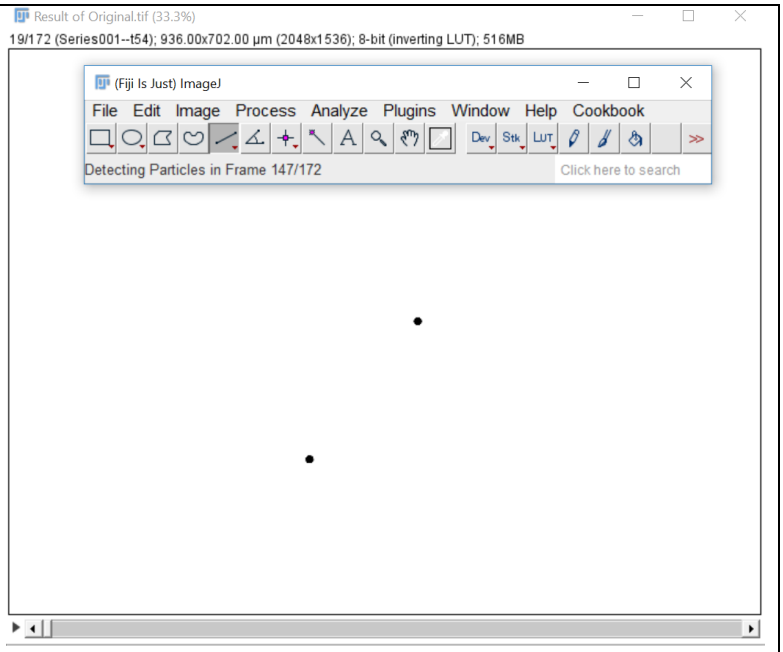

Figure 47 - Particle Tracker 2D/3D during linking particles trajectories in frame 147 / 172 of Location -1, experiment No. 2

8. After completing the particle tracking, the Results window will be displayed with a panel in the middle telling the total number of detected trajectories. More importantly, and to visualize these trajectories, a "**Visualize All Trajectories**" button must be clicked to display the results. However, a black background will appear which hardly could show the trajectories development with time, Figure (48 & 49).

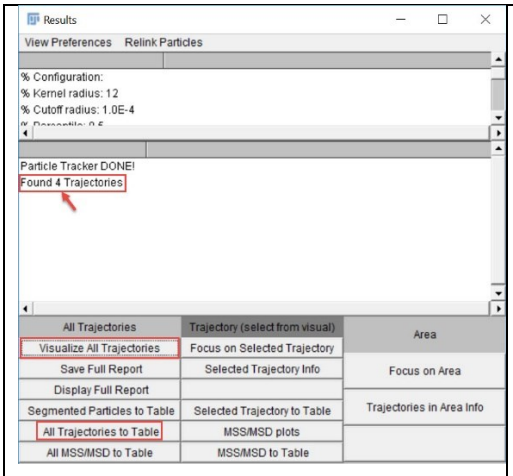

Figure 48 - Results Window of Particle Tracker 2D/3D plugin

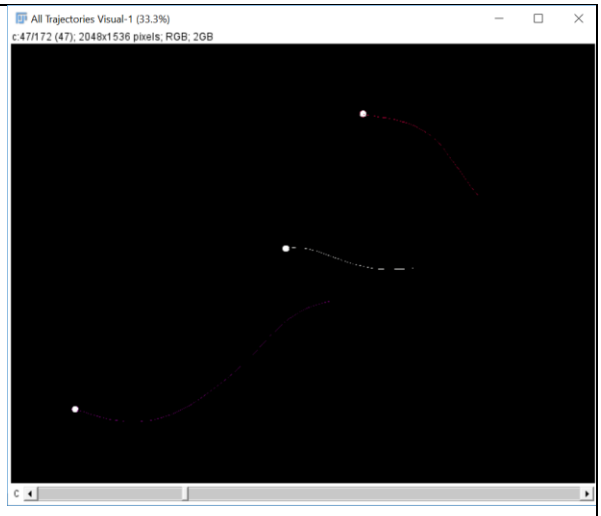

Figure 49 - Trajectories Visualization of Location -1, Experiment No. 2

Therefore, for better visualizations, we do some extra image processing steps on the complete results image stack (called from now on as hyper-stack).

- **Image → Duplicate →** and check the **Duplicate hyper-stack** box.
- **Image → type → 8-bit** (since the resulting hyper-stack is of RGB image type to highlight each trajectory was detected and tracked).
- **Edit → invert** (to display grayscale trajectories on white background).

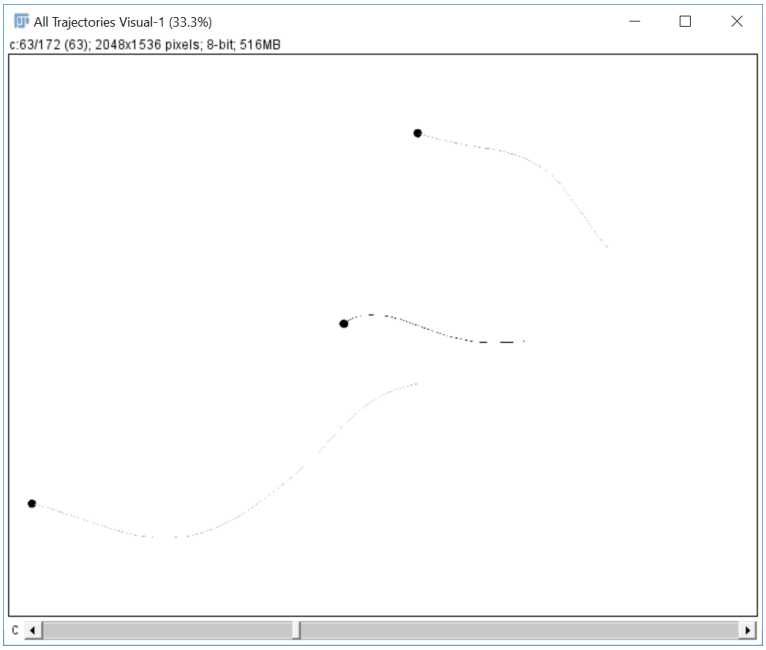

Figure 50 - Trajectories Visualization of Location -1, experiment No. 2, after inversion and convert to 8-bit type

In order to achieve clearer and thicker trajectories; and overlay them on the original background (the micromodel), few more steps were required:

- **Image → adjust → brightness/Contrast** (to threshold the hyper-stack and gain the best binary results). Figure 51 shows the setting for minimum and maximum intensity values being 254, 255 respectively**. This is another way for making binary.**

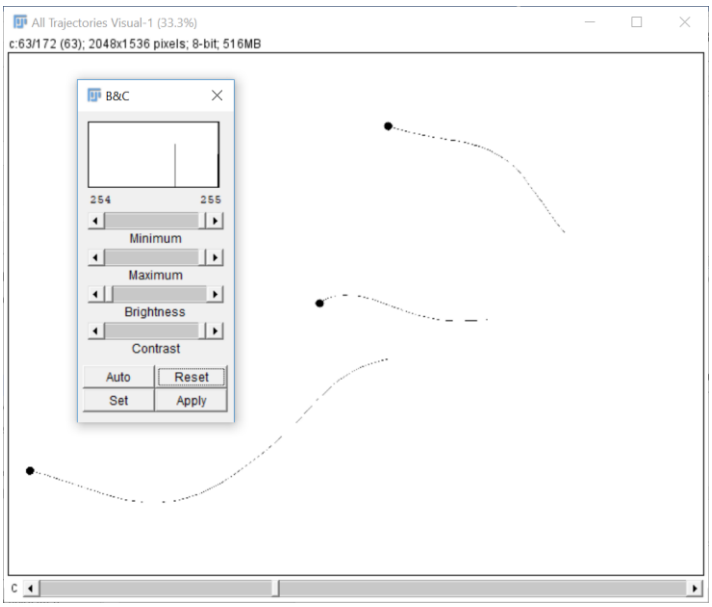

Figure 51 - Trajectories Visualization of Location -1, experiment No. 2, after inversion, convert to 8-bit type, and binarization

- Last, from **Process → Binary → dilate** (to thicken the trajectories), Figure 52.

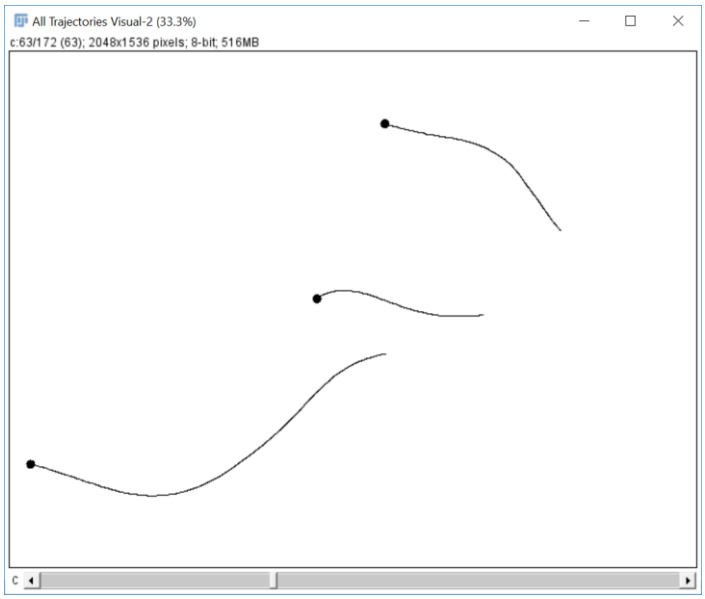

Figure 52 - Trajectories Visualization of Location -1, experiment No. 2, after inversion, convert to 8-bit type, binarization and dilation

However, showing these trajectories in their original environment would make these results more meaningful. To do so, we open the first image in this image sequence (named in our case as "Series001-t00.tif"), without closing the last results window (named in our case as "All Trajectories Visual 2"). Next, from the command sequence, **Process → Image Calculator → Operation AND.** As illustrated in figure (53 & 54), Image1 must be the hyper-stack "All Trajectories Visual 2", whereas Image2 must be

the first image in the original image sequence. Hence, a new hyper-stack will appear with a sliding bar to progressively observe the trajectories of particles inside our micromodel, with the advantage of having both ends of each trajectory constantly displayed.

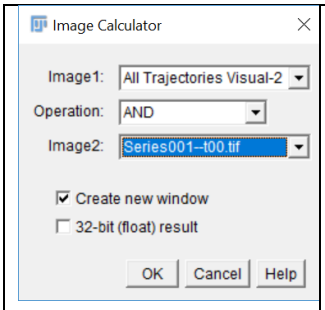

Figure 53 – AND function in ImageJ2/Fiji® and the respective settings

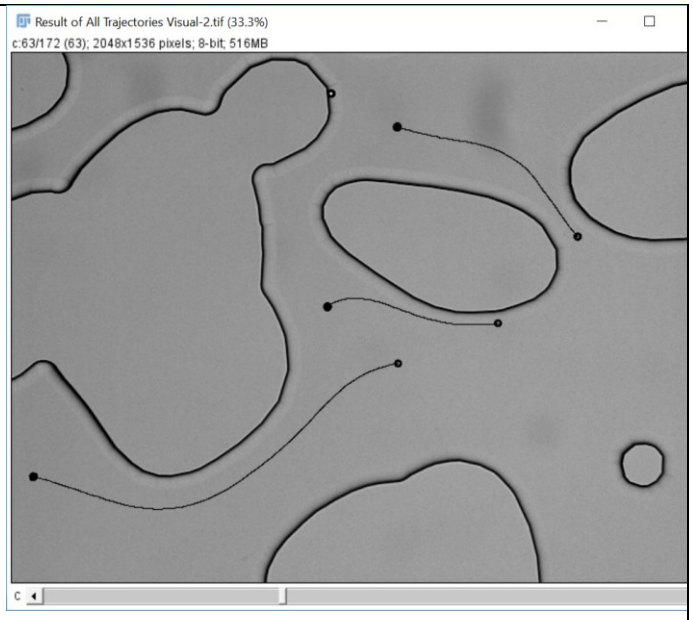

Figure 54 - Trajectories Visualization of Location -1, experiment No. 2, after inversion, convert to 8-bit type, binarization, dilation and Image calculating (via AND function) against first original image in the sequence.

Finally, we applied the exact Image processing settings and command sequence on the rest of the field of the views in experiment No. 2 namely; Location 2, 3, 4, 5, and 6.

As expected, no problems were faced in any of them except at location-6. In fact, this image sequence was intentionally acquired to witness the particles agglomeration phenomenon. Even if it was successfully traced, it will be not interpreted later in this study, since it is out of our research scope. Figure (55, 56, 57, 58) outline the final results:

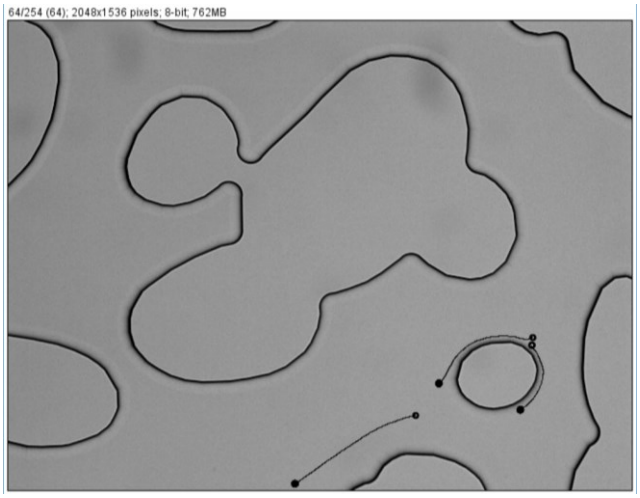

Figure 55: Trajectories Visualization of Location -2, experiment No. 2

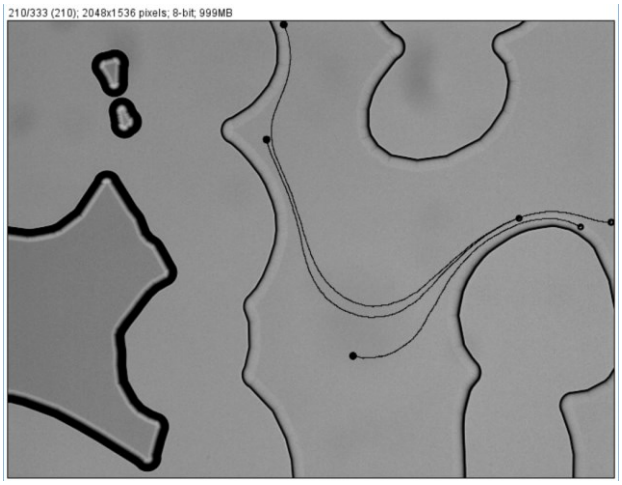

Figure 56: Trajectories Visualization of Location -3, experiment No. 2

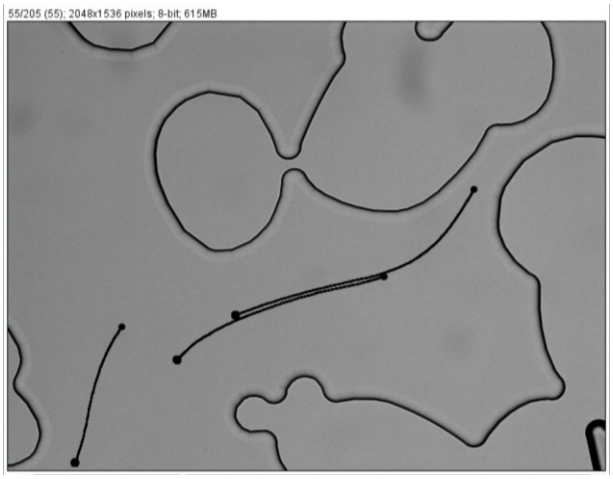

Figure 57: Trajectories Visualization of Location -4, experiment No. 2

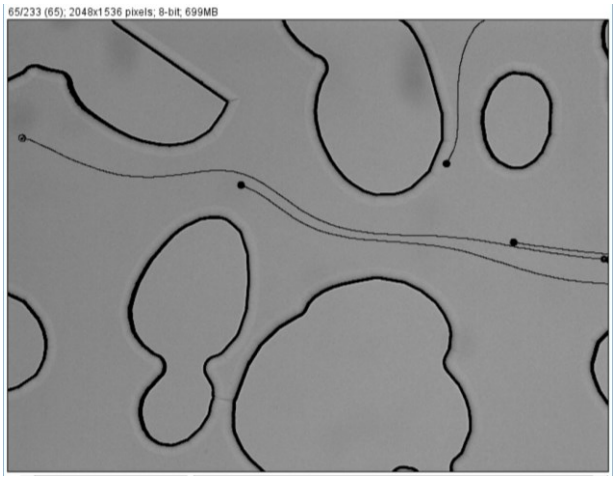

Figure 58: Trajectories Visualization of Location -5, experiment No. 2

4.2.6 Trajectories analysis workflow for Particle-tracing experiments with 5X magnification (experiments No. 3 and 4).

In order to validate the image processing workflow, which we developed for experiment No. 2, we tried to apply it on different experimental settings. This includes the injection flow rate and the field of view.

4.2.6.1 Experiment No. 3

In this experiment, we used the same flow rate (0.005 ml/Hour) as in experiment No.2, but on a larger field of view (5X magnification). Applying the same eight steps for trajectories analysis workflow, with similar settings except for the **µm** to **pixel** conversion factor and the Displacement parameter in Particle Tracker 2D/3D plugin. This is because particles and all other features have smaller sizes in the acquired images with the 5x magnification. This means that the same features are occupying less number of pixels in the new images. This is more evident in the image → properties command, which showed a new pixel width and height, figure (59).

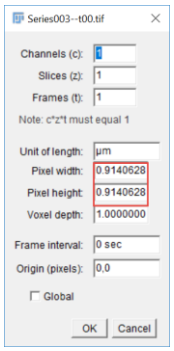

Figure 59: experiment No. 3 images properties

The corresponding results show the particles trajectories as following:

Figure 60: experiment No. 3 particles trajectories analysis

4.2.6.2 Experiment No. 4

For the first time in these experiments, we used a relatively high flow rate (0.02 ml/Hour). Combined with the same 5x magnification, a much faster particles' flow movement in the micromodel was observed. However, this was a manageable challenge with a camera of 4 fps, since all the particles had no blurring appearance even in the highest velocity areas of the micromodel. Therefore, we applied the same image processing procedures as before. The final particle trajectories analysis results were as in the figure next

Figure 61: experiment No. 4 particles trajectories analysis

4.2.7 Trajectories analysis workflow for Particle-tracing experiments with 2.5X magnification (experiments No. 5)

Global observation of the particle flow behavior was the ultimate goal in this experiment. The largest field of view with 2.5x magnification allowed, after implementing a proper trajectory analysis, to visually observe the particles preferential flow paths.

Interestingly, the same image processing and analysis workflow led to almost perfect results. Only minor artifacts were found at some parts of the microstructure. This was not contrary to expectations since much smaller particles (regarding the number of pixels each occupies in this large field of view), with much less intensity contrast were traced. Additionally, we injected a high particles concentration with the maximum flow rate that we could achieve without any blurring particles appeared (0.05 ml/Hour). The figure (62) shows the trajectories analysis results with inevitable artifacts (highlighted inside the red rectangles) resulted from the different experimental circumstance and dimensional settings.

"It is certainly a goal of digital image processing to establish protocols that eliminate variability, but currently a lofty goal. Even the most diligent of efforts to replicate circumstances generally fail to produce sets of images that can be thresholded with one fixed value" (imagej.net, 2017).

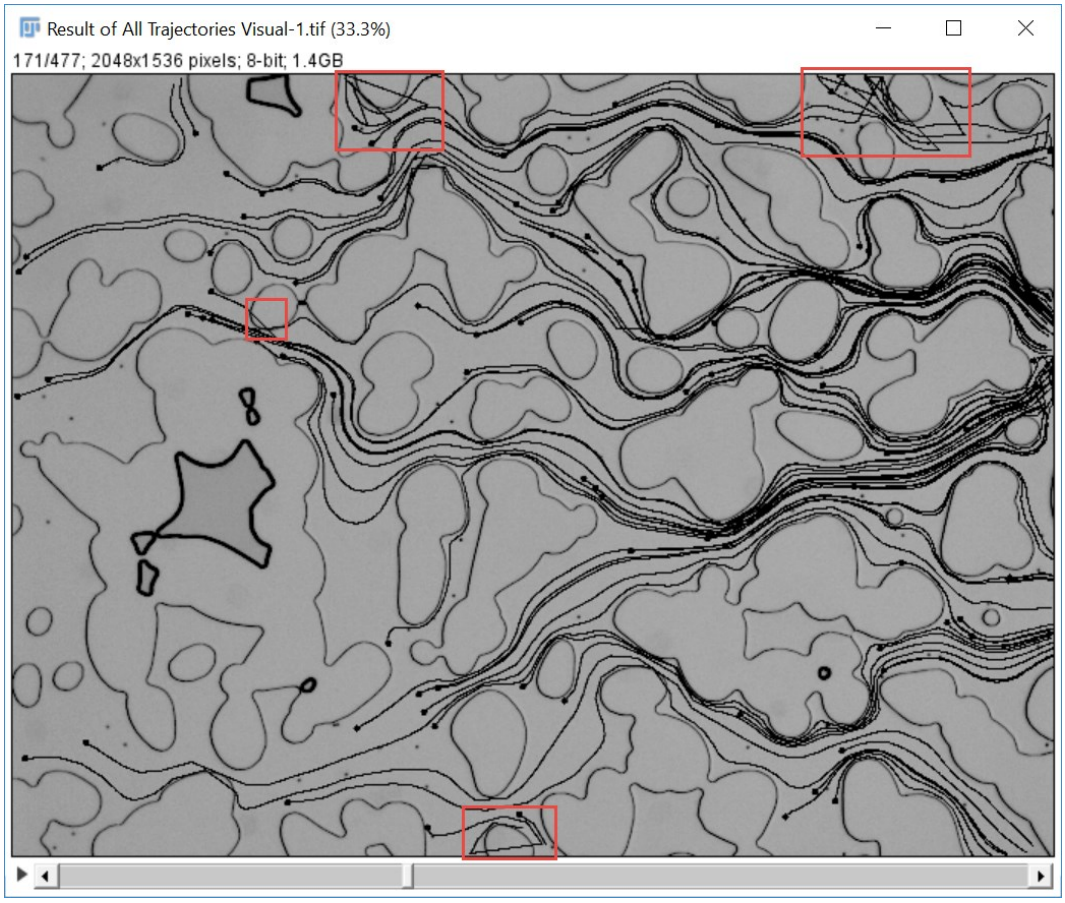

Figure 62: experiment No. 5 particle trajectories analysis

4.2.8 Fluorescent Particles trajectories (experiment No. 6)

"If intensity is the parameter which directly relates to the spatial characteristics of the objects, as often the case in fluorescence microscopy, a simple threshold would lead to satisfying results" (imagej.net, 2017). Fluorescence-based images will positively influence the features extraction by thresholding. Moreover, the quality of a µPIV is significantly improved by fluorescence imaging (Lindken, et al., 2009).

In our case, we used the fluorescence option in a new experiment with 5x magnification and a very small flow rate of 0.005 ml/hour in order to develop a trajectory analysis protocol for this new option (Experiment No. 6)

We acquired a sequence of images with the maximum fps we could achieve (25 fps). This was by a test camera, Zyla sCMOS camera, from ANDOR co., which we had for testing for only 3 days.

The high-intensity contrast between the fluorescent particles and the surrounding allowed the simplicity of trajectory analysis for this experiment without any need to preprocessing procedures or special plugins. Figure (6) illustrates the robust and secure method we used by the following command sequence on ImageJ2/Fiji®.

Image → Stacks → Z Project → Projection type: set to **Max Intensity**

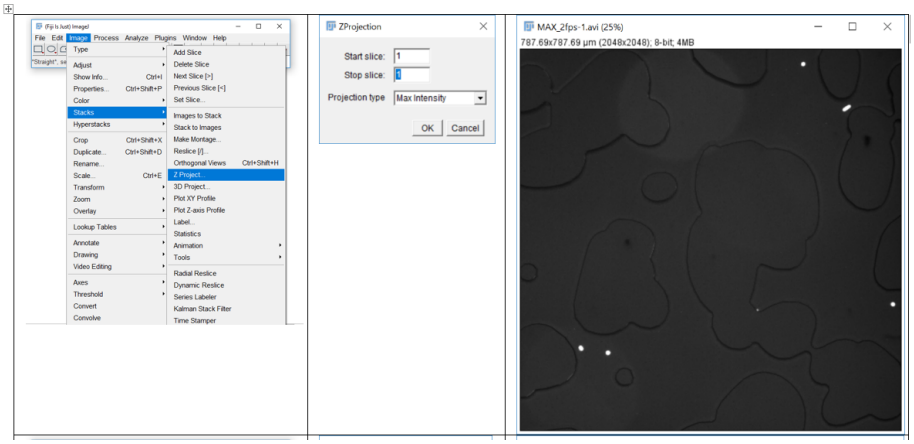

Figure 63- Trajectory analysis for fluorescent images from experiment No. 6

By increasing the number of slices to the maximum, the whole trajectory will be defined and visualized, Figure 64:

Figure 64 – Trajectories analysis from experiment No. 6

Also, for velocity calculation, since the distance between two steps is directly related to the velocity, then a function called **Grouped Z project,** will be useful to measure the velocity.

From the command sequence: **Image → Stacks → tools → Grouped Z project → Projection Method → Max Intensity**

By Z-projecting each two consecutive images, the length of the resulted strides will be a direct indication of the velocity. By measuring the total intensity value for each of them and subtract the total intensity value for one particle, the result will be the total intensity value of the crossed distance during a time step for each particle. Then by dividing by the time step, the velocity would be calculated. However, this method needs a development to be feasible in any future work.

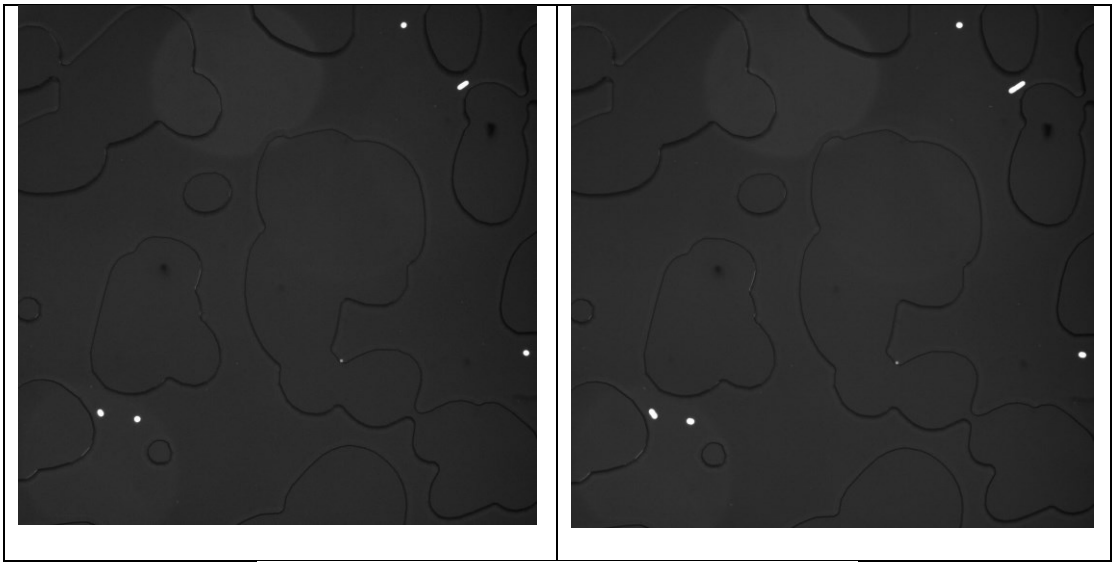

Figure 65- flow Velocity analysis for fluorescent images

4.2.9 Results and discussion

The outcomes of particles trajectories analysis by using Particle Tracker 2D/3D plugin from ImageJ2/Fiji®, showed many advantages such as the accurate tabular particles coordinates resulted when correct settings were adjusted for both image processing and Particle Tracker 2D/3D. In addition, the clear visualization of particles trajectories, even on the largest field of view, allowed the meaningful definition of particles preferential paths on a large scale of the micromodel.

However, trajectories visualizations are not enough to adequately describe the fluid flow behaviour in porous media, especially that these trajectories, if no extra time-consuming image processing steps were implemented, they disappear from the time slices when the concerned traced particle leaves the image boundaries. On the other hand, trajectory analysis combined with instantaneous velocity calculations (at each detected-particle coordinates) would provide a substantial exploration and explanation of fluids behaviour, and thus, serve much more applications of particles tracing experiments in porous media. Accurate measurements of particles breakthrough times, for example, would be possible with particles velocities calculations, especially if it is automatically computed for hundreds of particles passing across the micromodel simultaneously.

To do so, the output table of particle tracker 2D/3D plugin, which offers ultimately precise coordinates of detailed trajectories, with up to three-pixel decimal accuracy, would be a very handy tool for accurate interstitial velocity calculations.

Chapter 5

Velocity and flow paths analysis

Digital images are, as mentioned in the last chapter, represented with 2-dimensional regular grids. They consisted of 1-by-1 pixel elements and sampled with different intensity values at the grid vertices. Therefore, they form a perfect raw material for many applications by matrix-based programming language MATLAB®. The average and Instantaneous Interstitial Velocity calculations, for instance, would be possible in our case, if a sort of combination between Particle Tracker 2D/3D plugin, among many others in ImageJ2/Fiji®, and MATLAB®.

The output tables of the latter provide many information options about the detected particles and their trajectories. The "Display Full Report" option, for instance, provides detailed information about the number of detected particles and their exact locations in each frame. Accurate values with six-pixel decimals refer to the particles centroids coordinates in 2D dimensions (or 3D). This is illustrated in the figure next under the name "per frame information."

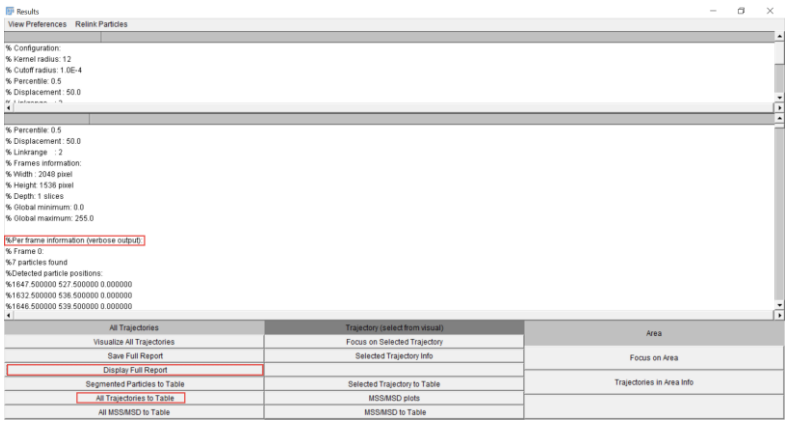

Figure 66: Particle Tracker 2D/3D results window

More interesting for trajectories analysis, is the output table of the linking part of **Particle Tracker 2D/3D** plugin. By calling "**All Trajectories to Table**" option in the Results above

window, a table of all trajectories will appear. These trajectories were generated by linking each detected particle with what is believed to be its counterpart in each time frame. Even in the case, a particle disappeared from some frames; the linking algorithm will perform an interpolation function to correlate the last detected coordinates with the next detection and fill these detection gabs. This all depends on the important **Displacement** parameter, which considers the maximum estimated distance (in pixel), which any particle can move between two consecutive frames. If we underestimate this distance, a particle will disappear in some frames. This issue was witnessed in many cases and will be mentioned later.

By default, in the **All Trajectories** output table, the 1st column indicates the trajectory number, the 2nd column indicates the frame number starting at zero for each trajectory, whereas the 3rd, the 4th, and the 5th define the X, Y, and Z coordinates of the corresponding particle centroid along the whole trajectory, respectively[8] Figure 67. "A trajectory will have at least two rows, each row represents a frame in this trajectory and holds the information about the particle related to this trajectory in that frame" (MOSAIC Group, 2006).

Results

File Edit Font Results

Trajectory	Frame	x	y	z	m0	m1	m2	m3	m4	NPscore
1	0	1640.922	532.754	0	359.104	7.768	66.704	607.171	5747.648	0.333
1	1	1627.407	517.265	0	364.760	7.827	67.588	617.875	5868.503	0.333
1	2	1613.069	500.031	0	355.369	7.734	66.198	601.027	5678.473	0.333
1	3	1599.080	480.846	0	361.255	7.824	67.587	618.342	5879.565	0.333
1	4	1582.002	455.973	0	357.434	7.769	66.729	607.539	5752.967	0.333
1	5	1564.447	431.543	0	365.223	7.797	67.107	611.613	5792.333	0.333
1	6	1544.845	404.046	0	360.513	7.792	67.074	611.743	5800.471	0.333
1	7	1526.517	378.861	0	362.149	7.764	66.586	604.993	5714.036	0.333
1	8	1513.161	360.789	0	361.536	7.770	66.710	606.786	5737.724	0.333
1	9	1502.154	348.780	0	361.467	7.770	66.702	606.696	5736.671	0.333
1	10	1495.023	339.882	0	359.193	7.760	66.585	605.586	5727.994	0.333
1	11	1486.963	332.819	0	360.515	7.785	66.959	610.269	5782.688	0.333
1	12	1478.500	324.822	0	363.097	7.786	66.939	609.430	5766.151	0.333
1	13	1471.272	319.562	0	364.506	7.811	67.334	614.565	5828.305	0.333
1	14	1464.583	314.832	0	362.995	7.785	66.928	609.415	5767.335	0.333
1	15	1457.021	310.048	0	355.972	7.711	65.831	596.318	5621.735	0.333
1	16	1450.219	305.781	0	362.416	7.785	66.938	609.629	5770.823	0.333
1	17	1442.594	301.565	0	364.057	7.760	66.513	603.860	5698.061	0.333
1	18	1436.935	298.377	0	359.575	7.747	66.348	602.304	5686.208	0.333
1	19	1431.554	294.584	0	363.954	7.751	66.381	602.195	5678.348	0.333
1	20	1425.407	290.609	0	363.124	7.736	66.141	599.109	5641.358	0.333
1	21	1417.567	286.765	0	362.492	7.743	66.272	601.005	5666.393	0.333
1	22	1409.613	283.520	0	363.254	7.731	66.053	597.974	5627.585	0.333
1	23	1400.611	279.821	0	361.669	7.730	66.062	598.338	5634.838	0.333
1	24	1388.537	275.679	0	362.117	7.705	65.657	593.016	5569.427	0.333
1	25	1378.519	271.918	0	360.809	7.730	66.063	598.400	5636.238	0.333
1	26	1372.856	271.028	0	359.666	7.765	66.651	606.365	5736.608	0.333
1	27	1370.446	269.416	0	363.954	7.751	66.381	602.195	5678.354	0.333

*Figure 67: **All Trajectories** output table of Particle Tracker 2D/3D plugin*

[8] The 6th, 7th, 8th, 9th, 10th, 11th columns define some important statistical intensity calculations. m0 defines the intensity moment of order 0 (total intensity) of the particle at the corresponding coordinates. m1, m2, m3, m4 define the intensity mean, variance, skewness, and intensity kurtosis respectively, whereas NPscore defines the non-particle discrimination score (MOSAIC Group, 2006). However, they are out of our interest in this study, since we are only interested in the particles velocity calculations.

5.1 Velocity Calculations with MATLAB®

Knowing the exact time step between every two points in the particle's trajectory would easily allow the calculation of this particle instantaneous velocity (known as interstitial velocity, to distinguish it from Darcy's velocity in porous media). Moreover, the three pixel-decimals accuracy of the X, Y, and Z coordinates would enable the extremely accurate calculations of the velocity vector's three components in three dimensions. This implies an accurate quantification of the colloidal microscopic flow field.

To do so, we used MATLAB® language in analyzing these trajectories-coordinates data, implementing the velocity calculations, and eventually visualize the computational results in a 2D MATLAB figure (since we are doing the trajectories analysis on 2D sets of data).

Hence, the resulting computational MATLAB figures would visualize the colloidal flow lines as well as the corresponding velocity field in the microporous structure (from which the original images were acquired). This when successfully implemented, would result in a relatively fast, user-friendly, easy to perform, efficient, and accurate technique for velocity calculations compared to other PIV methods and techniques. **PIV analysis** plugin in ImageJ2/Fiji® for example was implemented on the same data set from Experiment No. 2, Location-1. After 8 hours running the plugin on 171-slice image sequence using a computer with very high computational power, we got relatively Incomprehensible, difficult-to-read-and-interpret results with four different outcomes for velocity and flow directions, as well as a complex colour code for reading the results, Figure 68.

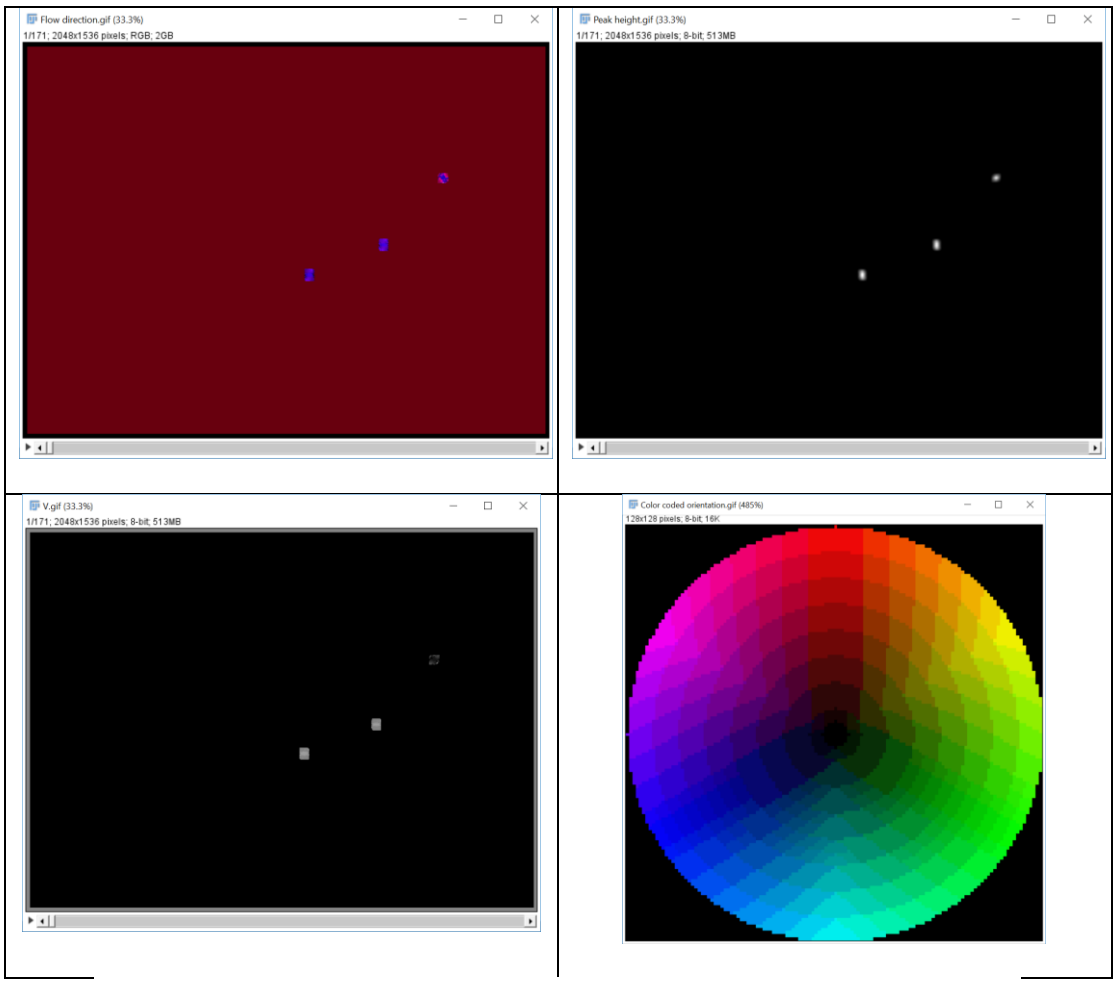

Figure 68 – PIV analysis from ImageJ2/Fiji® results of Experiment No. 2, Location -1

5.1.1 MATLAB® code development workflow

1. Save the Particle Tracker 2D/3D **All Trajectories** table in a new folder and name it as default "**Results.csv**." This will save the table in an excel sheet with all the data included. The **.csv** file extension will be necessary for being imported by any MATLAB® function. The **All Trajectories** table now is the input data for the MATLAB® code.
2. Make sure that the saved excel sheet looks like the one in Figure 69, case1, where the included data has the following columns order: 1. **Trajectory number**, 2. **Frame number**, 3. **X coordinate**, 4**. Y coordinate**, 5. **Z coordinate**. This is crucial for MATLAB®, since it reads the input data from the code-predefined column numbers in the **Results.csv** excel sheet.

   In some cases, the output **All Trajectories** table has different orders of these data when it is saved to an excel sheet (Results.csv), Figure 70, case2.

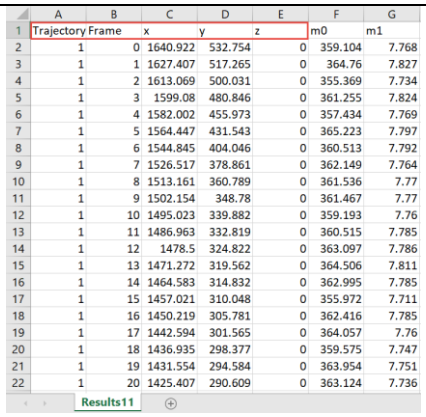

Trajectory	Frame	x	y	z	m0	m1
1	0	1640.922	532.754	0	359.104	7.768
1	1	1627.407	517.265	0	364.76	7.827
1	2	1613.069	500.031	0	355.369	7.734
1	3	1599.08	480.846	0	361.255	7.824
1	4	1582.002	455.973	0	357.434	7.769
1	5	1564.447	431.543	0	365.223	7.797
1	6	1544.845	404.046	0	360.513	7.792
1	7	1526.517	378.861	0	362.149	7.764
1	8	1513.161	360.789	0	361.536	7.77
1	9	1502.154	348.78	0	361.467	7.77
1	10	1495.023	339.882	0	359.193	7.76
1	11	1486.963	332.819	0	360.515	7.785
1	12	1478.5	324.822	0	363.097	7.786
1	13	1471.272	319.562	0	364.506	7.811
1	14	1464.583	314.832	0	362.995	7.785
1	15	1457.021	310.048	0	355.972	7.711
1	16	1450.219	305.781	0	362.416	7.785
1	17	1442.594	301.565	0	364.057	7.76
1	18	1436.935	298.377	0	359.575	7.747
1	19	1431.554	294.584	0	363.954	7.751
1	20	1425.407	290.609	0	363.124	7.736

Results11

Figure 69: Results.csv excel sheet Case-1

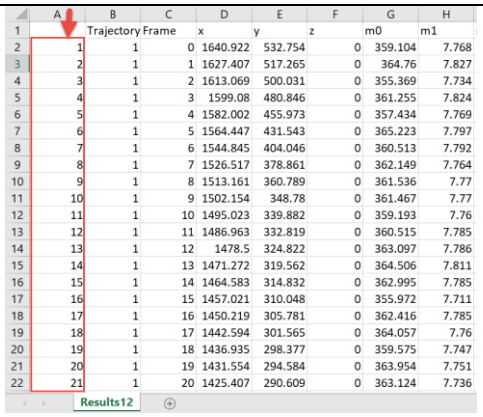

	Trajectory	Frame	x	y	z	m0	m1
1	1	0	1640.922	532.754	0	359.104	7.768
2	1	1	1627.407	517.265	0	364.76	7.827
3	1	2	1613.069	500.031	0	355.369	7.734
4	1	3	1599.08	480.846	0	361.255	7.824
5	1	4	1582.002	455.973	0	357.434	7.769
6	1	5	1564.447	431.543	0	365.223	7.797
7	1	6	1544.845	404.046	0	360.513	7.792
8	1	7	1526.517	378.861	0	362.149	7.764
9	1	8	1513.161	360.789	0	361.536	7.77
10	1	9	1502.154	348.78	0	361.467	7.77
11	1	10	1495.023	339.882	0	359.193	7.76
12	1	11	1486.963	332.819	0	360.515	7.785
13	1	12	1478.5	324.822	0	363.097	7.786
14	1	13	1471.272	319.562	0	364.506	7.811
15	1	14	1464.583	314.832	0	362.995	7.785
16	1	15	1457.021	310.048	0	355.972	7.711
17	1	16	1450.219	305.781	0	362.416	7.785
18	1	17	1442.594	301.565	0	364.057	7.76
19	1	18	1436.935	298.377	0	359.575	7.747
20	1	19	1431.554	294.584	0	363.954	7.751
21	1	20	1425.407	290.609	0	363.124	7.736
22	1	21					

Results12

Figure 70: Results.csv excel sheet Case-2

This depends on the Particle Tracker 2D/3D default settings, Figure 71. However, this problem can be solved by changing the settings from the **Results** tab in the **All Trajectories** table before saving it. Un-checking the "save row number" option will delete the extra column; otherwise, a code modification is necessary.

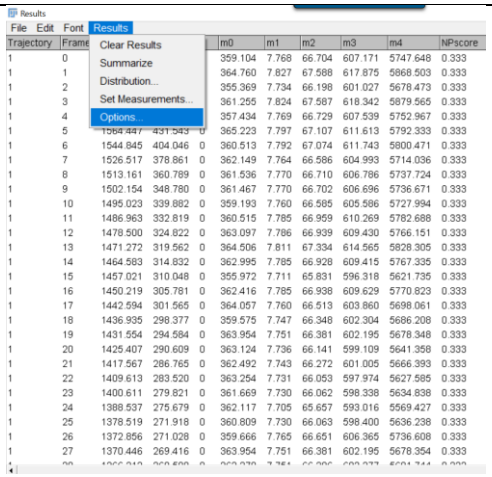

Figure 71: Results tab in All Trajectories output table

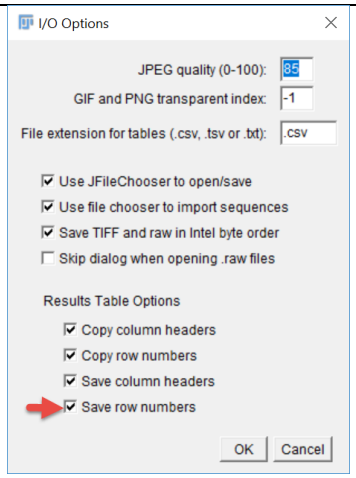

Figure 72: Saving the Results table options

3. Import the data from the **Result.csv** excel sheet as an input data for the further velocity calculations.
4. Import the first image in the concerned image sequence as a second input data for the final flow-field visualization. It is recommended to be a raw (unprocessed) image to assure no dilations or erosion happened to the grain boundaries thus no velocity vectors overlay on the boundaries.

5. Calculate the time step between every two subsequent points in each trajectory (in the **All Trajectories** Particle Tracker 2D/3D output table) from the following formula:

$$\boldsymbol{Time\ step} = (\boldsymbol{Texp.} + \boldsymbol{Tint.}) * \boldsymbol{Increment} * (\boldsymbol{Frame}\ (\boldsymbol{n}+\boldsymbol{1}) - \boldsymbol{Frame}\ (\boldsymbol{n}))$$

Where:

- ***Texp.*** : Exposure time in millisecond (given in the microscopic image acquisition settings)
- ***Tint.***: Time interval in millisecond (given in the microscopic image acquisition settings),
- ***Increment:*** Image Increment (we set it when we first import the image sequence for processing in ImageJ2/Fiji®),
- ***Frame (n)*** the Frame number in the 2nd column of the output **All Trajectories** table; n corresponds to the order of the trajectory point at which we compute the velocities, and not to the value in this column.
- ***Frame (n+1)*** the Frame number in the 2nd column of the output **All Trajectories** table; n+1 corresponds to the order of the next trajectory point at which we compute the velocities.

This **Frame-order** subtraction procedure was implemented to overcome the disappearance of particles in some frames due to some image processing artifacts or any related algorithm mistakes. This might happen due to wrong input parameters such as the aforementioned **Displacement** parameter. Figure 73 shows a case where some particles were not detected in some frames.

Trajectory	Frame	x	y	z	m0	m1	m2	m3	m4	NPscore
1	0	1809.629	4.117	0	22.306	2.045	5.136	14.381	43.361	0.011
1	2	1851.728	120.365	0	33.738	2.225	5.797	16.435	49.387	0.073
1	3	1820.753	121.247	0	34.16	2.279	6.05	17.45	53.289	0.04
1	4	1786.827	122.245	0	34.049	2.298	6.134	17.746	54.268	0.027
1	5	1741.361	106.064	0	28.656	2.23	5.87	16.862	51.408	0.021
1	7	1661.517	37.603	0	34.391	2.254	5.927	16.91	51.009	0.018
1	8	1646.154	25.257	0	32.778	2.207	5.721	16.167	48.504	0.028
1	9	1632.665	14.285	0	33.393	2.202	5.699	16.075	48.136	0.068
1	10	1621.5	4.213	0	30.85	2.148	5.474	15.297	45.631	0.011
2	0	814.672	7.437	0	32.931	2.144	5.422	14.959	43.817	0.038
2	1	811.392	9.484	0	33.315	2.169	5.537	15.394	45.386	0.069
2	2	808.176	11.585	0	32.146	2.12	5.321	14.606	42.668	0.044
2	3	804.627	14.373	0	32.546	2.118	5.305	14.513	42.211	0.041
2	4	800.824	17.638	0	33.094	2.197	5.669	15.941	47.571	0.05
2	5	797.39	22.193	0	33.295	2.203	5.696	16.025	47.799	0.088
2	6	793.273	27.38	0	33.308	2.182	5.599	15.663	46.515	0.089
2	7	788.243	34.103	0	32.135	2.175	5.582	15.653	46.678	0.019
2	8	781.815	42.25	0	33.709	2.277	6.041	17.408	53.101	0.036
2	9	773.279	52.5	0	32.546	2.118	5.305	14.513	42.211	0.046
2	10	760.5	64.5	0	34.085	2.218	5.759	16.236	48.419	0.035
2	11	743.56	73.512	0	33.89	2.212	5.735	16.162	48.234	0.045

Figure 73: Particle-disappearance case in trajectory No. 1

6. Calculate the Velocity X component (Vxn), and Y component (Vyn), and Z component (Vzn) for each trajectory point (n), for all the detected trajectories.

$$Vxn = \frac{Xn+1 - Xn}{time\ step}; \qquad Vyn = \frac{Yn+1 - Yn}{time\ step}; \qquad Vzn = \frac{Zn+1 - Zn}{time\ step},$$

Where

n: is the data point order in each trajectory, as mentioned before. Therefore, in the MATLAB code, it starts with number n=1 for each trajectory, and ends with (m) the total number of detected points for this trajectory.

This implies that we assigned the velocity at each particle coordinates point, based on the point its self and the next point's coordinates. Hence, the last point in each trajectory will have no next point to calculate its velocity. Therefore, we assigned a zero velocity value for the last points of all trajectories and ignored it in the later calculation of average interstitial velocity.

7. Calculate the Velocity magnitude for point (n) from the formula:

$$Vn = \sqrt{Vxn^2 + Vyn^2} \quad \text{(In a 2D case),}$$

8. Calculate the average velocity for each trajectory from the formula

$$Vavg = \frac{\sum_1^{m-1} Vn}{m-1},$$

Where

m-1: is the total number of detected points in each trajectory except the last point.

9. Display the microscopic velocity field vectors in 2 different output MATLAB® figures;
   - The first figure with the instantaneous velocity magnitude assigned to each velocity vector.
   - The second figure with the average velocity magnitude assigned to each trajectory.
10. Export all the calculated velocities to a new excel sheet (named as **Final_Results.xlsx**) as an extra output data saves all the necessary information for any further applications.

11. The full-text MATLAB® Code is included in Appendix B of this thesis.

5.1.2 MATLAB® code Considerations

It is noteworthy to consider the following points for successful application of the code:

A. All the input data for the code must be saved together in one folder. This includes the **Results.csv** excel sheet, the raw acquired image, as well as the two **MATLAB® .m-**files. The MATLAB window before running the code must look similar to Figure 74.

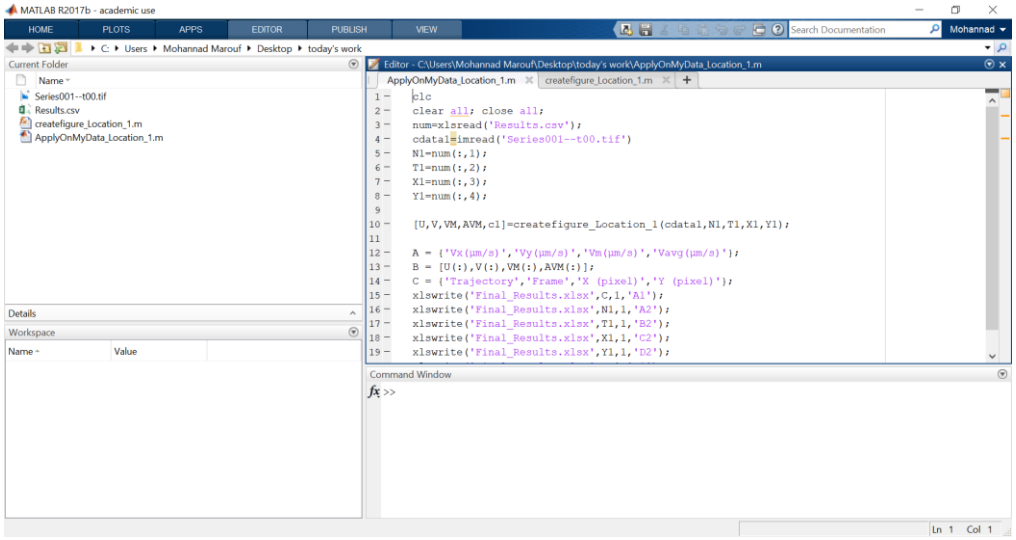

Figure 74: MATLAB® window before running the code

B. The name of the input image must match exactly the one in the code (inside the "imread" MATLAB command in line number 4 in **ApplyOnMyData_Location_1.m MATLAB® .m** file (look in the appendix). The same for the **Result.csv** input excel sheet.

C. Five **User-inputs** are requested after a few seconds of running the **ApplyOnMyData_Location_1.m** file. These are;

1. What is the exposure time in milliseconds?
2. What is the time interval in milliseconds?
3. What is the Images increment?
4. What is the pixel size in micrometer?
5. What is the required Velocity Arrows density?
   Please enter an integer number within the range [1, 10] with 1 for full density and 10 for least density!

These are necessary inputs for the velocity calculations as mentioned before. The user must be careful and accurate in entering them in order to achieve accurate results. Only the User-input number five is optional and up to the user.

D. All the output velocity values are in **µm/sec**, since a conversion factor, from **pixel/millisecond** to **µm/sec**, was used in the velocity calculations.

E. The **Final_Results.xlsx** output excel sheet will be automatically generated by MATLAB® immediately after running the **ApplyOnMyData_Location_1.m** file. This will be updated after each time we run the code (Figure 75).

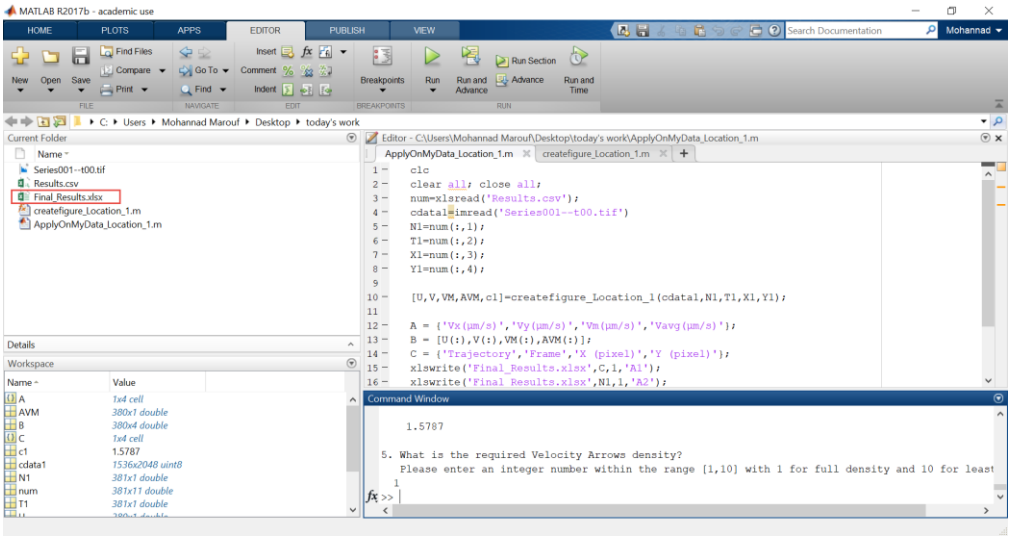

Figure 75: MATLAB® window after running the code

5.2 Results and Discussion

Applying the method mentioned above on the trajectory analysis' results from all the experiments (No.2, 3, 4 and 5), showed a relatively realistic average interstitial velocity values.

In experiment No. 2, Location -3 (10x & 0.005 ml/Hour) for example, the average interstitial velocity results showed a big interstitial velocity variation in this microscopic part of the micromodel, between 4 and 10 µm/sec, Figure (76).

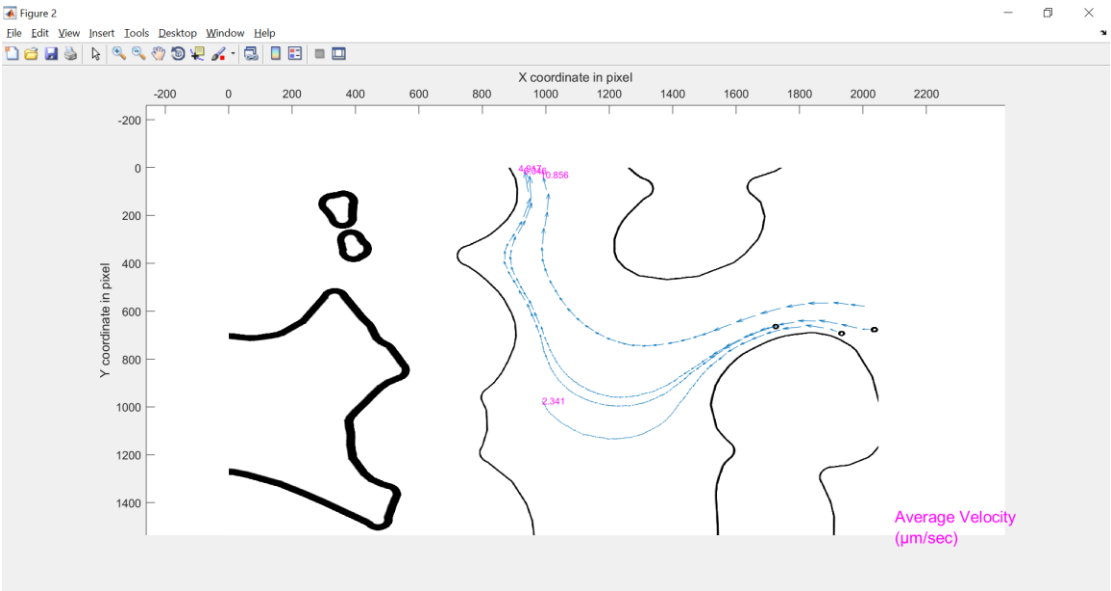

Figure 76 – Average Interstitial Velocity from Location- 3

This is much less than the average water interstitial velocity, calculated from Darcy's velocity across the whole model with a 0.005 ml/hour injection rate:

$$Vf,i = \frac{Vd\ (@\ 0.005\frac{ml}{hour})}{porosity} = \frac{12.0773}{0.57} = 21.1883\ \mu m/sec.$$

This is attributed to 2 main reasons:

- First, this area was by chance an extremely low interstitial-velocity area. This is normal for a complex microscopic geometry with very high-velocity variation. Therefore, this small part of the micromodel is not representative of the overall micro model, and the average velocity values are not indicative, which is the most likely reason,
- Second, the particles average interstitial velocity is generally slightly less than the average water interstitial velocity due to drag forces (Stokes' flow behaviour); and Brownian motion. However, dragging forces are linearly proportional to the particles interstitial velocity (Vi), the radius of the particle (r), and the fluid viscosity (µ) (Batchelor, 2000),

$$FD = 6\pi.\mu.r.Vi$$

This implies that with slow particles, it is less influencing, whereas Brownian motion will play a more significant role in this situation, and vice versa in high-velocity areas.

To investigate that into more details, we applied this method on a larger field of view in the same area of the micromodel (experiment No. 3). Both injection rate (0.005 ml/Hour) and investigation area were similar to experiment No. 2, but with 5x magnification. The results are shown next:

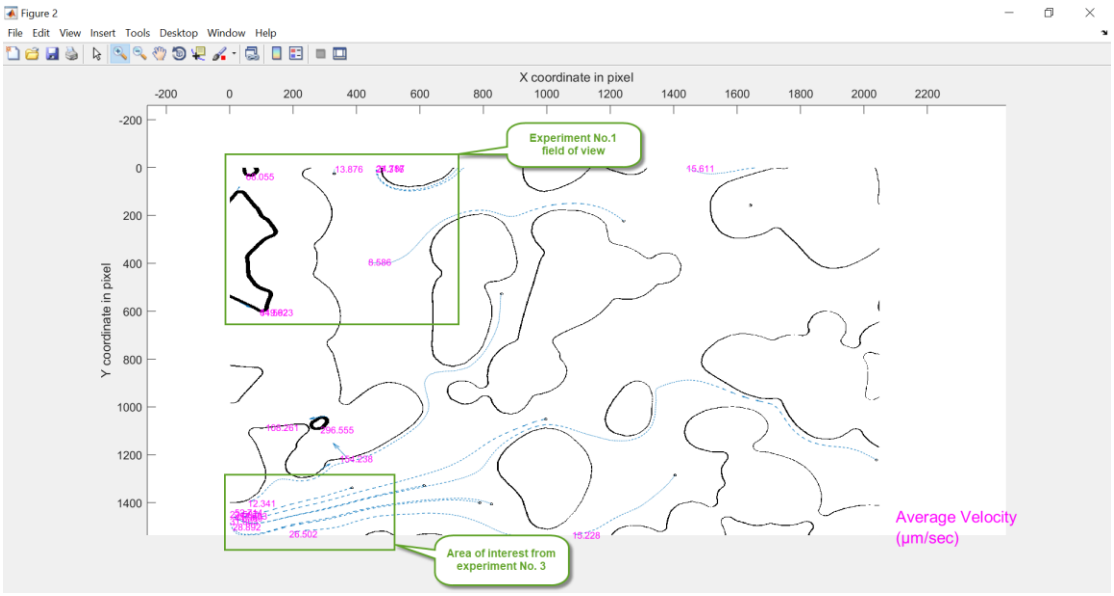

Figure 77 - Average Interstitial Velocity from experiment No. 3

This shows a potential particle preferential pathway at the bottom left corner of this field of view. Zooming into this part shows a relatively high average interstitial particle velocity. Two comparable and representative average velocity values (they belong to the most extended 2 streamlines in this field of view, but originated from two different directions) are highlighted next in green boxes for comparison, Figure 78.

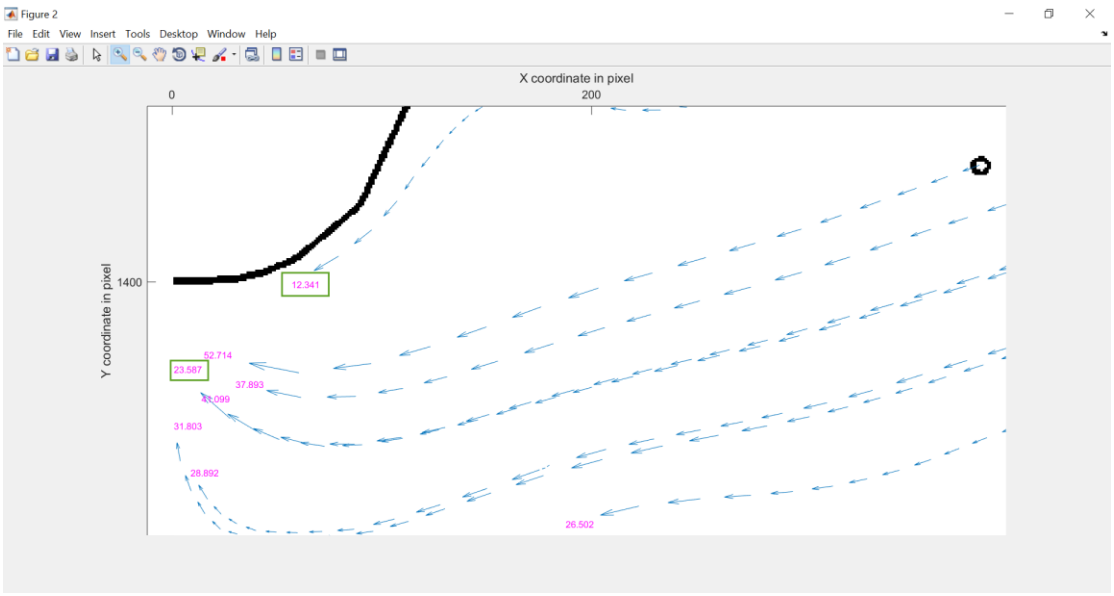

Figure 78 - Preferential flow paths from experiment No. 3

This shows that all particles that belong to the lower bundle of flow lines have a relatively high average interstitial velocity (23.587 µm/sec), compared to the single upper particle with an extremely low average velocity of 12.341 µm/sec. This would also be indicative if we compare the instantaneous velocities at this region instead of the average ones. Instantaneous velocities

at a cross-section of this area would indicate the fully developed parabolic velocity profile at the pore throats in such a complex geometry as was mentioned in the literature in Chapter 2, Figure 79. This issue needs more investigation in future if the code is developed to interpolate the instantaneous velocity values to cover each pixel of the images and thus a full velocity field visualization would be achieved.

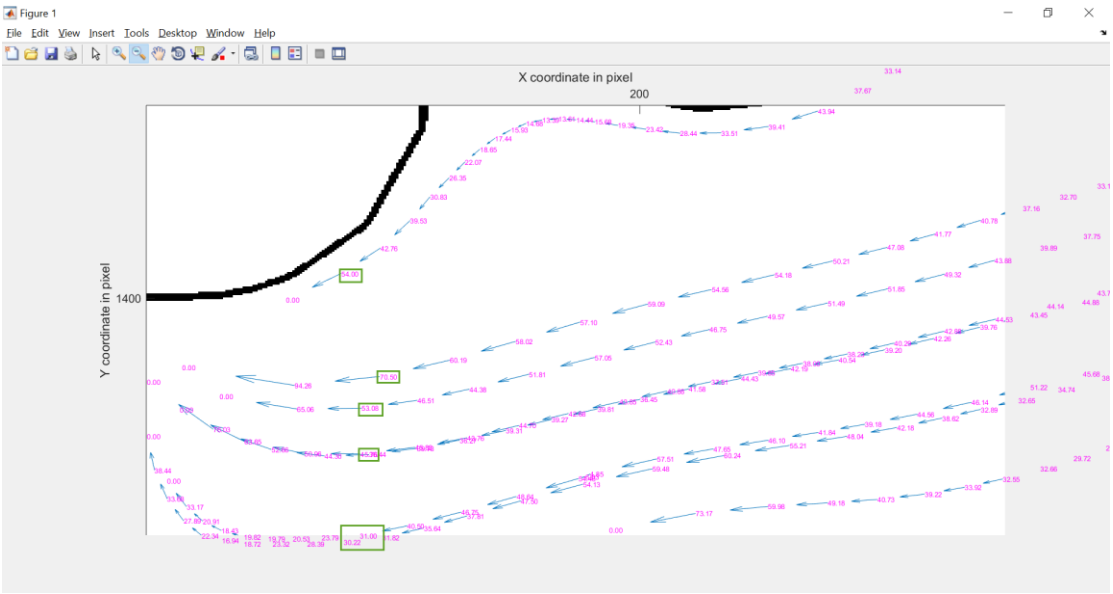

Figure 79 - Instantaneous velocity values from a preferential path cross-section

Overall, this leads to an essential inference that **most of the particles are flowing across relatively high-velocity paths called as colloidal preferential flow paths**, and if a particle takes non-preferable pathway, then it will be moving slowly and close to the walls.

Another example showed supporting evidence of preferential paths, by using a larger field of view (2.5X magnification). In experiment No. 5, an image sequence of 666-time slices was taken during sufficient experimental time of 100 seconds in steady state conditions. Applying the same method enabled us to visualize and quantify the colloidal flow field in a relatively accurate way. The figure next shows the corresponding results with many obvious particle preferential flow pathways defined by darker-blue and longer velocity field vectors, since not only the velocity values indicate the preferential paths, but also the number of particles flow lines.

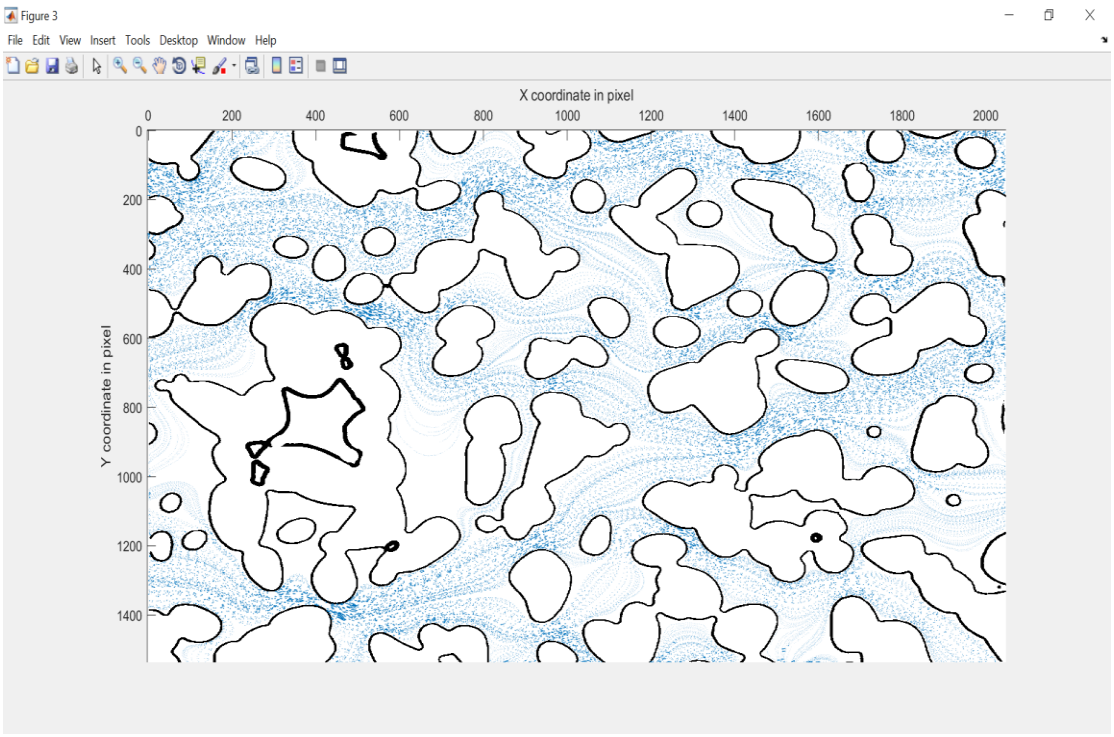

Figure 80 – the microscopic velocity field for experiment No. 5

Interestingly, another example from experiment No. 2 location -5, in a small field of view with 10x magnification, 835 acquired images during 200 seconds of steady-state conditions, showed with no doubt, a perfectly aligned particles' preferential flow lines, Figure (81).

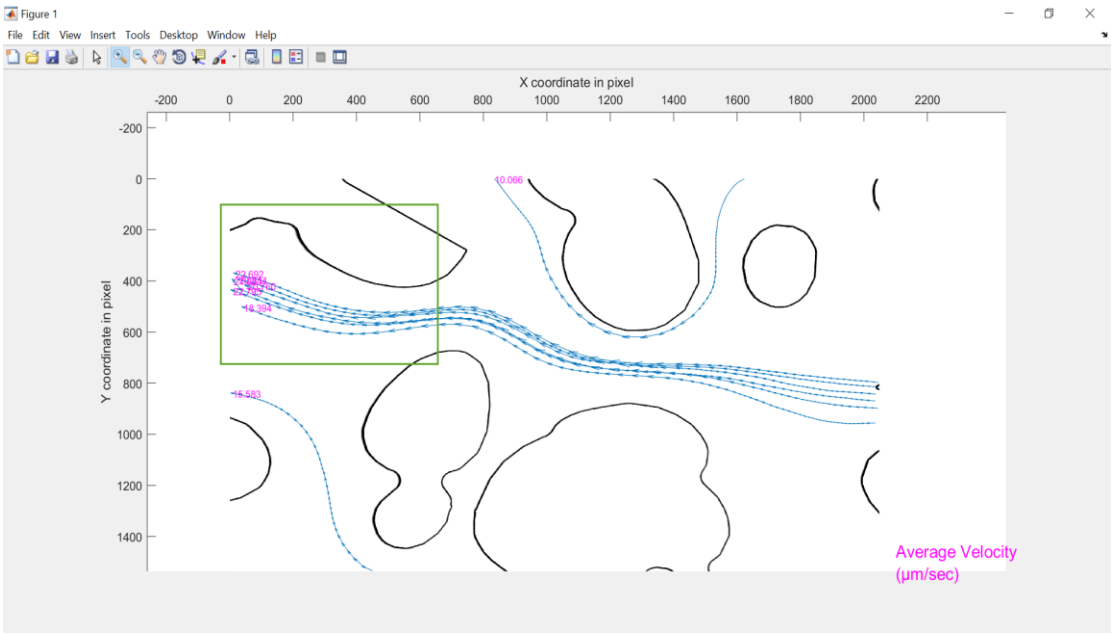

Figure 81 – Average Interstitial Velocity from experiment No. 2, Location -5

Since the average interstitial velocity of water in porous media is the average of all velocities in all the channels in an elementary representative volume (Malkovsky & Pek, 2009), we can investigate this part of the model assuming that it is a representative part of the micromodel.

Hence it has a similar water average interstitial velocity of 21.1883 µm/sec like the whole micromodel.

Investigating the average interstitial velocity along these preferential flow paths, showed values between 18.4 and 22.8 µm/sec, with an average of 21 µm/sec (slightly less than the calculated water interstitial velocity 21.1883 µm/sec). "The actual particle velocity should be close to the maximum velocity of the groundwater in the most permeable channel" (Malkovsky & Pek, 2009), Figure (82):

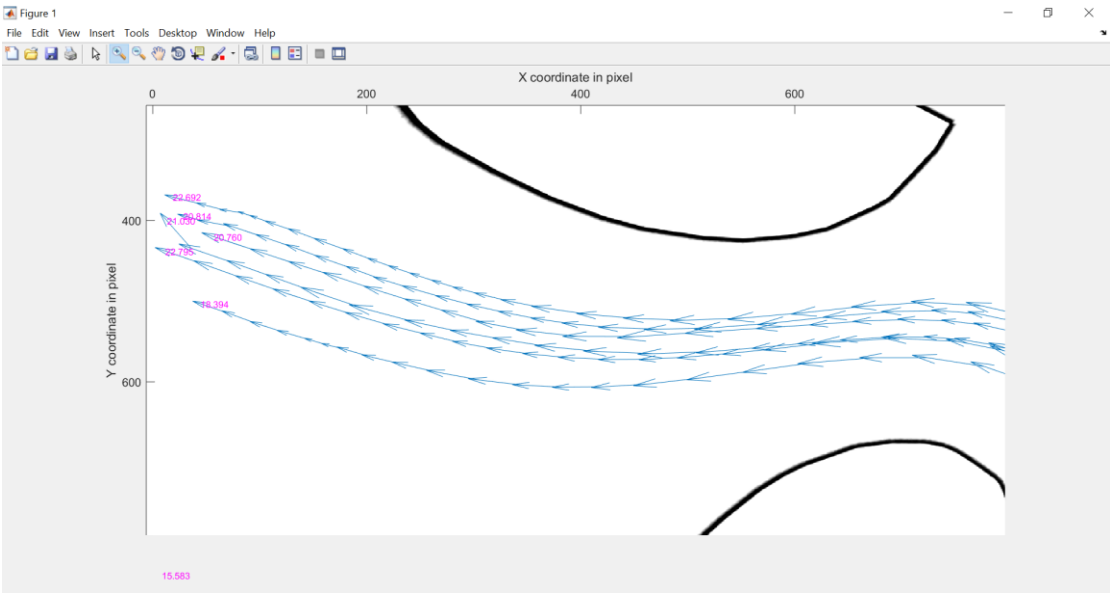

Figure 82 - Average Interstitial Velocity from experiment No. 2, Location -5, (zoomed in area)

This would be a perfect definition for a colloidal preferential path with a size-exclusion effect drives the large particles to take the most permeable channels, as well as dragging forces effect, which theoretically (in addition to minor Brownian dispersion effects), resist their movement in the fluid.

In other words, these particles due to the drag forces of Stokes' flow, and dispersion effect of Brownian motion have slightly less average interstitial velocity than the water molecules, but due to the size exclusion effect, they have reduced number of flow paths in the micromodels. This in total, led to the early particle breakthrough behaviors we observed in the first set of experiments (experiment No. 1) on a large scale includes the whole micromodel.

In fact, it in noteworthy to mention here that observing the dispersion effect in this example was difficult since it might be trivial with high-velocity movement (high advection forces). However, back to the first example in experiment No. 2, Location -3 (10x & 0.005 ml/Hour), a more obvious case, where extremely slow particles motion with tilted flow lines showed some indications of Brownian motion, Figure 83.

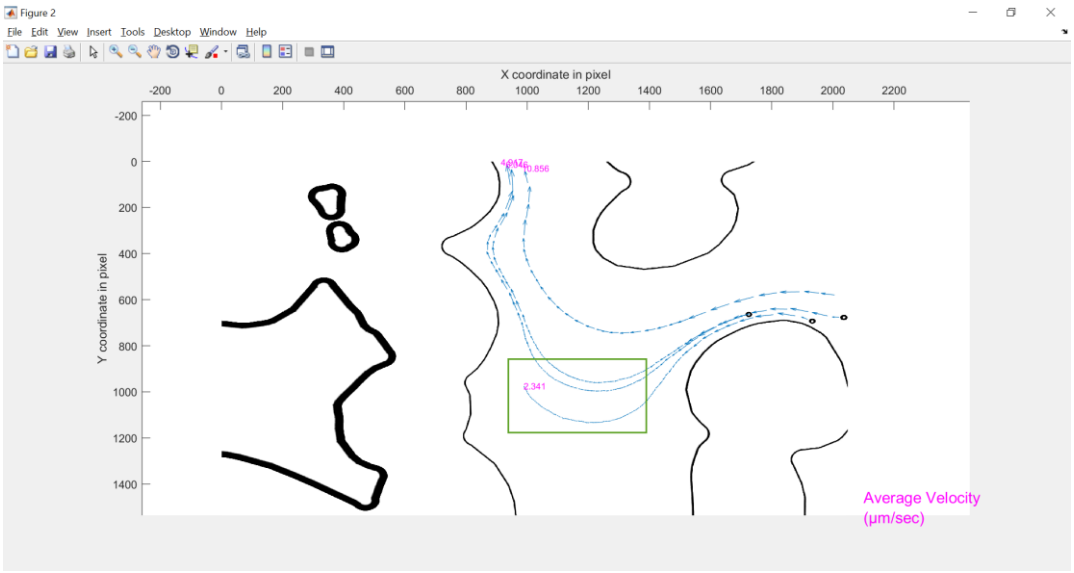

Figure 83 – Average Interstitial Velocity from Location- 3, experiment No. 2

Investigating this visualization by zooming into the in-green-box highlighted area showed that the assumption is in full agreement with experimental data as shown in Figure 84.

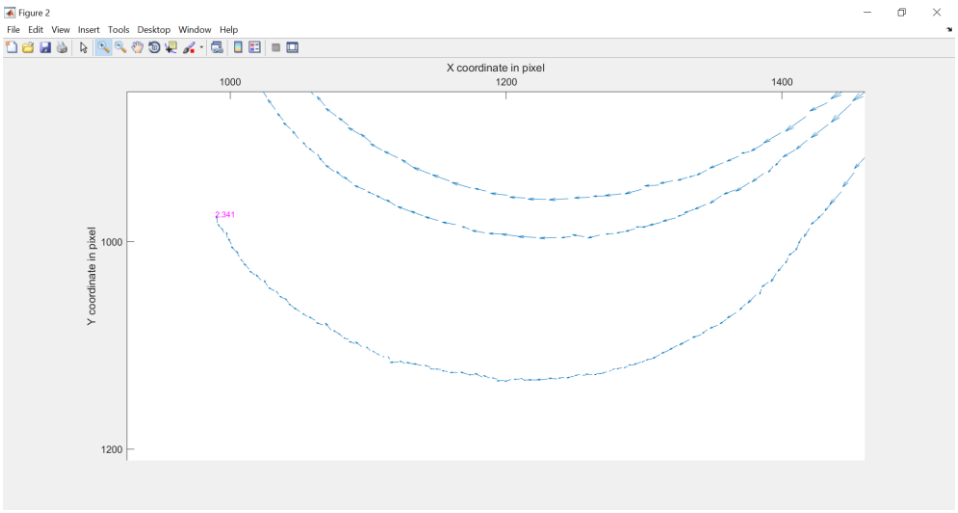

Figure 84 - Average Interstitial Velocity from Location- 3, Experiment No. 2 (zoomed in area)

More zooming into the lowermost flow line, which has the slowest average velocity, showed a highly tortuous flow line. This indicates the relatively high dissipation effect of Brownian motion on such a slow movement, due to the particles collisions with water molecules, which

results in a random movement of the corresponding colloid along the main flow line, Figure 85.

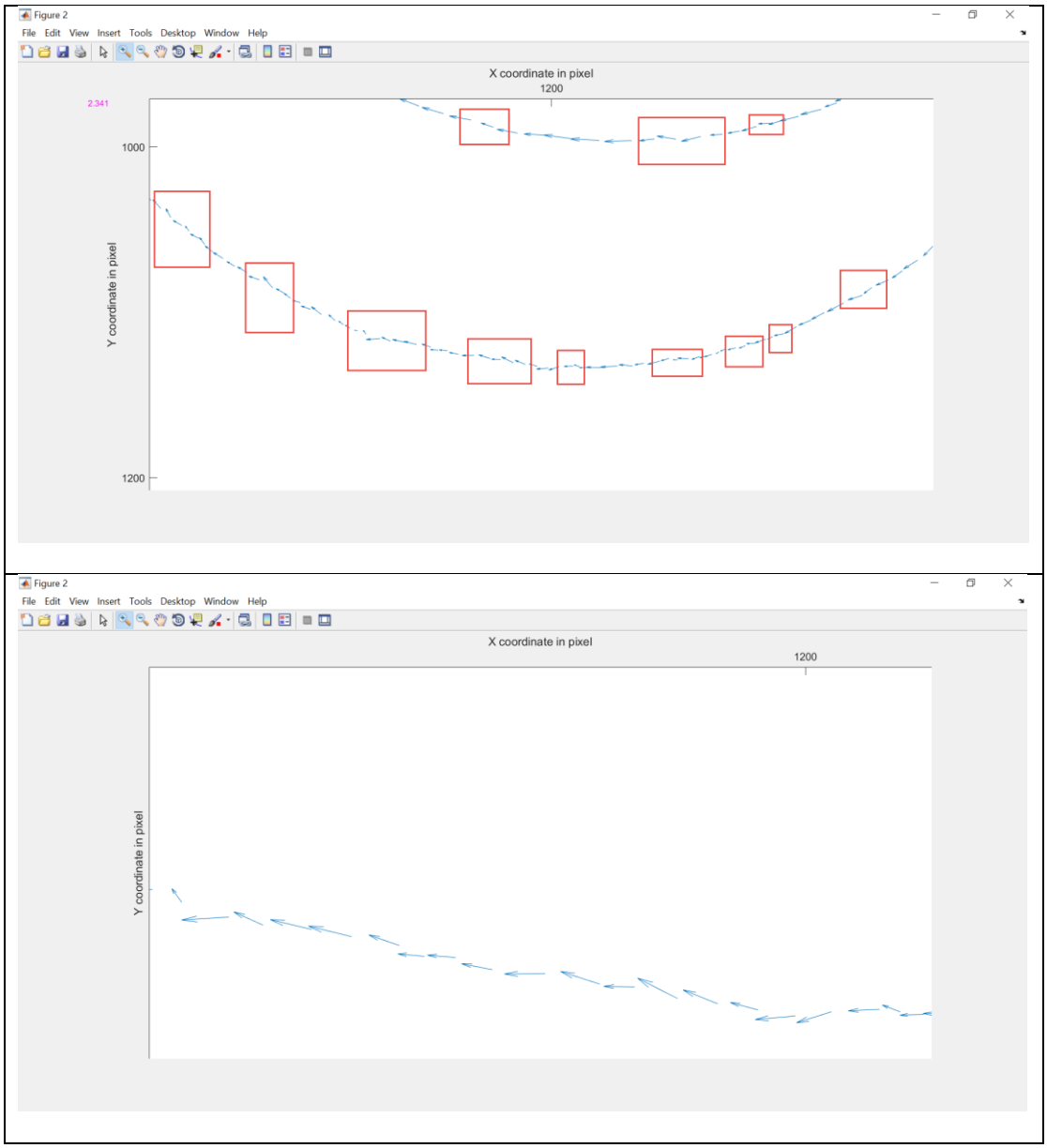

Figure 85 – Brownian motion effect in experiment No.2, Location -3

Many other interesting velocity-field visualization results from all the experiments are illustrated in the Appendix C.

Finally, we applied this method to compare the preferential flow paths in a water-saturated medium with a pre-established biomass system. This showed the effects of biomasses accumulation in changing some porosities in the structure, and blocking complete flow paths in the system. Figure 86

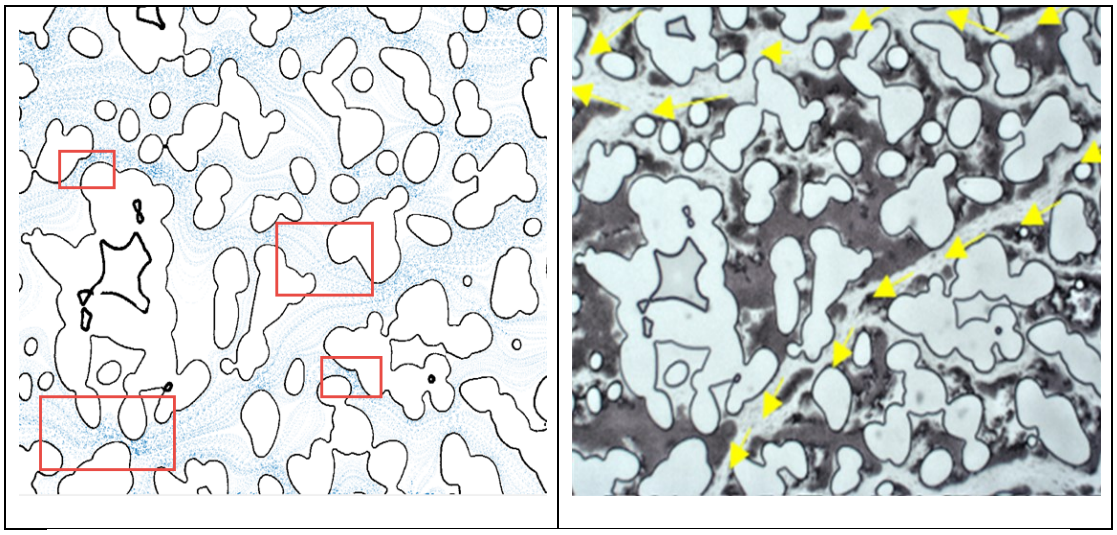

Figure 86- preferential flow paths comparison between water-saturated medium (left), and pre-established biomass – taken from PhD unpublished results - Montanuniversität leoben (right).

Chapter 6

6.1 Challenges and Recommendations

In this chapter, the main challenges we faced during this work, will be highlighted and addressed to help avoiding them and guiding future work in particle tracing:

Two main challenges have been the most time consuming and needed the most effort to tackle:

- Cleaning issues, which have been incredibly difficult to solve, since we needed a perfectly clean micromodel to avoid any porosity and permeability changes, and hence any flow lines distribution changes due to any contaminants in our micromodel.
  However, this issue must have standard procedures and solutions from the utilized-micromodel manufacturer (micronit co.).
- Low flow rates were used in this work due to the limitation we had in processing the images with blurring particles in high velocity areas. This will lead to particles disappearances from these areas. An example from experiment No. 5 showed some evidences of the blurring particles at 0.05 ml/hour, Figure 87.

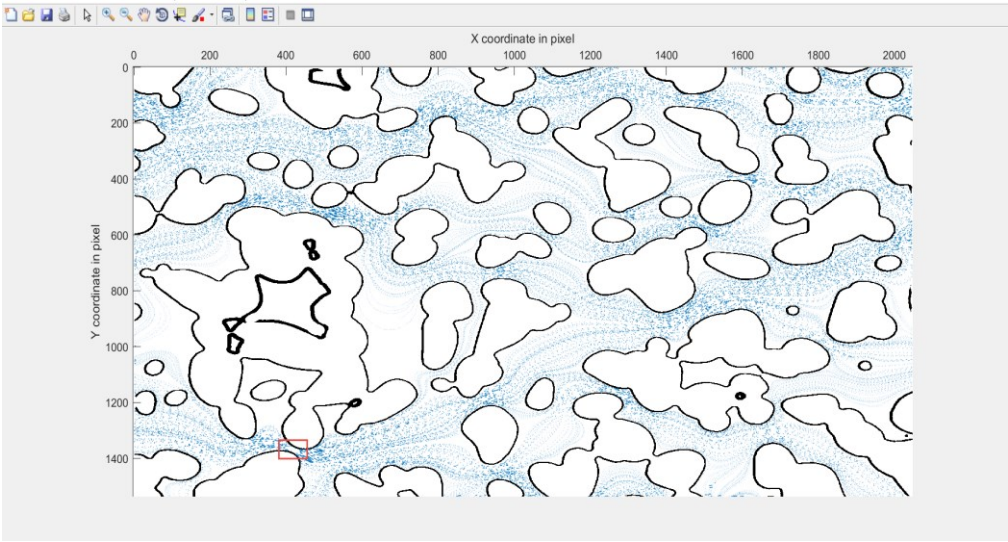

Figure 87- Blurring particles effect in experiment No. 5

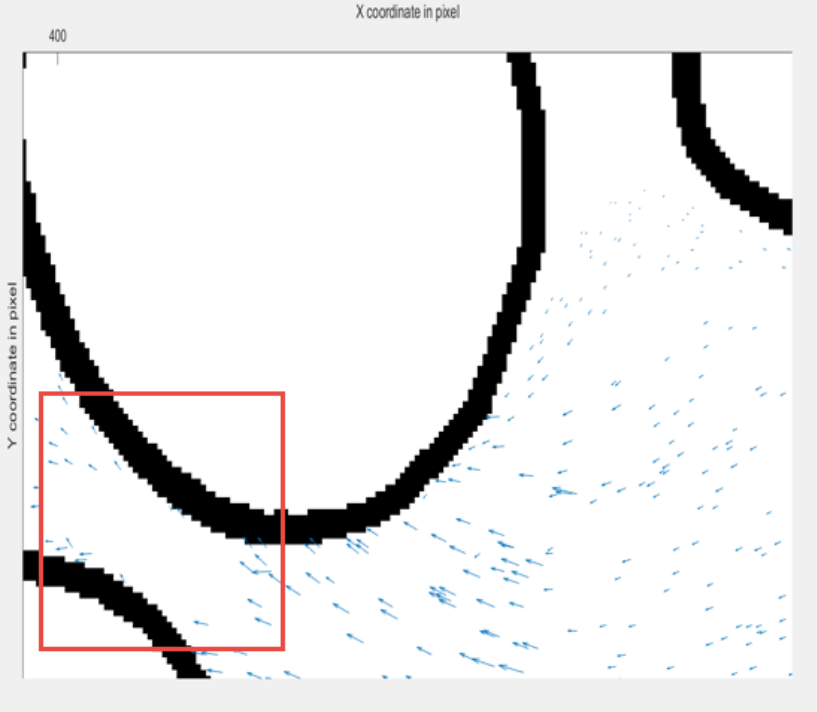

Figure 88- Blurring particles effect in experiment No. 5 (zoomed in)

This was attributed to the low-camera-fps capabilities. This problem can be solved by purchasing higher fps cameras, and suitable for fluorescent microscopy.

6.2 Future Work

By solving these issues, many important applications of particle tracing can be investigated and studied in future work :

- Compare the results between the obtained velocity profile of the microporous structure and the data from numerical simulations which uses Navier-Stokes equation for solving the flow behavior. However, the result must have a difference since it assumes that particles faithfully follow the fluid streamlines and ignores the inertia term of particles.
- Studying the effect of different factors on the colloidal flow behavior such as particles size and concentration, flow rate, differential pressure, as well as the diffusion (dispersion) effect on the flow properties.
- Studying many other phenomenon like particle filtration and straining and their influencing factors.
- Applying the same method in unsaturated micromodel and in 3D dimensions (since both particle tracker 2D/3D and the code are upgradable to a 3D mode).
- Applying other plugins in ImageJ2/Fiji® for automatically counting the particles and hence, statistically define the most possible preferential pathways in any field of view.
- These are few of many more applications of particle tracing in the porous media which are worth investigation in the future.

Chapter 7

Conclusion

A quantitative flow visualization method was developed by implementing a robust protocol for image processing and analysis, and combining Particle tracker 2D/3D tool from ImageJ2/Fiji® with MATLAB® language in particle tracing experiments. We could quantify the colloidal flow field at the pore scale in a 2D water-saturated micromodel represents an actual physical piece of rock. The direct observation and average velocity measurements of 10-µm particles' flow proved us the early breakthrough behavior of colloids in saturated porous media. In comparison with the results from the particle tracing flow-visualization quantitative method, we had a supporting evidence of colloidal preferential flow pathways in porous-media. Moreover, by applying this method, the clear visualization and accurate quantification of particles flow-lines in dead ends illustrated the diffusion effect on slow-motion particles. It indicated a Brownian motion effect, which was difficult to observe on large size particles with more than 2µm diameter.

Chapter 8

References

Artinger, R. K. B. S. W. K. J., 1998. Effects of humic substances on the 241Am migration in a sandy aquifer: column experiments with Gorleben ground-water/sediment systems. *J. Contam. Hydrol.,* Volume 35, p. 261–275.

Auset, M. & Keller, A., 2005. *Pore-scale processes that control dispersion of colloids in saturated porous media.* s.l.:Water Resources Res..

Batchelor, G. K., 2000. *An Introduction to Fluid Dynamics.* s.l.:Cambridge University Press.

Bian, X., Kimb, C. & Karniadakis, G., 2016. 111 years of Brownian motion. *Royal Society of Chemistry,* p. 6331.

Buffle, J. et al., 1998. A Generalized Description of Aquatic Colloidal Interactions: The Three-colloidal Component Approach. *Environmental Science and Technology,* 32(19), pp. 2887-2899.

Cardinale, J., 2008. *imagej.net/Background_Subtractor.* [Online] Available at: http://mosaic.mpi-cbg.de/Downloads/BGS_manual.pdf

Cey, E., Rudolph, L. D. & Niemi, J., 2009. Influence of macroporosity on preferential solute and colloid transport in unsaturated field soils. *Journal of Conatminant Hydrology,* 107(1-2), pp. 45-57.

Chenouard, N. et al., 2014. Objective comparison of particle tracking methods. *Nature Methods,* 11(3), pp. 281-289.

Chrysicopoulos, C. V. & Abdel-Salam, A., 1997. Modeling colloid transport and deposition in saturated fractures. *Colloids and Surfaces A: Physicochemical and Engineering Aspects ,* 121(2-3), pp. 189-202.

Chrysikopoulos, C. V. & Sim, Y., 1996. One-dimensional virus transport in homogeneous porous media with time-dependent distribution coefficient. *Journal of hydrology,* 185(1-4), pp. 199-219.

Chrysikopoulos, V. C. & Katzourakis, V. E., 2015. Colloid particle size-dependent dispersivity. *Water Resources Research,* Volume 51, pp. 4668-4683.

Clancy, L. J., 1975. Aerodynamics, Chapter 3. In: *Aerodynamics.* s.l.:Wiley.

deMarsily, G., 1986. *Quantitative Hydrogeology.* Orlando: Academic Press.

DeNovio, N. M., Saiers, J. E. & Rayan, J. N., 2004. Colloid Movement in Unsaturated Porous Media: Recent advances and Future directions. *Vadosezone Journal.*

Engineering_ToolBox, n.d. *Reynolds Number.* [Online] Available at: https://www.engineeringtoolbox.com/reynolds-number-d_237.html

Fetter, C. W., 2001. *Applied Hydrology.* 4th edition ed. New Jersey: Prentice-Hall.

Gong, Y. & Sbalzarini, I. F., November, 2014. *Image Enhancement by Gradient Distribution Specification.* Singapore, s.n.

Haase, R., 1971. Survey of Fundamental Laws. In: *Physical Chemistry.* s.l.:Academic Press, pp. 24-28.

Holman, J. P., 2002. *Heat Transfer.* New York: McGraw-Hill companies, Inc..

Hu, Z., Zhao, J., Gao, H. & Nourafkan, E., 2017. Transport and Deposition of Carbon Nanoparticles in Saturated Porous Media. *Energies,* 10(8), p. 1151.

imagej.net, 2016. *imagej.net.* [Online] Available at: https://imagej.net/Principles#Image_acquisition_principles

imagej.net, 2017. *imagej.net.* [Online] Available at: https://imagej.net/Principles#What_else_is_critical_during_binarization_and_further_object_analysis.3F

imagej.net, 2017. *imagej.net.* [Online] Available at: https://imagej.net/Principles#Image_processing_principles

imagej.net, 2017. *imagej.net.* [Online] Available at: http://imagej.net/Particle_Analysis#Setting_a_threshold

Incropera, F. P. & Dewitt, D. P. B. T. L. A., 2005. *Fundamentals of Heat and Mass Transfer.* Sixth edition ed. s.l.:John Wiley & Sons, Inc..

Jan Brocher, T. W., 2015. *www.biovoxxel.de.* [Online] Available at: https://imagej.net/BioVoxxel_Toolbox#Threshold_Check

Karimi, A. et al., 2012. Wettability Alteration in Carbonates using Zirconium Oxide Nanofluids: EOR Implications. *Energy & Fuel,* 26(2), pp. 1028-1036.

Keith J. Laidler, J. H. M., 1982. *Physical Chemistry.* s.l.:Menlo Park, Calif. : Benjamin/Cummings Pub. Co., ©1982..

Kirby, B. J., 2010. *Micro- and Nanoscale Fluid Mechanics: Transport in Microfluidic Devices.* New York: Cambridge University Press.

Knapp, R. C. M. D. W., 2000. An experimental exploration of the transport and capture. *Water Resour. Res. ,* 36(11), p. 3139–3149.

Levy, G., 2006. *MosaicSuite.* [Online] Available at: http://mosaic.mpi-cbg.de/ParticleTracker/doc/ParticleTrackerUserManual.pdf

Lindken, R., Rossi, M., Große, S. & Westerweel, J., 2009. Micro-particle Image Velocimetry (μPIV): Recent developments, applications, and guidlines. *Lab on a Chip,* 7 September, 9(17), pp. 2551-2567.

Loitsyanskii, L., 1973. *Mechanics of Fluid and Gas.* Nauka, Moscow: s.n.

magej.net, 2017. *imagej.net.* [Online] Available at: https://imagej.net/Principles#Why_not_simply_choose_a_manual_threshold.3F

Mahesh, j. C., 2009. Chapter 1. In: *Textbook of Engineering Physics- Part 1.* s.l.:PHI Learning Pvt. Ltd., p. 9.

Mahesh, J. C., 2009. Fundamental forces and laws: a brief review. In: *Textbook of Engineering Physics-Part 1.* s.l.:PHI Learning Pvt. Ltd., p. 10.

Malkovsky, I. V. & Pek, A. A., 2009. Effect of Elevated Velocity of Particles in Groundwater Flow and Its Role in Colloid-facilitated Transport of Radionuclides in Underground Medium. *Transport in Porous Media,* 78(2), pp. 277-294.

McCarthy, J. S. W. S. P., 1998. Lanthanide field tracers demonstrate enhanced transport of transuranic radionuclides by natural organic matter. *Environ. Sci. Technol,* 32(24), p. 3901–3906.

Meijering, E., Dzyubachyk, O. & Smal, I., 2012. Methods for Cell and particle tracking. *Methods in Enzymology,* Volume 504, pp. 184-197.

microtechnologies, m., 2018. *www.micronit.com.* [Online] Available at: https://store.micronit.com/microfluidic-platforms/enhanced-oil-recovery-platforms/

MOSAIC Group, C. f. S. B. D. (. M. P. I. o. M. C. B. a. G., 2006. *MosaicSuite/Particle analysis.* [Online]
Available at: http://mosaic.mpi-cbg.de/ParticleTracker/doc/ParticleTrackerUserManual.pdf

Niehren, S. & Kinzelbach, W., 1998. Artificial colloid tracer tests: development of a compact on-line microsphere counter and application to soil column experiments. *Journal of Contaminant Hydrology,* 35(1-3), pp. 249-259.

Pei, H. H. et al., 2015. *Investigation of Nanoparticle and Surfactant Stabilized Emulsion to Enhance Oil Recovery in Waterflooded Heavy Oil Reservoirs.* Calgary, Alberta, Canada, Society of Petroleum Engineers.

Reimus, P. W., Robinson, B. A., Nuttall, H. E. & Kale, R., 1994. Simultaneous Transport of Synthetic Colloids and a Nonsorbing Solute Through Single Saturated Natural Fractures. *MRS Material Research Society,* Volume 353, pp. 363-370.

ResearchGate, n.d. *ResearchGate.* [Online] Available at: https://www.researchgate.net/figure/Velocity-profile-and-shear-stress-in-laminar-flow_fig13_307994348

Rhodes, M., 2007. Single Particles in a Fluid. In: *Introduction to Particle Technology, Second Edition.* Ballnarring: John Wiley & Sons, Ltd, pp. 29-30.

Rueden, C. T. & Schindelin, J. &. H. M. C. e. a., 2017. ImageJ2: ImageJ for the next generation of scientific image data. *BMC Bioinformatics,* Volume 18, p. 529.

Ryan, N. J. & Elimelech, M., 1996. Colloid mobilization and transport in groundwater. *Research Gate Journal,* Volume 107, pp. 1-56.

Santiago, J. G. et al., 1998. A Particle Image Velocimetry system for microfluidics-Experiments in Fluids. *Springer Link,* Volume 25, pp. 316-319.

Sbalzarini, I. F. & Koumoutsakos, P., 2005. Feature Point Tracking and Trajectory Analysis for Video Imaging in Cell Biology. *Journal of Structural Biology ,* 151(2), pp. 182-195.

SCIENCEFORUMS, n.d. *SCIENCEFORUMS.* [Online] Available at: https://www.scienceforums.net/topic/63070-suction-or-vacuum-power-bernoulli/

Sirivithayapakorn, S. & Keller, A., 2003. Transport of colloids in unsaturated porous media: A pore-scale observation of processes during the dissolution of air-water interface. *Water Resources Research,* 39(4), p. 1109.

Smith, D. F. D. B. S., 2003. An inventory of long-lived radionuclides residual from underground nuclear testing at the Nevada test site. *J. Environ. Radioact,* 67(1), pp. 35-51.

Tiago Ferreira, W. R., 2012. *imagej.net.* [Online] Available at: http://imagej.net/docs/guide/146-7.html#sec:Image-Types

Zheng, C. & Bennett, G. D., 1995. *Applied Contaminant Transport Modeling: Theory and Practice.* Wiley: Technology and Engineering.

Zhuang, J., Flury, M. & Jin, Y., 2003. Colloid-facilitated Cs transport through water-saturated Hanford sediment and Ottawa sand. *Environ. Sci. Technol.,* 37(21), p. 4905–4911.

Appendix A

Physical-Rock network micromodel from Micornit®

Product Code	FC_EOR.PR.20.2_PACK
Number of chips per pack	3
Distance between channel and top surface	1100 µm
Distance between channel and bottom surface	680 µm
Channel location	N/A
Total chip thickness	1800 µm
Chip size	45 mm x 15 mm
Channel width	50 µm
Channel height	20 µm
Rockpore volume	2.3 µl
Combined volume inlet and outlet channel	0.9 µl
Combined volume of inlet and outlet hole	2.5 µl
Total internal volume	5.7 µl
Porosity	0.57

Fig 1 – Physical Rock network micromodel specifications from micronit®_1

Permeability	2.5 Darcy
Number of Inlets	1
Number of outlets	1
Inlet/outlet hole sizes on top of the chip	1.70 mm
Inlet/outlet holes size at channel	0.60 mm
Optical properties	Optical clear view from all sides
Supplied in Fluidic slide?	Yes
Material chip	Borosilicate glass
Material black cartridge	Polypropylene

Fig 2 - Physical Rock network micromodel specifications from micronit®_2

Appendix B

MATLAB® code for Location No. 1

B.1 First .m file: *ApplyOnMyData_Location_1 .m*

```
clc
clear all; close all;
num=xlsread('Results.csv');
cdata1=imread('Series001--t00.tif')
N1=num(:,1);
T1=num(:,2);
X1=num(:,3);
Y1=num(:,4);

[U,V,VM,AVM,c1]=createfigure_Location_1(cdata1,N1,T1,X1,Y
1);

A = {'Vx(µm/s)','Vy(µm/s)','Vm(µm/s)','Vavg(µm/s)'};
B = [U(:),V(:),VM(:),AVM(:)];
C = {'Trajectory','Frame','X (pixel)','Y (pixel)'};
xlswrite('Final_Results.xlsx',C,1,'A1');
xlswrite('Final_Results.xlsx',N1,1,'A2');
xlswrite('Final_Results.xlsx',T1,1,'B2');
xlswrite('Final_Results.xlsx',X1,1,'C2');
xlswrite('Final_Results.xlsx',Y1,1,'D2');
xlswrite('Final_Results.xlsx',A,1,'F1');
xlswrite('Final_Results.xlsx',B,1,'F2');
```

B.2 Second .m file: *createfigure_Location_1 .m*

```
function [U,V,VM,AVM,c1]=createfigure_Location_1(cdata1, N1,
T1, X1, Y1)
%CREATEFIGURE(cdata1, X1, Y1, U1, V1, VM1)
%  CDATA1:  image cdata
%  N1:      the trajectory number
%  T1:      the frame number
%  X1:      quiver x (x coordinate in pixel)
%  Y1:      quiver y (y coordinate in pixel)
%  U:       quiver u (Velocity X component in µm/sec )
%  V:       quiver v (Velocity Y component in µm/sce )
%  VM:      Velocity Magnitude in µm/sec
%  AVM:     Average Velocity for each trajectory in µm/sec
%  c1:      Conversion factor

%           Generated by Mohannad Marouf on 02-Aug-2018
14:09:42

%% necessary inputs from ImageJ:

prompt = '1. What is the exposure time in milliseconds?\n  ';
Exposure = input(prompt);
prompt = '\n2. What is the time interval in milliseconds?\n ';
Interval = input(prompt);
prompt = '\n3. What is the Images increment?\n  ';
Increment = input(prompt);
prompt = '\n4. What is the pixel size in micrometer?\n  ';
Pixel = input(prompt);
c1=(Exposure+Interval)*Increment/(1000*Pixel)
%%%c1=1.5787;

prompt = '5. What is the required Velocity Arrows density?\n
Please enter an integer number within the range [1,10] with 1
for full density and 10 for least density!\n  ';
ArrowsDensity = input(prompt);

for k=1:1:2

% Create figure
figure1 = figure;
colormap(gray);

% Create axes
axes1 = axes('Parent',figure1);
hold(axes1,'on');

% Create image
image(cdata1,'Parent',axes1);

%% Calcualte the instantaneous and average velocities

U1=zeros(numel(N1)-1,1);
V1=zeros(numel(N1)-1,1);
```

```
VM1=zeros(numel(N1)-1,1);
AVM1=zeros(numel(N1)-1,1);

i=1;
for j=1:1:max(N1)
    L(j)= i;
  while (i<numel(N1) && N1(i)==j)
        U1(i)=(X1(i+1)-X1(i))/(c1*(T1(i+1)-T1(i)));
        V1(i)=(Y1(i+1)-Y1(i))/(c1*(T1(i+1)-T1(i)));
        VM1(i)=sqrt(U1(i)^2+V1(i)^2);
        i=i+1;
  end
    U1(i-1)=0;%U1(i-2);
    V1(i-1)=0;%V1(i-2);
    VM1(i-1)=0;%VM1(i-2);
    AVM1(i-1)=mean(VM1(L(j):i-2));
end
U=U1;
V=V1;
VM=VM1;
AVM=AVM1;

%% create quiver
quiver(X1(1:ArrowsDensity:numel(U)),Y1(1:ArrowsDensity:numel(U
)),U(1:ArrowsDensity:numel(U)),V(1:ArrowsDensity:numel(U)),'Au
toScaleFactor',1);

%% Display velocity values on the trajectories

%%% First:   Instantaneous Velocity

if k==1

   text(max(xlim)-500,max(ylim)-100,{'Instantaneous
Velocity','(μm/sec)'},'Color','m','FontSize',13);
   i=1;
   while i<=numel(VM)
        if ~isnan(VM(i))
            VelocityMagnitude = num2str(VM(i),'%.2f\n');

text(X1(i),Y1(i),VelocityMagnitude,'FontSize',6,'color','m');
        end
      i=i+ArrowsDensity;
   end

else

%%% Second:   Average Velocity
   text(max(xlim)-400,max(ylim)-100,{'Average
Velocity','(μm/sec)'},'Color','m','FontSize',14);
   i=1;
    while i<=numel(AVM)
         if (~isnan(AVM(i))&& AVM(i)~=0)
            AverageVelocity = num2str(AVM(i),'%.3f\n');
```

```
text(X1(i),Y1(i),{AverageVelocity},'Fontsize',8,'color','m');
          end
        i=i+1;
    end
end
%% axes labels
%Create ylabel
ylabel('Y coordinate in pixel');

% Create xlabel
xlabel('X coordinate in pixel');

%% X and Y limits and increments

% Comment (ctrl+r) the following line to Automatically Change
the X-limits of the axes
xlim(axes1,[-260 2448]);

% Comment (ctrl+r) the following line to Automatically Change
the Y-limits of the axes
ylim(axes1,[-260 1536]);

axis(axes1,'ij');

%% Set the remaining axes properties
set(axes1,'Layer','top','XAxisLocation','top','YTick',...
 -200:200:numel(cdata1(:,1))+200,'XTick',...
 -200:200:numel(cdata1(1,:))+200);
```

Appendix C

MATLAB® results figures

C.1 Experiment No. 2

C.1.1 Location -1

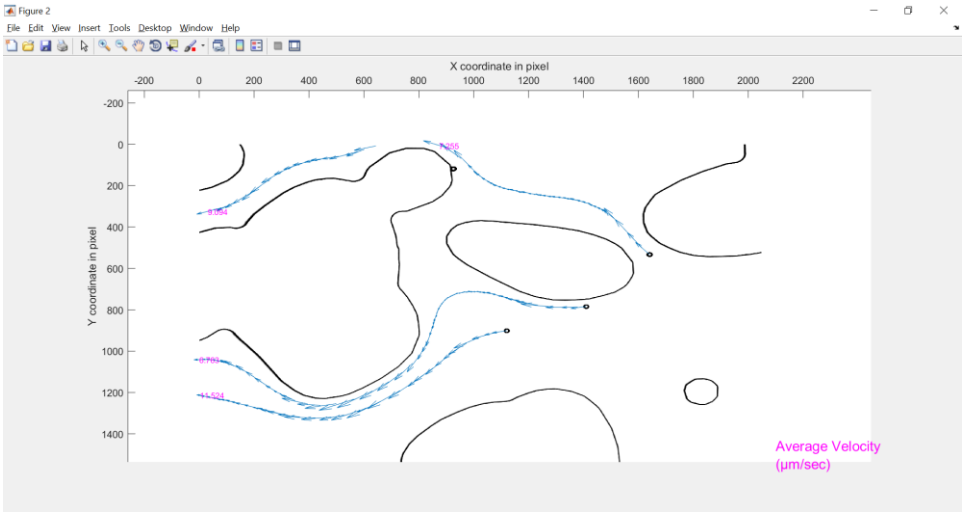

Fig 3 - Average Interstitial Velocity from Location- 1

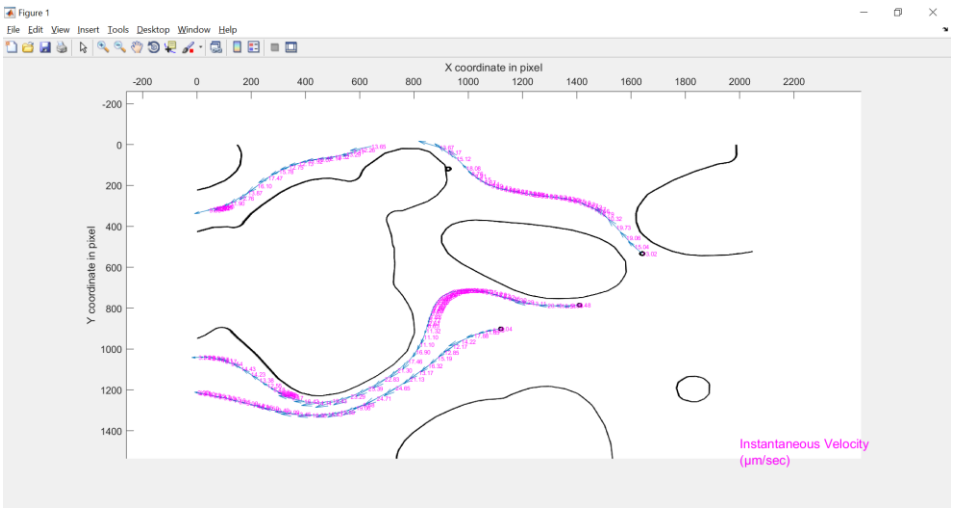

Fig 4 - Instantaneous Interstitial Velocity from Location -1

C.1.2 Location -2

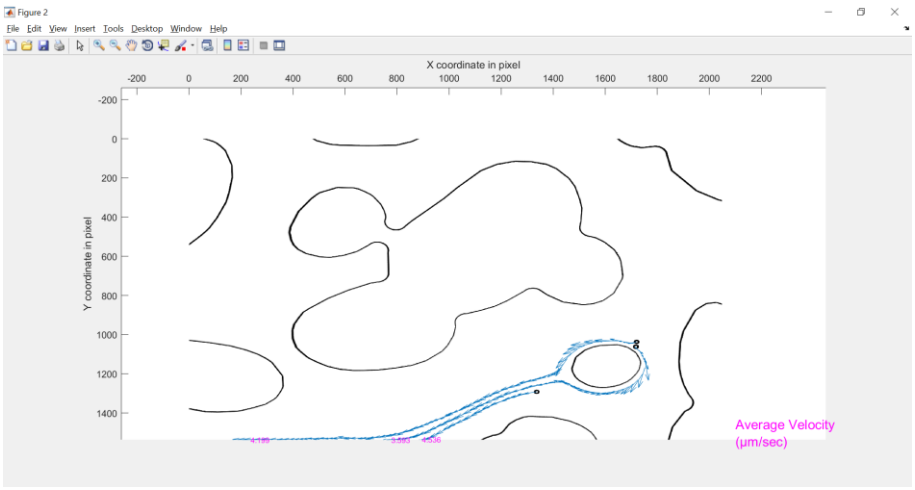

Fig 5- Average Interstitial Velocity from Location- 2

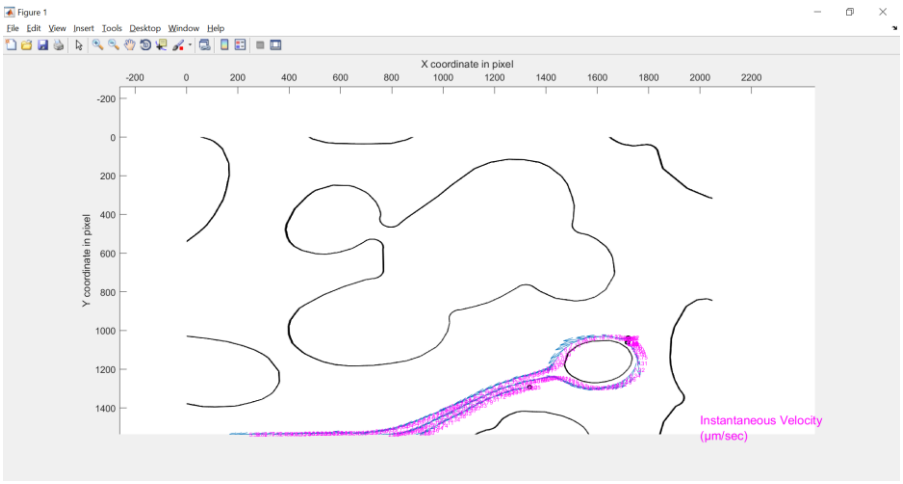

Fig 6- Instantaneous Interstitial Velocity from Location -2

C.1.3 Location -3

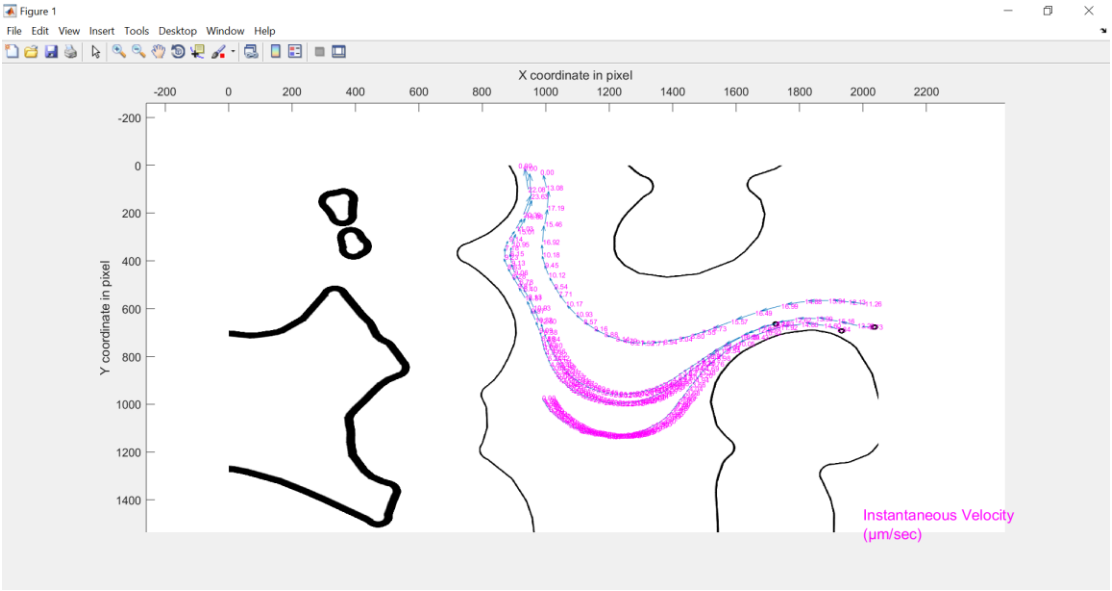

Fig 7 - Instantaneous Interstitial Velocity from Location -3

C.1.4 Location -4

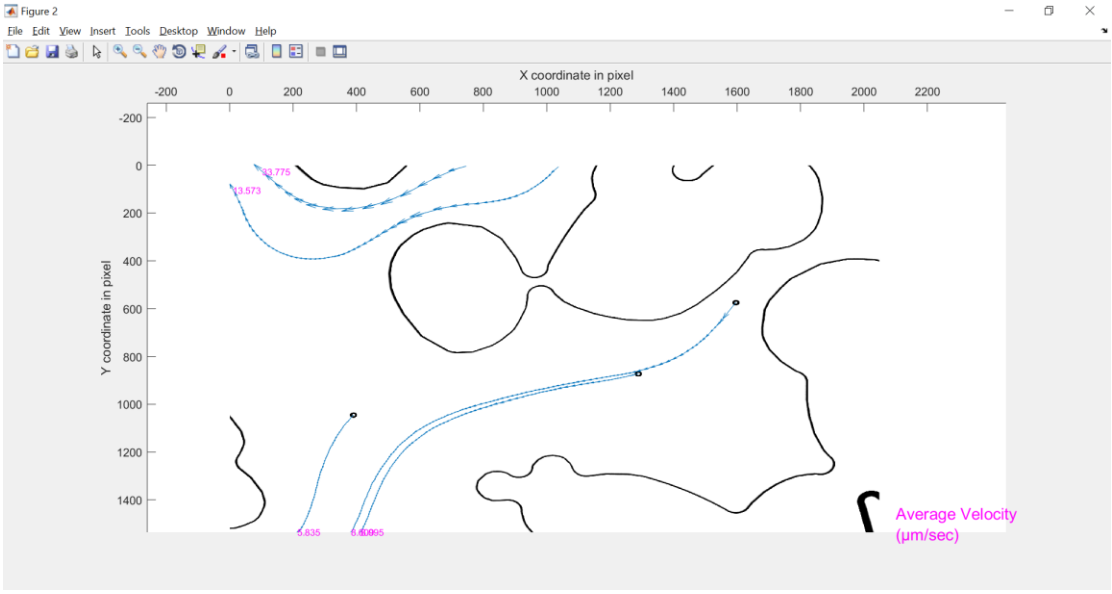

Fig 8- Average Interstitial Velocity from Location- 4

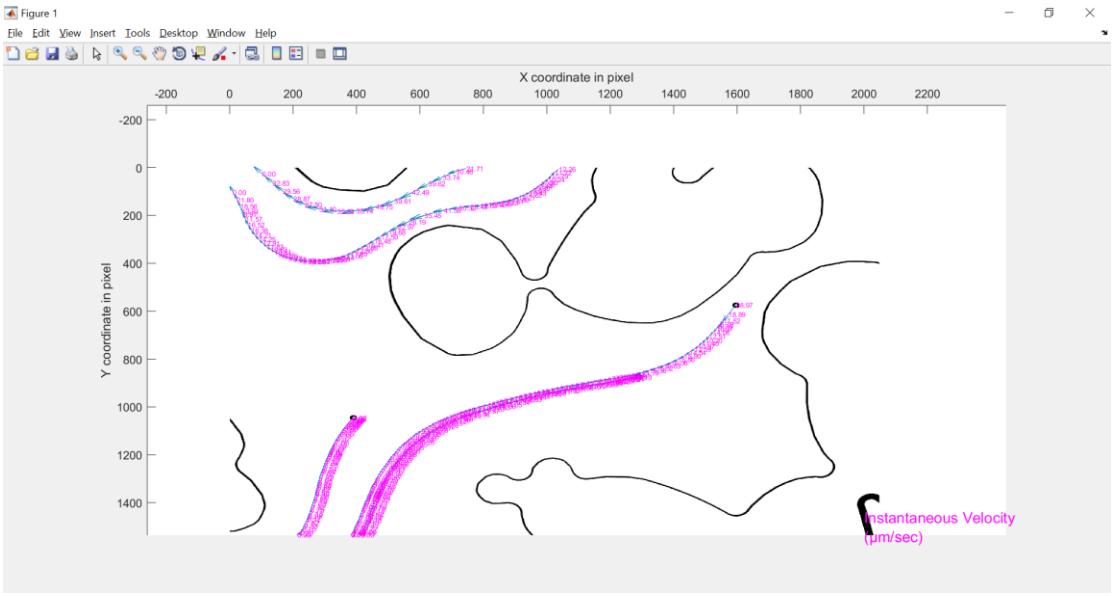

Fig 9- Instantaneous Interstitial Velocity from Location -4

C.1.5 Location -5

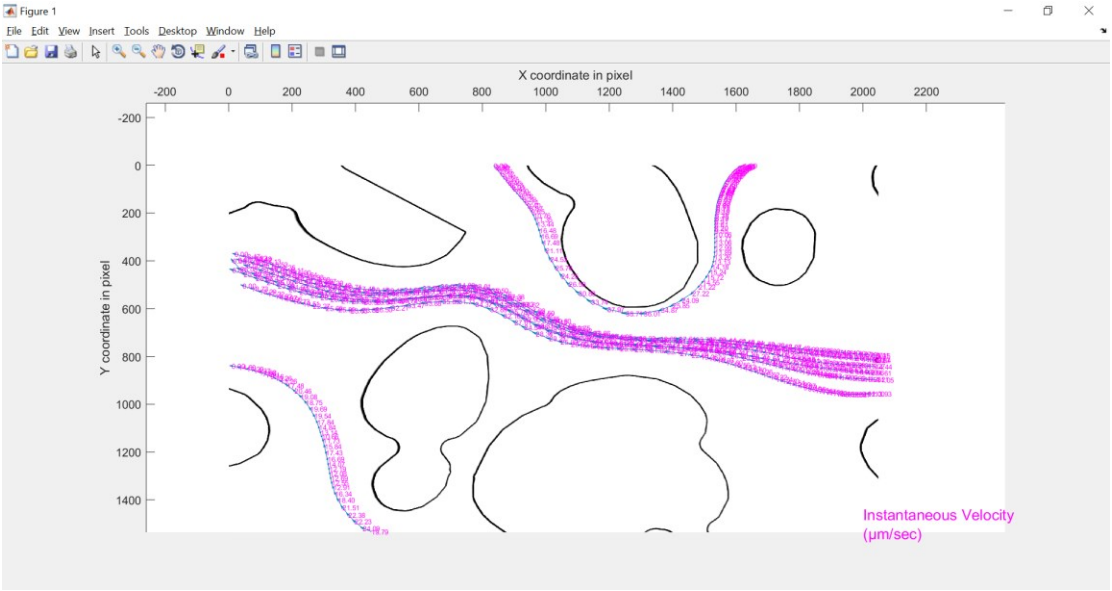

Fig 10 - Instantaneous Interstitial Velocity from Location -5

C.2 Experiment No. 3 (5x & 0.005 ml/Hour)

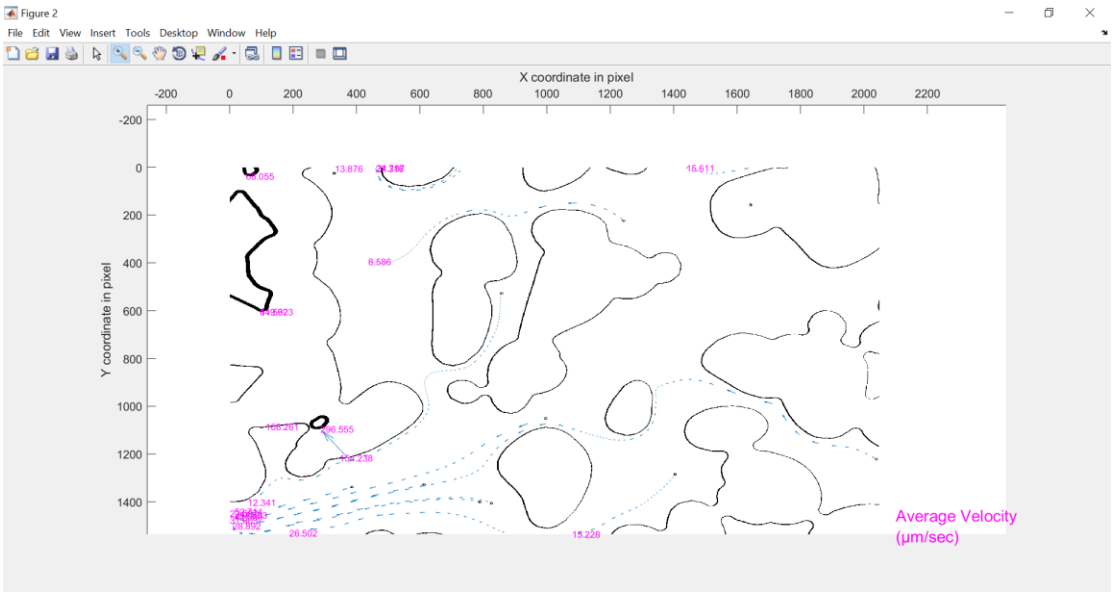

Fig 11 - Average Interstitial Velocity from Experiment No. 3

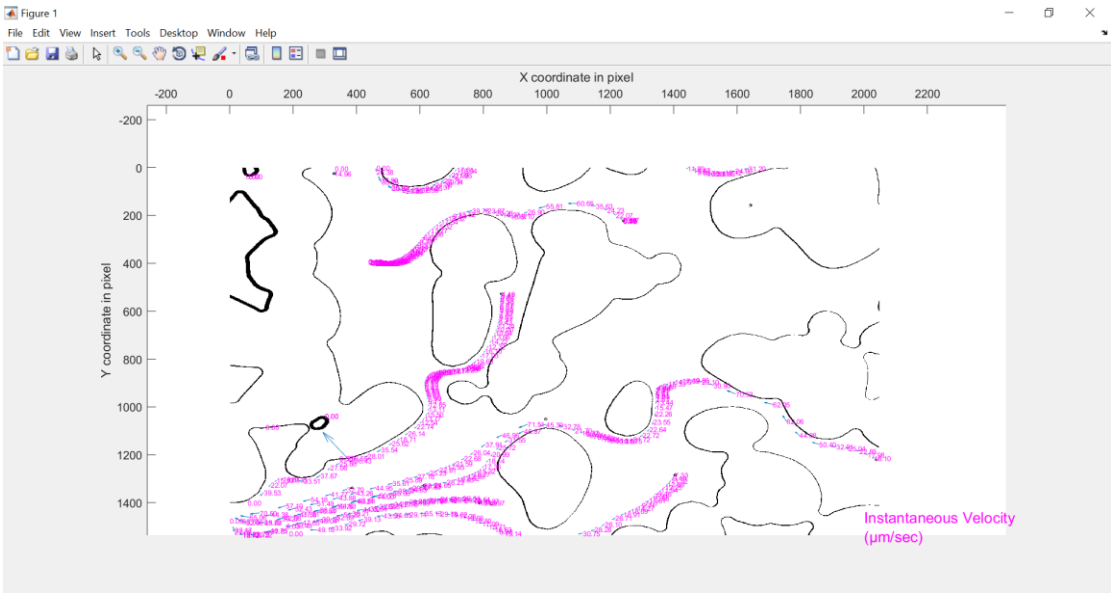

Fig 12 - Instantaneous Interstitial Velocity from Experiment No. 3

C.3 Experiment No. 4 (5x & 0.02 ml/Hour)

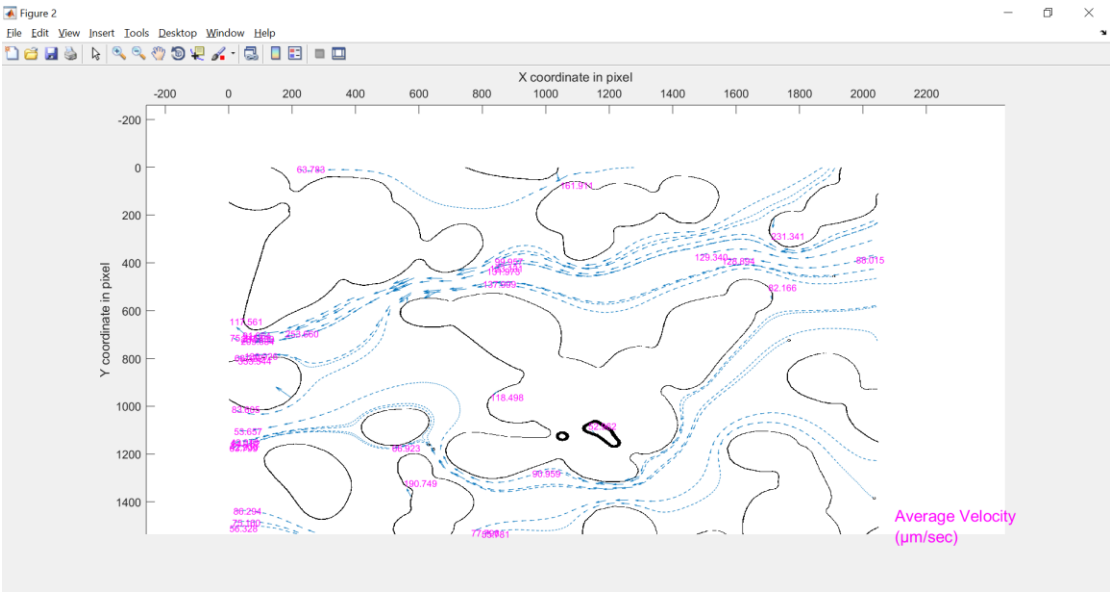

Fig 13 – Average Interstitial Velocity from Experiment No. 4

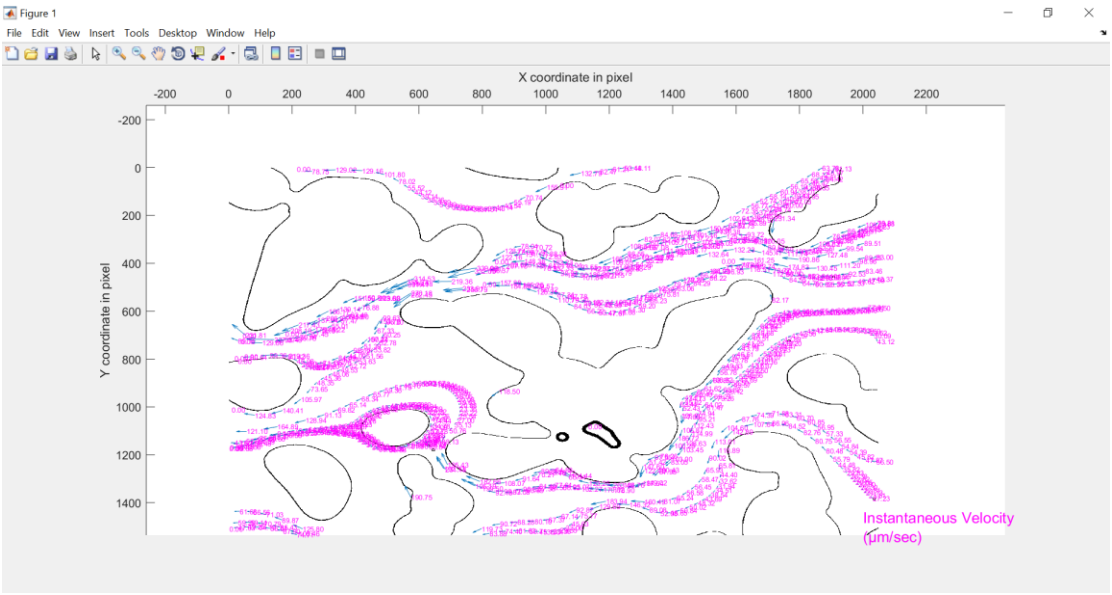

Fig 14 - Instantaneous Interstitial Velocity from Experiment No. 4